Early events in DNA double strand break repair after damage induction with a laser microbeam

Dissertation
zur Erlangung des akademischen Grades
doctor rerum naturalium (Dr. rer. nat.)

vorgelegt dem Rat der Biologisch-Pharmazeutischen Fakultät
der Friedrich-Schiller- Universität Jena

von Dipl. Biophys.

Paulius Grigaravičius

geboren am 30. März 1979
in Vilnius, Litauen

This work was performed in

Leibniz Institute for Age Research
Fritz Lipmann Institute (FLI)

Supervisor: Prof. Dr. Karl Otto Greulich
Leibniz Institute for Age Research – Fritz Lipmann Institute

Gutachter: Prof. Dr. Zhao Qi Wang
Leibniz Institute for Age Research – Fritz Lipmann Institute

Gutachter: Prof. Dr. Cristina Cardoso
Molecular Cell Biology
Technical University Darmstadt

Day of defense: 18.06.09

Content

Summary

In the present thesis DNA double strand break (DSB) induction and repair are analysed after laser-microbeam irradiation. Live cell imaging of DNA repair proteins fused to Green Fluorescent Protein (GFP) as well as immunofluorescent detection of endogenous protein are used.

Laser induced DNA damage, detected by γ-H2AX foci staining depend on a subtle combination of used laser pulse wavelength, pulse energy and dose. The recruitment times of repair proteins depend inverse linearly on laser pulse energy. By extrapolation to zero, the recruitment time at biological relevant conditions is calculated. Interestingly, considerable spatial dynamics of the foci is found. Two neighbouring foci even can fuse within ~20 min.

Recruitment time comparison of molecules representing early and late Non-Homologous end Joining (NHEJ), Homologous Recombination Repair (HRR) and the Mre11-Rad50-NBS1 (MRN) complex reveals that the whole NHEJ machinery is assembled to DSBs within 1 min. Recruitment of latest NHEJ factor (XRCC4) is faster than NBS1 and is not directly influenced by the absence of NBS1. XRCC4 persists at DSBs longer in the G1 cell cycle phase than in G2 where the replacement of NHEJ by HRR molecules occurs. Rad51 is recruited when XRCC4 is released with the complementary kinetics. DNA-PKcs phosphorylation at two sites, known to facilitate DNA end processing, occurs between the recruitment of NHEJ and HRR.

Recruitment of DNA repair proteins gives only an indirect view on DNA double strand breaks in the form of foci. A new modification of Comet-assay technique the Immunofluorescent Comet-assay (IFCA) is developed in this work for direct visualisation of DSBs in single cells. IFCA uses the immunofluorescent detection of histone H1 in neutral and alkaline Comet-assay, and enables simple and clear visualisation of details in the comet tail, which are hardly detectable by conventional DNA staining dyes such as SYBR Green. Comparison of fragmentation patterns after different treatments reveals, that 10 μJ of highly localized laser-microbeam irradiation induces similar fragmentation pattern as whole cell treatment with 20 Gy of ionizing radiation. Using IFCA, the fragment size at the end of the neutral comet tail is determined for the first time.

Zusammenfassung

In der vorliegenden Arbeit werden die DNS-Doppelstrangbruch (DSB) Induktion und Reparatur nach der Laser-Mikrobestrahlung erforscht.

Die Lebendzellmikroskopie wurde verwendet zur Untersuchung von Reparaturenzymen, die mit grünfluoreszierendem Protein (GFP) gelabelt wurden. Desweiteren wurden endogene Proteinen immunofluoreszenzoptisch analysiert.

Die durch den Laser induzierten Schäden, nachgewiesen durch die γ-H2AX-Färbung, sind abhängig von einer subtilen Kombination der angewendeten Laserpulswellenlänge, der Pulsenergie und der Dosis. Die Akkumulationszeit der Reparaturproteine hängt reziprok-linear von der Laserpulsenergie ab. Durch die Extrapolierung gegen Null wird die Rekrutierungszeit unter biologisch relevanten Bedingungen berechnet. Deutliche räumliche Dynamiken der beschädigten Stellen werden erkennbar. Zwei benachbarte Foci können innerhalb von 20 Minuten fusionieren.

Ein Vergleich der Akkumulationszeiten von Molekülen, welche die frühe und späte nicht-homologe End-zu-End-Verknüpfung (NHEJ), die homologe Rekombinationsreparatur (HRR) und den Mre11-Rad50-NBS1-Komplex (MRN) repräsentieren, zeigt, dass sich alle NHEJ Enzymen am DSB innerhalb einer Minute ansammeln. Die Rekrutierung des letzten NHEJ-Faktors (XRCC4) erfolgt schneller als die von NBS1, wird aber nicht direkt durch das Fehlen des NBS1 beeinflusst. Das XRCC4 verweilt an den DSBs in der G1-Zellzyklusphase länger als in der G2-Phase, in welcher der Austausch von NHEJ durch HRR stattfindet. Das Protein Rad51 wird akkumuliert, wenn sich XRCC4 mit vergleichbarer Kinetik ablöst. Die DNS-PKcs-Autophosphorylierung erfolgt genau zwischen den Rekrutierungen von NHEJ und HRR.

Die Rekrutierung der DNS-Reparaturproteine gibt nur einen indirekten Einblick auf die DNS-Doppelstrang-Brüche in Form der Foci. Eine neue Modifikation der Comet-Assay-Technik, der Immunofluoreszent-Comet-Assay (IFCA), wurde in dieser Arbeit für die direkte Visualisierung der DSBs in einzelnen Zellen entwickelt. Die IFCA benutzt den immunofluoreszenten Nachweis an H1-Histonen in neutralem und alkalischem Comet-Assay und ermöglicht eine einfache und deutliche Visualisierung der Details im Cometenschweif. Diese sind mit einer herkömmlichen DNS-Färbung, wie etwa SYBR Green, nur schwer erkennbar. Ein Vergleich verdeutlicht, dass 10 μJ der hochlokalisierten Laser-Mikrobestrahlung ein ähnliches Fragmentierungsmuster induziert wie eine gesamte Zellbehandlung mit 20 Gy ionisierender Strahlung. Die Anwendung von IFCA dokumentiert zum ersten Mal die Größe der Fragmente am Ende des Schweifs.

1. Introduction

DNA is a molecule preserving our genetic information and therefore determining the way how and who we ***are*** from a biological point of view. Additionally it plays a crucial role for our health and longevity - the intact DNA is a basis for our healthy life. Unfortunately it is under enormous damaging load. Each cell in the human body suffers from thousands of various DNA damage per day. Another important fact is that damaged DNA molecules can not be replaced by an intact one as for example damaged proteins. Thus, it has to be repaired. If not, it can lead to mutations and genetic instability. This can further cause various diseases, cancer and also premature aging. In order to keep our DNA intact the nature has developed a huge DNA repair mechanism involving more than hundred genes and tens of different pathways dealing with broad range of different types of DNA damage (Hoeijmakers, 2001; Wood et al., 2001; Wood et al., 2005) (Figure 1.1).

Among the high variety of DNA damage types the DNA double strand breaks (DSBs) are particularly harmful lesions, since, in this case, the second DNA strand can no longer be used as a template. Furthermore, it is the most lethal damage, since one DSB is sufficient for cell cycle arrest, cell death and cellular malfunctioning leading to aging. In mammals two major pathways are responsible for repair of DSBs. The most utilized is a error prone NonHomologous End Joining (NHEJ) working throughout the cell cycle. Another major repair pathway is Homologous Recombination Repair (HRR), which uses homologous information from the undamaged sister chromatid to restore the intact genetic information, therefore this pathway is error free and better conserves the information preserved in DNA.

Although most genes involved in the above mentioned pathways are well known, we still do not completely understand the mechanism of DSB repair in the cell nucleus, since it is a very complex issue involving not only proteins but also a lot of their posttranslational modifications such as phosphorylation, acetylation and ubiquitinylation (Karagiannis and

El Osta, 2007; Huen and Chen, 2008). It turned out that studying the kinetics of the recruitment of DNA repair molecules to sites of damage in the cell nucleus significantly helps to understand the repair mechanisms. In order to study kinetics, a time point and the position of damage has to be highly defined. This is possible only if damage is introduced exogenously.

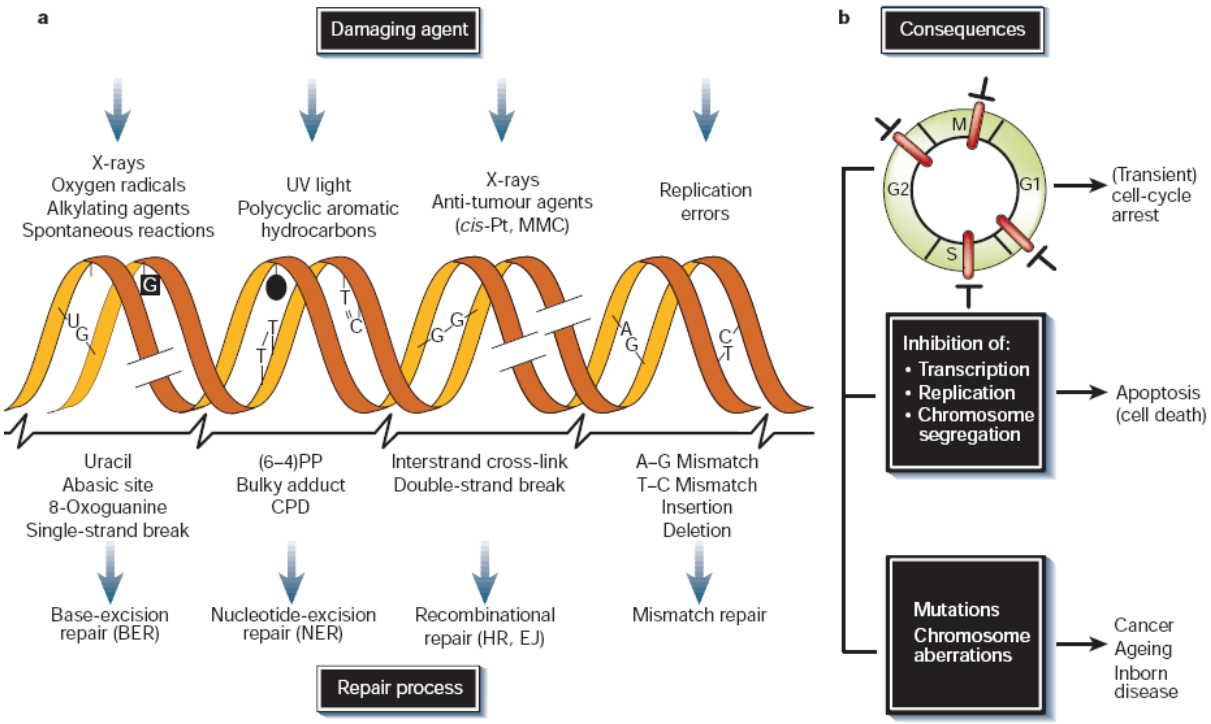

Figure 1.1 DNA damage and repair mechanisms and consequences. A - examples of DNA damaging, induced lesions and their subsequent repair. B - consequences of DNA damage processing showing transient arrest in G1, S, G2 and M cell cycle phases, cell death or genetic instability. Adapted from Hoeijmakers, 2001.

1.1. DNA double strand break repair

As mentioned above, DSBs are repaired by two major pathways, an error prone NHEJ and error free HRR, which together with the Mre11-Rad50-NBS1 (MRN) complex will be described in the following sections.

NHEJ

As recently numerous reviews have described (Weterings and Chen, 2008; van Gent and Van der Burg, 2007) the NHEJ is active throughout the cell cycle and is initiated by very strong binding of Ku70/80 heterodimer to DNA ends with a dissociation constant K_d in the

range 1.5 - 4.0 × 10^{-10} M (Dynan and Yoo, 1998; Walker et al., 2001). Figure 1.2 shows that it is followed by the recruitment of the catalytic subunit of DNA-Protein Kinase (DNA-PKcs) from the PIKK family (Burma et al., 2006). It was suggested that DNA-PKcs mediates tethering of two DNA ends by forming a synaptic complex which in its natural form hides DNA termini from processing and thus repair (Weterings and van Gent, 2004; Weterings et al., 2003). Only after autophosphorylation, DNA-PKcs molecules undergo conformational changes and liberate DNA ends for further processing (Ding et al., 2003; Weterings et al., 2003; Block et al., 2004). Here the phosphorylation of clusters around two positions, Ser2056 and Thr2609, are known to be involved in conformational changes (Weterings and Chen, 2007).

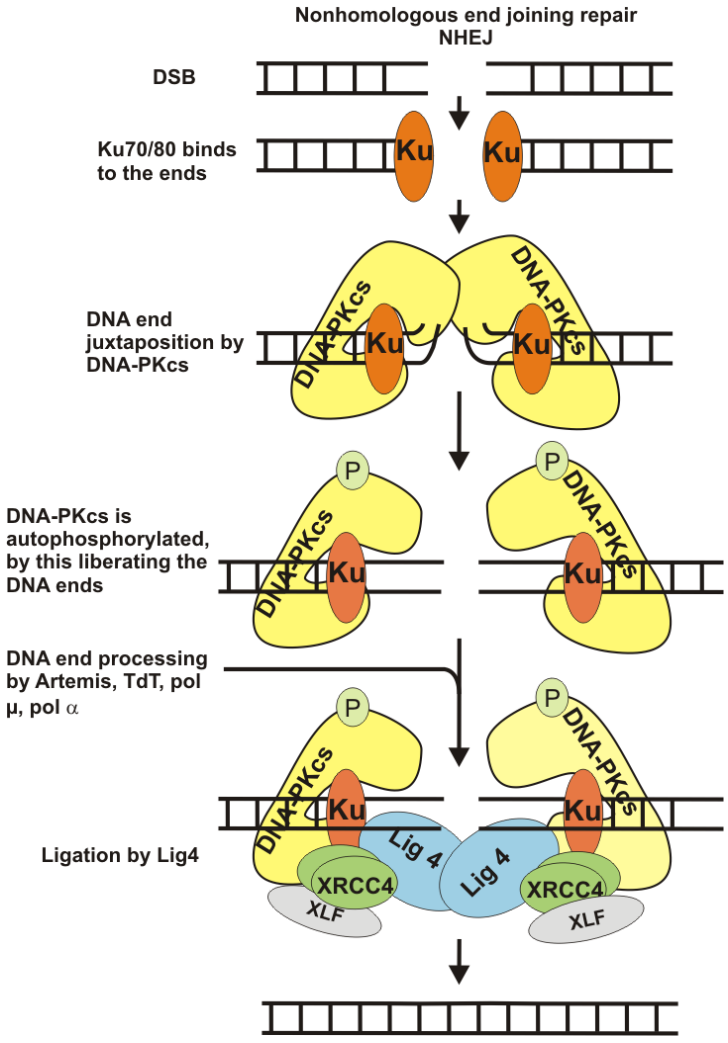

Figure 1.2 Double strand break repair by Non Homologous End Joining (NHEJ).

Those clusters are called PQR and ABCDE correspondingly. The cluster at Ser2056 is autophosphorylated by the kinase domain of DNA-PKcs, whereas phosphorylation of the cluster at Thr2609 was shown to be mediated by ATM (Ataxia telangiectasia mutated) (Chen et al., 2007) or even by ATR (Yajima et al., 2006). Interestingly, it was suggested that the PQR cluster phosphorylation is working in the opposite direction than a ABCDE since upon phosphorylation of the PQR cluster the DNA end processing is inhibited (Cui et al., 2005). Recently additional autophosphorylation sites in the C-terminal region of DNA-PKcs were identified at positions 3821, 4026 and 4102 (Ma et al., 2005).

After DNA-PKcs autophosphorylation DNA ends can be processed by μ and λ polymerases, terminal deoxynucleotidyltransferase, polynucleotide kinase and Artemis endonuclease (Wyman and Kanaar, 2006; van Gent and Van der Burg, 2007). The final step of NHEJ is thought to be accomplished by recruitment of the recently identified XRCC4 like factor (XLF, also named Cernunnos) (Ahnesorg et al., 2006) and subsequently the XRCC4/LigIV complex (Lee et al., 2000), which ligates the DSBs. So far it is not really known whether factors involved in the latest NHEJ step are recruited before or after the DNA end processing. Yano et al. reported that recruitment of indeed all factors is crucial for NHEJ complex stability (Yano and Chen, 2008). This indicates that for a proper repair all the enzymes have to be assembled sequentially in a small time window. This hypothesis was supported by the finding that DNA end processing by polymerases and endonucleases is mediated by the XRCC4/Lig4 complex (Budman et al., 2007). It means that the complex involved in the latest NHEJ step is present at DSBs very early, facilitates DNA end processing and only after that performs ligation. Correspondingly, Ku70/80, DNA-PKcs and XLF are estimated to be recruited within the first minute after irradiation (Mari et al., 2006; Uematsu et al., 2007; Yano et al., 2008). In contrast, XRCC4 has been reported to reach the maximum only in ~ 6 min (Yano and Chen, 2008). This inconsistency might appear due to below described problem, arising when experiments are done using different laser-microbeam system or even at the same set up but different settings.

HRR

Unlike NHEJ, the HRR is an error free repair pathway requiring resection and also the homologous sequence from the sister chromatid (Li and Heyer, 2008; Wyman and Kanaar, 2006; Sung and Klein, 2006). In mammals it is available only in the late S/G2 cell cycle phase and is a major repair pathway of replication generated DSBs with one DNA end. DNA nucleases such as MRE11 and CtIP (Buis et al., 2008a; Sartori et al., 2007) play a

crucial role in HRR since they produce 3´-overhangs (Figure 1.3). After resection, the single stranded DNA is covered by the RPA (Replication protein A) proteins, which are then exchanged by the Rad51 nucleoprotein filaments. This replacement is facilitated by Rad52 protein, while Rad54 mediates the strand invasion and recombination after correct positioning of the sister chromatid by cohesins.

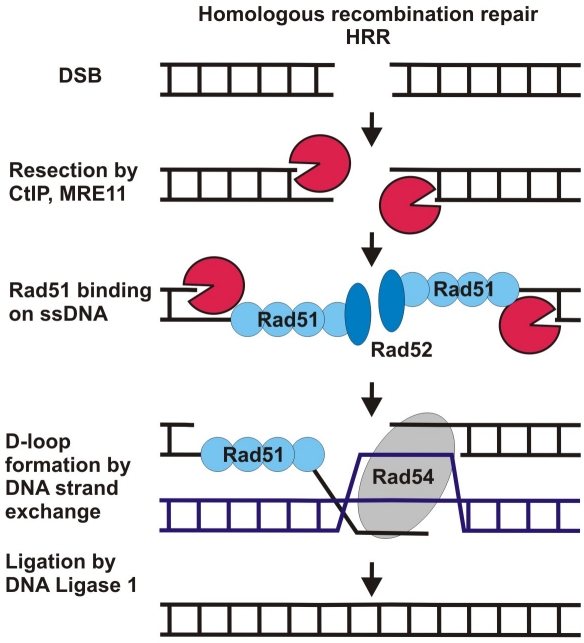

Figure 1.3 Simplified scheme of DSB repair by Homologous recombination repair (HRR)

The MRN complex

One of the key players in DSB repair is the MRE11-Rad50-NBS1 complex (MRN), which is involved in different stages of DNA damage response (Williams et al., 2007). As shown in Figure 1.4 one of the functions is the detection of DNA double strand breaks through the Mre11 (Meiotic recombination 11) DNA end binding domain (Lavin, 2007; Buis et al., 2008b; Williams et al., 2008). According to the literature this binding is essential for activation of ATM – a PIKK 3 family kinase, which normally forms a dimer and only upon activation is phosphorylated and monomerized. The activated ATM phosphorylates a huge number of proteins involved in DSB repair. One of them is a histone H2AX, which is phosphorylated at Ser139 in megabase regions around the DSB (Rogakou et al., 1998). In

this way γ-H2AX is forming an irradiation induced focus, which is thought to be a specific marker of DBSs and can be clearly visualized by fluorescence microscopy. However, the intial phosphorylation is directly connected with the DSB sensing by MRN and then activation of ATM Figure 1.4. The following γ-H2AX signal spreading is mediated by MDC1 (Mediator of DNA damage checkpoint protein 1) protein and works like a chain reaction, where MDC1 binds to initial γ-H2AX, recruits MRN complex with ATM and in this way phosphorylates the next H2AX, which again is detected by MDC1 (Figure 1.4) (Celeste et al., 2003; Stucki and Jackson, 2006). Here the second second function of MRN complex becomes obvious, as it is involved in the posttranslational modification of chromatin, surrounding the DSB (Lee and Paull, 2007). When and how this reaction stops is still not understood. It is known that it provides a basis for the binding of different DSB repair proteins by this ensuring the efficient repair and finally plays a crucial role in the cell cycle checkpoint activation. Where again the MRN complex was reported to be involved (Shiloh, 2003). Finally, the MRN complex was shown to play a crucial role in mediating the choice of NHEJ and HRR pathways (Yang et al., 2006). It is also important for the production of 3'- overhang by the nuclease activity of Mre11.

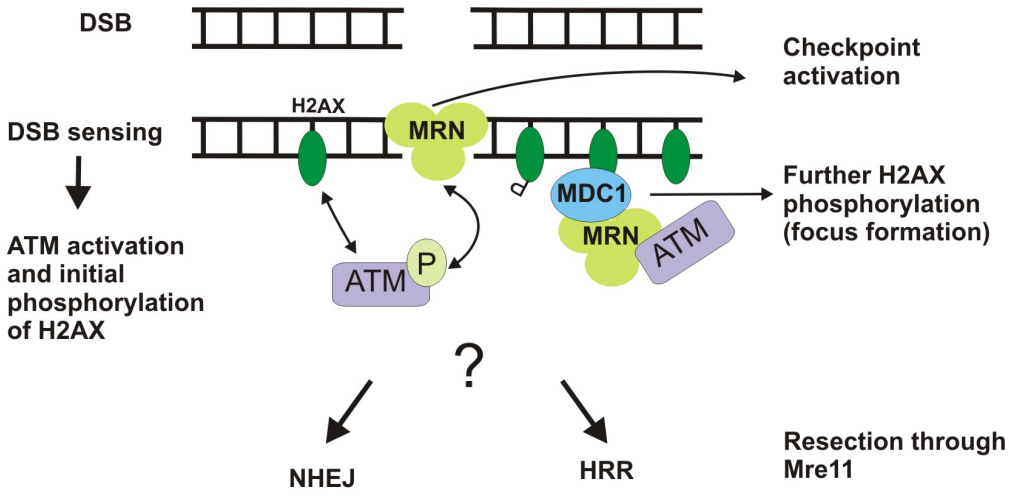

Figure 1.4 Mre11-Rad50-NBS1 (MRN) complex as a multifunctional player in DSB repair

1.2. Laser-microbeam as a precise tool to study DNA damage and repair

A number of tools are available to experimentally induce DNA double strand breaks (Essers et al., 2006). One can use toxins or different types of irradiation such as ionising or

UV-A radiation (Rapp and Greulich, 2004). However these treatments normally induce damage in whole cell nucleus and their time resolution is poor since damaging procedure can last up to 30 min. Another possibility is a stable genetical integration of a recognition site for a rare cutting enzyme and then subsequent generation of damage by inducing the enzyme translocation into the nucleus (Rodrigue et al., 2006; Miyazaki et al., 2004). Here again timing of damage induction can not be controlled exactly. Thus, the starting time point of DNA damage repair can not be highly defined.

There are two available techniques capable to induce highly localized damage with high temporal resolution. One of them is an ionising microbeam delivering heavy ions and alpha particles of different energies and linear transfer energies to a desired part of the cell nucleus (Tartier et al., 2003; Heiss et al., 2006; Prise et al., 1998; Hamada et al., 2006; Desai et al., 2005; Greubel et al., 2008). Although some systems already exist for the observation of living cells during and immediately after irradiation (Hauptner et al., 2006; Jakob et al., 2005), these instruments are extremely costly, rarely available, very complex and limited to a narrow spectrum of beam parameters.

Another technique is the laser-microbeam generating ultraviolet, visible or near infrared light (Greulich, 1999). Micro-focused laser light has proven to allow very precise micromanipulation and microprocessing of cells (Berns and Greulich, 2007). Recently, an interest in laser microbeams has turned towards application in DNA repair research, because of their high resolution in space (x,y,z) (Meldrum et al., 2003) and time. Unlike the above presented tools for DNA damage induction, lasers can be simply directed to the preselected sub nuclear locus at user defined time points. Recently, the damage induction and repair exclusively in the heterochromatin of mouse cells was shown (Ayoub et al., 2008). A distinct advantage is that the laser beam is incorporated into the same microscope that is used for imaging. Therefore the specimen does not need to be transferred and thus it allows detecting fast events: ~ 1 s if combined with live cell imaging and ~2 min if combined with immuno-histochemistry (Essers et al., 2006; Lukas et al., 2005).

One of the first attempts to use a laser-microbeam for DNA double strand break repair studies was presented in 1999 by Rogakou et al (Rogakou et al., 1999). The authors used LaserScissors Module 390/20 with a pulsed UV-A laser at 390 nm to induce damage in cells pre-sensitized with halogenated thymidine analogs and/or DNA intercalating dyes such as Hoechst. Following this experiment, numerous publications appeared using different laser systems for DNA damaging. Some groups used pulsed UV-A lasers from

337 nm (nitrogen laser) to 405 nm either with the pre-sensitization as mentioned above (Lukas et al., 2004; Bekker-Jensen et al., 2006; Tashiro et al., 2000; Walter et al., 2003; Celeste et al., 2003; Mortusewicz et al., 2005; Kruhlak et al., 2006) or without it (Lan et al., 2005; Uematsu et al., 2007). Some of the researches tried also to use low energy pulsed diode laser at 405 nm, however 100 line scans were needed to produce detectable double strand breaks (Lan et al., 2005). Higher energy pulsed laser systems have an advantage that DSBs can be induced just with one pulse. This increases temporal resolution as well as reduces unwished thermal effects. Recently also lasers in the visible and the near infrared range have been used. The second harmonic of Nd:YAG (Kim et al., 2005) at 532 nm was used to study the assembly of proteins involved in NHEJ and HRR after two photon damage induction. It was also reported that pulsed near infrared Ti:Sa lasers at 800 nm can be applied to induce DNA damage due to three-photon absorption (Meldrum et al., 2003; Bradshaw et al., 2005; Mari et al., 2006).

Despite the wide usage of laser, DNA damaging effects of microbeams are understood only to a limited extent (Konig et al., 1999; Mohanty et al., 2002; Dinant et al., 2007) especially in terms of beam quality. Unfortunately, each group uses microbeams with different parameters - pulse energy, dose and wavelength even though DNA damage induction was shown to be highly dependent on the quality (pulsed vs continuous laser) of the irradiation source (Mohanty et al., 2002; de With and Greulich, 1995). The variation of various parameters may induce different responses, from moderate photodamage to complete destruction of the DNA. In consequence, the activated DNA repair response may vary largely depending on the laser system used (Dinant et al., 2007). Therefore, comparison of results obtained in different laboratories became a quite challenging issue. Obtaining first information on such differences is one of the aims of this work.

1.3. Comet-assay for detection of DNA fragmentation

The level of induced double strand breaks (DSBs) primarily can be estimated from the dose of applied noxes although dose definitions for each of the damaging agents are different. Grays [Gy] are used for ionizing irradiation, concentration [µg/ml] for biochemical damaging like drugs or enzymes and Joules [J/cm^2] for UV and visible light. Consequently they can not be compared directly. This lack of comparability of DNA fragmentation induced by different noxes has the consequence that the synergies in the knowledge on DNA damage and subsequent repair are presently not optimally used.

One way to compare different damaging tools is to look at the DNA damage response for example by measuring the presence of DNA repair proteins such as γ-H2AX or RPA (Bekker-Jensen et al., 2006). However, it is not clear if these markers do really represent DSBs. Therefore, in this work another additional method was developed for direct detection of DNA damage. Correspondingly, in the case of DSBs the fragmentation levels will be analysed.

For the detection of DNA breaks at a single-cell level, the neutral Comet-assay has been developed in 1984 (Ostling and Johanson, 1984; Olive et al., 1992). The basic principle of the Comet-assay is presented in Figure 1.5. The induced damage level can be quantified by the DNA content in the comet tail after electrophoresis of single cells embedded in the agarose gel. Therefore another name for this technique is a Single Cell Gel Electophoresis (SCGE). It is widely believed that the conventional neutral Comet-assay, where lysis and electrophoresis are done at pH 8, detects DNA strand breaks. Whether it detects solely DSBs or also single strand breaks (SSBs) is still under discussion (Collins, 2004; Collins et al., 2008). However, the common DNA dye based staining techniques used in previous approaches provide only limited resolution of the comets. Thus, visualization of details is not possible and the subtle differences in neutral comets after various treatments can not be revealed.

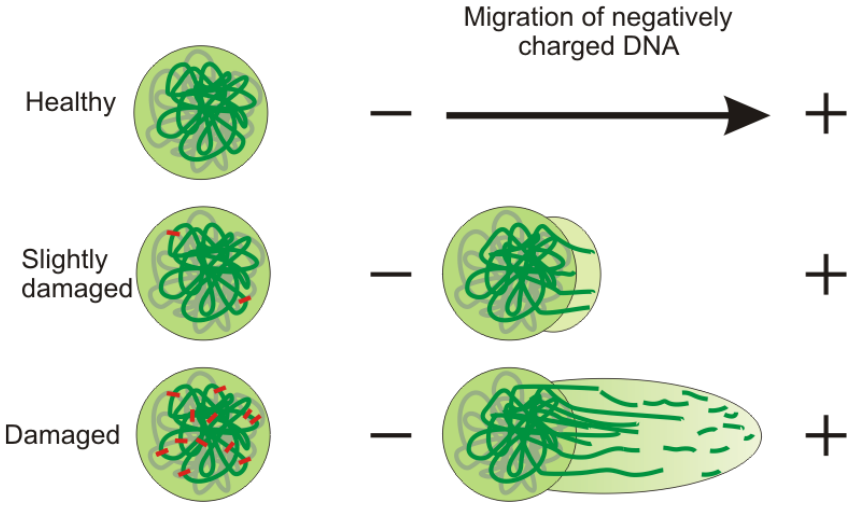

Figure 1.5 DNA stretching in single cell gel electrophoresis. By increasing the number of damage (marked in red) the amount of DNA stretched out of the cell nucleus increases, by this forming a tail.

Therefore in this work a novel staining method - the Immuno Fluorescent Comet Assay (IFCA) using antibodies against histone H1, will be introduced. This enables direct visualization of fragmented chromatin with high resolution, exploiting the fact that the linker histone H1 is tightly bound to the DNA. It has already been reported in the literature that even after proteinase treatment some proteins still remain bound to DNA in the Comet-assay (Singh et al., 1999b; Werner and Petzelt, 1981).

Using IFCA it is possible to provide a detailed look into the neutral version of the Comet-assay at high resolution, and even gives an estimate for the size of fragments at the end of the comet tail. Importantly, it allows comparing fragmentation patterns of single cells after different damaging treatments.

1.4. Aim of the thesis

Both, the NHEJ and HRR pathways as well as MRN function, seem to be well studied separately. However, it is still very poorly understood how these pathways interact with each other in real time. There are only few reports in literature where the timing of NHEJ and HRR are compared. Kim et al. have found that NHEJ and HRR are recruited sequentially, however only the Ku80 molecule involved in the earliest NHEJ step was analysed, and only the information whether the proteins are assembled or not was obtained (Kim et al., 2005). Furthermore, immunofluorescence staining was performed by fixing cells around 20 min after irradiation. Therefore, the information of the earliest steps could not be recorded. An interesting finding was obtained by Allen et al. who reported that HRR is increased in the absence of DNA-PKcs but decreased when DNA-PKcs is catalytically inactive, suggesting that DNA-PKcs is a protein at the interface of NHEJ and HRR pathways (Allen et al., 2003; Shrivastav et al., 2008), which might cooperate (Rapp and Greulich, 2004). However, we still do not understand how these pathways do cooperate or compete on the DSBs.

Therefore, one of the main aims of this work is to understand the cross talk of those pathways. In this case the recruitment kinetics are measured of early and late NHEJ, the MRN complex and the HRR machinery at exactly the same conditions in human cells, by combining laser-microbeam for damage induction with live cell imaging and immunofluorescence.

Since laser-microbeams are used for the study, the influence of the variation of different laser parameters on the DNA double strand break induction has to be investigated. Following it, the comparison of laser micro-irradiation against other treatments such as ionizing radiation and chemicals in terms of the DSB induction has to be done. For this purpose a novel Comet-assay staining method, allowing measuring of DNA fragmentation with high resolution, is developed.

2. Materials and Methods

2.1. Cell culture

The human osteosarcoma U-2 OS, HeLa, HaCat (kindly received from Petra Baukamp) and NIH 3T3 mouse fibroblasts cell lines were maintained in RPMI containing 10% FCS, 10.000 U/L Penicillin, 100 mg Streptomycin at standard conditions at 37°C, 5% CO_2. Stable U-2 OS cell lines expressing EGFP tagged Ku80, XRCC4 or NBS1 where maintained with 300 µg/ml of G418. Wilde type and NBS1 null mouse embryonic fibroblasts kindly received from Z.Q.Wang and Ku80 deficient MEFs kindly received from M.Löbrich were maintained in DMEM with 10% FCS, 10.000 U/L Penicillin, 100 mg Streptomycin at 37°C, 10% CO_2. Depending on the experiment the cells were seeded in chambered cover-slips (Nunc), µ-dish (ibidi) or 3.5 cm culture dishes two days before the experiment. In the case of transient transfection, one day before the experiment cells were transfected with vectors as described. All experiments were done in unsynchronised cells.

2.2. Cloning

In order to visualise the proteins of interest in the living cells, they were fused with Enhanced Green Fluorescent Protein or monomer Red Fluorescent Protein (EGFP or mRFP). Therefore the coding sequences of investigated proteins were amplified from U-2 OS cells and then cloned into expression vectors containing coding sequences of fluorescent proteins. Finally, generated vectors were amplified in *Escherichia coli* (*E.coli*) and analysed by restriction analysis and sequencing. Vectors coding proper fusion proteins were further used for transient transfection or for the generation of cell lines stably expressing fusion proteins.

DNA agarose gels

DNA gels were used either to analyse restriction digestions (analytic gels), by detecting the correct number and size of bands, or to purify certain nucleic acids from an inhomogenous mixture e.g. after polymerase chain reaction (PCR) (preparative gels). Preparative gels were with larger slots to accommodate large amounts of DNA. Gels contained 1.0% agarose type II in TAE buffer with 5 µl of ethidium bromide per 100 ml gel. DNA samples were mixed 6:1 with 6×DNA loading buffer and run at 5 V/cm in TAE buffer.

RNA Gels

RNA gels were used to analyse the RNA content after RNA isolation from mammalian cells. They were prepared with 1.2 % agarose type II in formaldehyde (FA) gel buffer with 3 µl of ethidium bromide per 50 ml gel. RNA samples were mixed 10:1 with 10×RNA Loading-buffer, denatured for 5 minutes at 65°C and then run at 5 V/cm in FA Running-buffer.

Generation of cDNA library

RNA isolation of U-2 OS cells was carried out according to RNeasy® Mini Kit Protocol for animal cells (Qiagen). The RNA concentration was measured in RNase-free cuvettes (UVette, Eppendorf) using the BioPhotometer (Eppendorf) and a RNA gel was run to test the RNA quality. cDNA synthesis was performed using the ThermoScript™ Reverse Transcriptase Kit (Invitrogen) with Oligo (dT) primers. The result was controlled by running the DNA gel.

Gene amplification

The coding sequence of human gene of interest was amplified using PCR and the specifically designed primers shown in Table 2.1. Each primer has a sequence of a target and a certain restriction site at their 5' end for direct cloning into desired vector. Primers were designed using Clone Manager Software (Sci-Ed Software) so that tagged fluorescent protein sequence in final vector is in frame with the insert. Synthesis of the primers was done by Eurofins MWG Operon.

Table 2.1 Primers and their annealing temperatures used for gene amplification.

Gene name	Gene bank ID, NM_	Primer name	Primer sequence (restriction sites are underlined)	Product length, bp	Restriction site	Annealing Temp. °C
Ku70	001469	Ku70-fw2	aaccgcggatgtcagggtgggagtcatattac	1845	SacII	60
		Ku70-rv2	aaggatccaagtcctggaagtgcttggtgag		BamHI	
Ku80	021141	Ku80-fw2	aaccgcggatggtgcggtcggggaataag	2214	SacII	60
		Ku80-rv2	aaggatccaatatcatgtccaataaatcgtccacatc		BamHI	
XRCC4	003401	XRCC4-fw	aagagctcatggagagaaaaataagcagaatc	1021	SacI	56
		XRCC4-rv2	aaccgcggaaaaatctcatcaaagaggtcttctg		SacII	
OGG1	002542	OGG1-fw	aagtcgacgaaatgcctgcccgcgcgc	1038	SalI	62
		OGG1-rv	aagcggccgcaagccttccggccctttggaaccctttc		NotI	

Table 2.2 PCR setup.

Component	Amount
10x Accu Prime™ *Pfx* Reaction Mix	5 µl
Primer Mix (10 µM each)	1.5 µl
cDNA template	2 µl
Accu Prime™ *Pfx* DNA Polymerase (2.5 U/µl)	0.5 µl
dH_2O	Up to 50 µl

The sequence of interest was amplified by PCR using the AccuPrime™ *Pfx* DNA Polymerase Kit (Invitrogen) and certain primers. The reaction mix is shown in Table 2.2. Primer annealing temperatures used for PCR reactions in a Thermocycler (Eppendorf) are shown in Table 2.1, and the whole reaction programme is given in Table 2.3.

PCR products were separated on a preparative DNA agarose gel, bands with the correct length were cut out with a scalpel and the DNA was extracted using the QIAquick Gel Extraction Kit (Qiagen) according to manufacturer's instructions. Product concentrations were determined by measuring absorption at 260 nm using a photometer.

Table 2.3 Thermocycler programme for PCR.

Step	Temperature	Time	
Denaturation	95°C	5 minutes	
Denaturation	95°C	30 seconds	35x
Primer Annealing	Individual for each primer	45 seconds	
DNA synthesis	68°C	3 minutes	
Completion of synthesis	68°C	10 minutes	

Plasmid ligation, amplification and isolation

The restriction digestion reaction of amplified products and the target vectors, was performed. Approximately 3-10 µg of each PCR-product and 5-10 µg of the designated target vectors were digested by enzymes given in Table 2.1. The digestion in reaction mix shown in Table 2.4 took place at 37°C for four hours or over night. The reaction was terminated by heating at 65°C for 20 minutes, followed by the preparation of a preparative DNA agarose gel in order to cut out and purify digested product (as described above).

Finally products were ligated into target vectors using the T4 DNA ligase (Invitrogen) at 16°C over night. Amount of digested vector and insert molecules was set to be equal in the ligation reaction mix of 20 µl volume containing T4 DNA ligase and appropriate buffer. Next day the ligation was terminated by heating at 65°C for 10 min and the ligation product was transformed into competent "One shot top 10" *E.coli* cells (Invitrogen). 25 ng of DNA from ligation mix were added to 50 µl of fresh thawed cells and gently mixed. The mixture was kept on ice for 30 minutes, followed by a heat shock in a 42°C water bath for 45 seconds. After keeping the cells on ice for a few more minutes, 250 µl of a warm SOC-medium was added and the cells were incubated at 37°C and constant rotation for one hour to allow the expression of resistance genes. After that, 150 µl of cells were spread on a petri-dish containing 2% agarose/LB, 100 µg/ml kanamycin or ampicillin depending on the used target vector and were grown over night at 37°C. Single growing colonies were transferred in sterile glass-tubes containing 5 ml of LB-medium with kanamycin or ampicillin (100 µg/ml) and incubated at 37°C and constant rotation (225 rpm) over night.

Table 2.4 Setup for restriction reaction.

Component	Amount
10x Reaction buffer (enzyme specific)	3.0 µl
100x BSA	0.3 µl
Enzyme 1	2.0 µl
Enzyme 2	2.0 µl
Nucleic Acid	(dependent on concentration) 10 µg
dH_2O	Up to 30.0 µl

Plasmids from grown *E.coli* cultures were isolated using the QIAprep Spin Miniprep Kit (Qiagen) according to manufacturer's instructions. To verify that the plasmids contain the correct insert, a test digestion was performed by choosing unsymmetrical restriction sites, one located in the insert and one in the original vector. Plasmids whose restriction analysis showed bands with correct length, were sequenced further by MWG Biotech. To obtain bigger amounts of the desired plasmids, after sequencing one clone was chosen and another transformation into "One shot top 10" cells was performed as described above using the

purified plasmids as a transformation agent. Growing colonies were transferred to sterile glass-tubes containing 50 ml of LB-medium/Kanamycin (100 µg/ml) and grown at 37°C and constant rotation (225 rpm) over night. Plasmids were isolated using the QIAgen HiSpeed Plsmid Midi Kit according to manufacturer's instructions.

OGG1 was cloned into pDEST47 plasmid using the Gateway system (Invitrogen) therefore pENTR vector was used as a primary target plasmid. After the confirmation of correct sequence the insert, flanked by attL sites, in pENTR vector was further transferred into pDest-47 vector containing attR sites by the Gateway® LR Clonase (Invitrogen) recombination reaction according to manufacturer's instructions. The principle of Gateway system is shown in Figure 2.1.

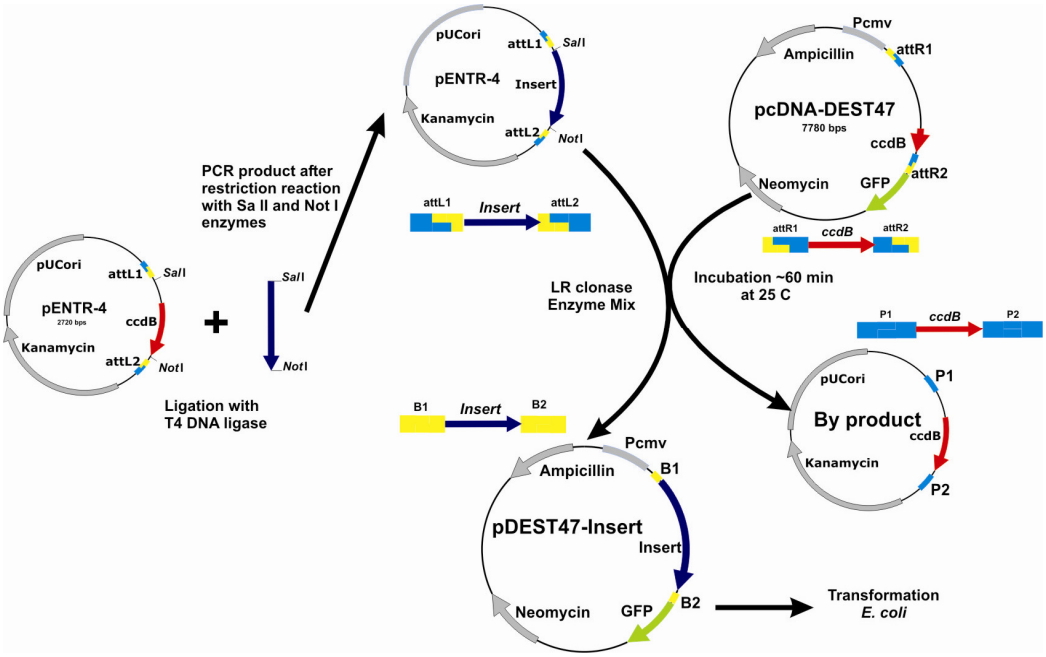

Figure 2.1 Scheme of Gateway cloning system.

2.3. *Transient transfection*

In general, U-2 OS cells were seeded in chambered cover glasses one day prior to transfection and grown over night to be approximately 60% confluent during transfection. Then the appropriate amount of FuGENE 6 was directly pipetted into serum free Optimem 1 Medium without touching the plastic surface of the tube, mixed shortly and incubated for five minutes at room temperature. Subsequently DNA was added, carefully mixed and

incubated for 20 minutes. Afterwards, everything was added directly to the culture medium of the cells and incubated over night under normal culturing conditions. Next day the medium was changed.

2.4. Stable cell line generation

The DNA plasmids coding Ku80-EGFP, XRCC4-EGFP and NBS1-EGFP fusion proteins were stably introduced into the genome of U-2 OS cells in order to have similar expression levels in all cells through many passages. For stable transfection of U-2 OS cells, 10 µg of plasmid vectors containing the respective EGFP-fusion proteins were linearized via enzymatic digestion to ensure an insertion into the cell's genome without disrupting any functional gene within the vector. The digestion was carried out as described in section 2.2, Ase I restriction enzyme was used to linearize all in this work used constructs. Afterwards the linear plasmids were purified using the QIAquick PCR Purification Kit according to manufacturer's instructions. For stable transfection, U-2 OS cells were grown in 6-well plates to a density of 90%. The medium was changed shortly before transfection. 4.0 µg of the linear constructs as well as 10 µl of Lipofectamine 2000 were separately mixed with 250 µl of Optimem 1 medium each and incubated at room temperature for five minutes. Both mixtures were combined and incubated together for 20 minutes, then applied to one well of cells and incubated at normal culturing conditions over night. For selection of transfected clones, cells were trypsinized and each well was transferred to a 5 ml culturing flask containing half the effective concentration of G418 (100 µg/ml). During a period of two weeks, cells were cultured in media containing increasing concentrations of G418 until 1.5 times the effective concentration (300 µg/ml) was reached and the formation of resistant colonies was visible. At this point, cells were seeded at low density in 96-well plates and growing colonies were checked for green fluorescence under the laser-scanning microscope. Cells from positive wells were transferred to 96-well plates to gain individual clones. Clones containing the plasmid thus fluorescing in green were isolated, grown in culture flasks and finally frozen.

2.5. Western Blot analysis

Western blot was used to detect the expression levels of exogenous protein in stable U-2 OS cell lines.

Cell lysate preparation

U-2 OS cell lines expressing the exogenous fusion protein were grown in 6 cm dishes then trypsinized, collected in medium and cell number was counted by using Neubauer cell counting chamber and centrifuged at 1100 g for 5 minutes. After the removal of the medium, the cell pellet was resuspended in the whole cell protein extraction buffer. The volume of added buffer (300 µl) was selected in order to keep the same cell number per ml for all samples. During the resuspension the cell pellet was gently pipetted up and down and than gently shaken on ice for 30 minutes. After sonication (two times, 5 seconds, 30% amplification, Bandelin electronic) the solution was centrifuged at 14000 rpm in a cooled microcentrifuge for 15 minutes. The supernant - whole cell extract was finally aliquoted and frozen.

Protein separation

In order to separate proteins according to their size 10% SDS polyacrylamide gels with a thickness of 1 mm were prepared using the "Mini-PROTEAN 3 Cell" rag-system from Biorad. First, the separating gel was poured and the surface and flattened with buthanol. After gel polymerisation buthanol was removed and the stacking gel solution was added. Before analysis protein extract was mixed 6:1 with SDS-loading buffer containing DTT for 5 min incubation at 95°C and finally placed on the ice for several minutes. Equal amount of proteins were loaded in each pocket. 4 µl of prestained protein standard (PageRuler Prestained Protein Ladder Plus) was also loaded in one empty pocket. The electrophoresis was carried out in SDS-Running-buffer at 120 V for variable time periods depending on the size of the detected protein. After electrophoresis separated proteins were visualized on one of the gels by Coomassie staining with Rotiphorese brilliant blue (Roth) for 20 minutes and subsequently destained over night.

Blotting

For the transfer of the separated proteins from the SDS gel to a nitrocellulose membrane (Hybond-ECL), the membrane was soaked for ten minutes in dH_2O and shortly in Transfer buffer. The same procedure was done for the blotting paper. The SDS gel was removed from the electrophoresis chamber and also shortly covered with transfer buffer. A stack containing blotting paper, membrane, SDS gel and another blotting paper was placed on the semi dry Transfer Cell (Bio-Rad). Transfer was performed at 9 V for 90 minutes.

Protein detection

Proteins on the membrane were temporarily visualized by staining with Ponceau Red (Roth), and destained by dH_2O washing. Further the membrane was blocked with 4% non-fat dried milk in PBST-0.05% for 1 hour at room temperature and washed in PBST-0.05% for 10 minutes. The primary antibody (Table 2.5) was diluted in 2 ml of PBST-0.05%, BSA 2% and applied to the membrane with constant shaking at 4°C over night. Next day the membrane was washed three times with PBST-0.1% for 10 minutes each. Then it was incubated with 10 ml of the HRP-labelled secondary antibody (1:10000 in 4% non-fat dried milk in PBS) at room temperature for one hour. Subsequently the membrane was washed with PBST-0.01%, PBST-0.05% and PBS for ten minutes each. Finally the membrane was covered with ECL (Pierce) or ECL-Plus (Amersham) solution for one to three minutes depending on the strength of the signal. The ECL was removed and the membrane was exposed to a sheet of Hyperfilm ECL for one up to 60 minutes under safelight illumination conditions. Afterward the film was developed using the Classic E.O.S. processor (AGFA).

Table 2.5 Antibodies used for Western Blot analysis.

Antigene	Species and clonality	Dilution
Ku80	mouse monoclonal	1:1000
XRCC4	mouse polyclonal	1:1000
NBS1	rabbit polyclonal	1:1000
Alpha-Tubulin	mouse monoclonal	1:1000

2.6. Immunohistochemistry

For visualisation of endogenous and also exogenous fusion proteins in the cell nucleus the Immunohistochemistry was used. Medium was removed and the cells were shortly washed with PBS and then fixed in 3.7% formaldehyde, 0.1% Triton X-100 in PBS for 20 minutes at room temperature. After wash in PBS for 5 minutes the cells were permeabilized in 0.7% Triton X-100 in PBS for 15 minutes at room temperature and washed again as above. The cells were incubated in 7% BSA in PBS plus primary antibody at 4°C overnight. The primary antibodies used in this study are shown in Table 2.6. After the incubation with

primary antibody the slides were washed in PBS, PBST-0.05% and again in PBS for 10 min each at room temperature. Finally for indirect immunochemical detection the secondary antibodies were used: donkey anti-mouse conjugated with Alexa488 or Alexa594 and anti-rabbit conjugated with Alexa488, Alexa555 and Alexa594, at 1:400 dilution (Molecular Probes). Secondary antibodies were diluted in PBS with 7% BSA and incubated on the slides for 1 hour at room temperature. After washing as described above the specimens were covered with ProLong Gold antifade reagent containing DAPI and sealed with a coverslip.

Table 2.6 Antibodies used for immunohistochemistry.

Antigene	Species and clonality	Dilution
γ-H2AX	mouse monoclonal	1:400
Ku80	mouse monoclonal	1:200
XRCC4	mouse polyclonal	1:400
NBS1	rabbit polyclonal	1:200
Rad51	rabbit polyclonal	1:200
53BP1	rabbit polyclonal	1:400
DNA-PKcs (phospho Ser2056)	rabbit polyclonal	1:400
DNA-PKcs (phospho Ser2609)	mouse polyclonal	1:400
Cyclobutane pyrimidine dimers	mouse monoclonal	1:400
OGG1	mouse monoclonal	1:200
Histone H1	mouse monoclonal	1:50

2.7. Immunofluorescent Comet-assay (IFCA)

General procedure of neutral and alkaline Comet-assays

The Comet-assay was performed immediately after the DNA damage was induced to avoid DNA repair. The principle scheme of Comet-assay procedure is shown in Figure 2.2.

Embedding of the cells for alkaline and neutral versions of Comet-assay was performed in the same way as described below.

Slide preparation

Two types of slides were used in this work: fully frosted and partially frosted with two clear windows. For both of them the ground agarose layer was added in order to strengthen the binding of later agarose layers with cells. For that reason 100 µl of melted 1% agarose type II in PBS were applied to the slides, spread into a very thin ground layer and air dried. Slides with two windows could be further proceeded for cell embedding, while fully frosted slides need a thick middle layer in order to reduce the amount of light appearing due to the scattering by frosted glass. For this, 400 µl of the same agarose-solution was applied to a ground-layered slide, covered with a glass coverslip and immediately polymerized on a cold metal plate (4°C) to form the middle layer.

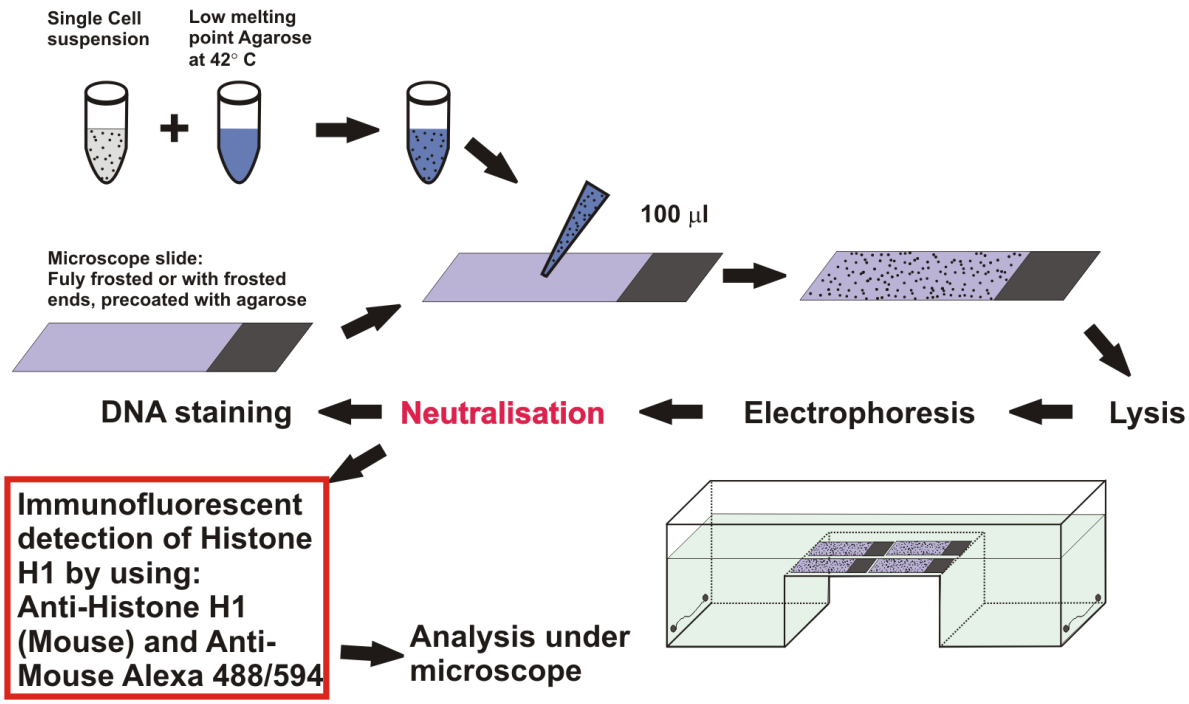

Figure 2.2 Scheme for comet assay procedure. Red box shows the step done only in IFCA. In red text the step of neutralisation is shown, which is necessary only for Alkaline Comet-assay. Washing steps are skipped.

Cell embedding on slides

Cells were washed with PBS, trypsinized and suspended in medium with FCS to block the trypsin activity, afterwards cells were centrifuged for 10 min at 2000 g. After removal of medium the cells were resuspended in PBS thereby setting the concentration of cells to ~10^5 cells per ml or less and incubated at 41°C in a water bath for several minutes. Then cells in PBS were mixed with 1% low melting point agarose (Type VII) in PBS. 100 µl of the cell suspension in 0.8% agarose were added on the prewarmed slides with middle layer and sealed with cover slip. Polymerisation was performed by putting slides on the cold (4°C) metal plate for several minutes. Afterwards, slides were lysed depending on the Comet-assay version used.

Alkaline Comet-assay

Slides were incubated in alkaline lysis buffer for 60 min at 4° C. Subsequently they were placed in electrophoresis buffer pH>13 for 25 min in order to unwind the DNA, and electrophoresed at 1 V/cm for 25 min or 2 hours in the same buffer, after electrophoresis slides were neutralised in Tris buffer (pH7.5) for 5 min.

Neutral Comet-assay.

Slides for the neutral Comet-assay were incubated in neutral lysis buffer at room temperature for 40 min, then incubated for 10 min in 1xTBE buffer and electrophoresed in 1xTBE buffer at 1V/cm for the times indicated in the results section.

Enzymatic induction of DNA fragmentation

For generation of defined numbers of SSBs and DSBs the nicking and restriction endonuleases Nt.BbvCI and BbvCI (New England Lab) were used respectively. Both enzymes recognize the sequence 5´-CCTCAGC, but induce either a SSB (nick) (Nt.BbvCI) or a DSB (BbvCI). Untreated HeLa cells were embedded in microgels, lysed in neutral lysis buffer as described above and subsequently washed in TE buffer for 10 min, then two times for 15 min in 1× restriction reaction buffer. Then, 15 units of the enzyme diluted in 100 µl of the 1× restriction reaction buffer were added to the slides. One unit is the amount of Nt.BbvCI enzyme required to convert 1 µg of supercoiled plasmid DNA to open circular form in 1 hour at 37°C in a total reaction volume of 50 µl. When for BbvCI one unit is defined as the amount of enzyme required to digest 1 µg of λ DNA at the same conditions. The slides were covered with a plastic cover slip and incubated at 37° C in humid chamber

for 3 hours, washed with PBS for 15 min, incubated in 1×TBE and electrophoresed as described above.

Immunofluorescent Comet-assay (IFCA)

As shown in Figure 2.2 slides of both Comet-assay versions after single cell gel electrophoresis were washed in PBS, followed by the addition of mouse monoclonal anti-Histone H1 antibody (AE-4, SantaCruz) diluted 1:50 in 60 µl of PBS with 7% BSA and sealed with a plastic coverslip. Incubation was performed in a humid chamber overnight. Next day the slides were washed in PBS, PBST-0.05% and PBS for 15 min each and incubated with secondary donkey anti-mouse antibody conjugated with Alexa 488 or Alexa 594 fluorescent dyes (dilution 1:400 in PBS with 7% BSA). After 1.5 hours of incubation the slides were washed again as described above and mounted in DAPI/antifade (1 µg/ml DAPI, 100 mM DABCO, 45% glycerol, 10 mM Tris-HCl (pH 8.0) or for colocalization experiments slides were embedded in SYBR Green solution with antifade and finally sealed with a glass coverslip.

Lambda DNA (48.5 kbp) and low range PFGE (2-200 kbp) marker migration in neutral Comet-assay

Frosted slides with two windows (Erie Scientific Company) were covered with 400 µl of 0.8% low melting point agarose in PBS, sealed with cover slip and cooled down. After 10 min of incubation in an electrophoresis tank with 1xTBE buffer the, 25µg/ml Lambda DNA (New England Lab) diluted in PBS was added by the following. With the top of the 10 µl tip a small pocket was formed in agarose layer (as shown in Figure 3.5 G) and ~0.2 µl of 1:1 lambda DNA and DNA loading dye mixture was loaded. After 25 min of electrophoresis, 30 µl of antifade solution containing YOYO1 or SYBR Green was added to the slides and sealed with a cover slip. A slightly different procedure was done for electrophoresing the low range PFGE marker purchased from New England Lab. The marker DNA is delivered in 1% agarose, thus it was cut into small pieces with diameter of ~500 µm. These pieces were attached to the frosted slide with two windows and covered with 400 µl of 0.8 % low melting point agarose in PBS. Consequently the slides were covered with a cover glass and cooled down. Further processing was done as described above.

Sequence analysis

In silico restriction fragmentation analysis for fragmentation of the whole human genome by cutting BbvCI enzyme was done by using Clone manager (for sequence manipulation and analysis) and OriginPro (for data analysis and graphical representation) software.

In silico calculation for the number of potential DSBs arising due to closely induced SSBs by the nicking Nt.BbvCI enzyme was done only for the human chromosome 6. Sequences of all human chromosomes were obtained from the website of National Centre for Biotechnology Information (NCBI, http://www.ncbi.nlm.nih.gov/).

2.8. *Damage induction and quantitative calculation of used photons, doses and molecule number by ionizing radiation, UV-A laser-microbeam irradiation and bleomycin treatment*

For the following calculations of applied doses and photon numbers of different treatments the assumption was done that the size of a HeLa cell nucleus is $10\times10\times3$ μm^3 and it has the volume of 300 μm^3 or 300 fl. The weight of such cell nucleus is 300 pg (assuming a density of 1 g/ml).

Ionizing radiation:

Gamma irradiation was performed using a Gammacell GC40 with ^{137}Cs (Nordion). Doses were defined via the time of exposure (dose rate: 1.17 Gy/min) of the gamma source. Since 1 Gray strictly is a dose absorbed by the tissue, and not the dose emitted by the gamma source, one has to assume that the biological material absorbs the ionizing radiation like water. This assumption is in agreement with medical literature.

The ionizing irradiation dose is defined as the absorbed energy per 1 kg of biological tissue, thus 1 Gy = 1J/kg = 10^{-3} J/g. In this case one cell nucleus will absorb 0.3 pJ (10^{-3} J/g x 300×10^{-12} g = 300×10^{-15} J = 0.3 pJ). This energy is an equivalent for (0.3×10^{-12} J) /(1.6×10^{-19} J/eV) = 1.5×10^{6} eV. One gamma photon of ^{137}Cs has an energy of 662 keV. Thus, one single cell nucleus formally absorbs the whole energy of (1.55×10^{6} eV)/(662 000 eV) = 2.3 gamma photons. However a 3 µm thick nucleus is not able to absorb the whole energy of the one photon because the linear energy transfer (LET) of gamma photons is 0.8 keV/µm. Thus, 625 gamma photons with 0.8 keV LET are needed in order to apply 1 Gy irradiation dose on one single nucleus.

Laser-microbeam:

Laser microirradiation was performed by a pulsed UV-A laser-microbeam (frequency tripled Nd:YLF laser generating ~20 ns pulses at 349 nm from Spectra Physics) coupled via the epifluorescence illumination path into a confocal laser scanning microscope (LSM 510, Zeiss).

The pulse energy used to irradiate the single cell nucleus was about 10 µJ in the optical plane of sample. In the following the absorbed dose will be converted into an equivalent for ionizing radiation (J/kg) and will find out how many photons this irradiation does need for induction of double strand breaks. The penetration depth of such wavelength in biological tissue is around 60 µm (Greulich, 1999). By using the Lambert- Beer law the pulse in the depth of 3 µm will have the energy $I_{3\mu m} = I_0 e^{-dl}$: $I_{3\mu m} = I_0\ e^{-3/60} = 0.95\ I_0$ from here the absorbed energy is $I_A = 0.05\ I_0 = 0.5$ µJ or 3.13×10^{12} eV. A single photon at 349 nm has an energy of 3.5 eV thus the cell nucleus absorbs around 1×10^{12} photons. Note that in the case of laser-microbeam the energy is absorbed locally only in the irradiated region with a volume of 3 μm^3 (for a 3µm thick nucleus) or 3 pg. From these numbers one can calculate the absorbed energy per mass unit: $(0.5\times10^{6}$ J$)/3\times10^{-12}$ g $= 0.5/3\times10^{-6}$ J/g $= 0.17\times10^{9}$ J/kg. This is a dimension of Gy that is usually used only for ionising radiation.

Bleomycin:

For chemical damage with bleomycin (BLM), BLM was added to the medium to a final concentration of 12 µg/ml. The cells were then incubated at standard conditions for 30 min.

The molecular weight of bleomycin is 1415 g/mol. Thus the molarity in the cell nucleus is 8.5 µM, if one assumes that bleomycin is equally distributed in the solution and the cell, this represent 5.12×10^{18} molecules in 1 litre. With a volume of the cell nucleus of 300 fl the number of bleomycin molecules in the single cell nucleus will be (5.12×10^{18} molecules/l) × (0.3×10^{-12} l) = 1.5×10^{6} moleculess. All important parameters of different treatments are summarised in Table 3.1 in 3.3.3 section.

2.9. DNA damaging by laser irradiation

No sensitisation was used for all laser irradiation experiments.

2.9.1. Optical setup for irradiation at 420-455 nm

For highly localized irradiation of the living cells in a broad range of the spectrum a tunable femtosecond Ti:Sa laser system was used (Figure 2.3). Fundamental (700-930 nm), frequency doubled (350-465 nm) and frequency tripled (250-310 nm) radiation of a Ti:Sa laser (Tsunami, Spectra Physics) were coupled into an Axiovert 135M microscope (Carl Zeiss) via the epifluorescence illumination path as shown in Figure 2.3. In Table 2.7 properties of used beamsplitters are shown.

Table 2.7 Beamsplitters used for combining the fundamental, second and third harmonics of Ti:Sa laser.

	Reflection (HR)	Transmision (T)
1	250-340 nm	350-550
2	250-550	600-1000
3	650-1000	
4	450-600	330-450

In order to investigate DNA damaging by different doses of laser light, pulse frequencies from 0.4 kHz to 4 MHz where changed by a pulse picker (Spectra Physics). Laser microbeam was focused into the middle of the field of view by using a 100X, NA 1.3 Plan Neofluar oil immersion objective (Zeiss). Cells in a 400 μm × 500 μm area were irradiated by moving the motorised x,y table, which was driven by an MCU 26 controller (Zeiss) at slowest available speed – 294 μm/s. At the lowest frequency (0.4 kHz) ~1.3 pulse per 1 μm hits the cell nucleus where in contrast at 800 kHz ~2600 pulses per μm hit the cell in irradiated region. Energies from 375 pJ to 7.5 pJ per ~200 fs pulse were used in order to investigate the pulse energy influence on DNA damage. Following the irradiation, which took usually around 10 min per plate (μ-Dish, Ibidi), the cells were incubated at normal growing conditions for one hour, then washed with PBS and fixed for immunofluorescence.

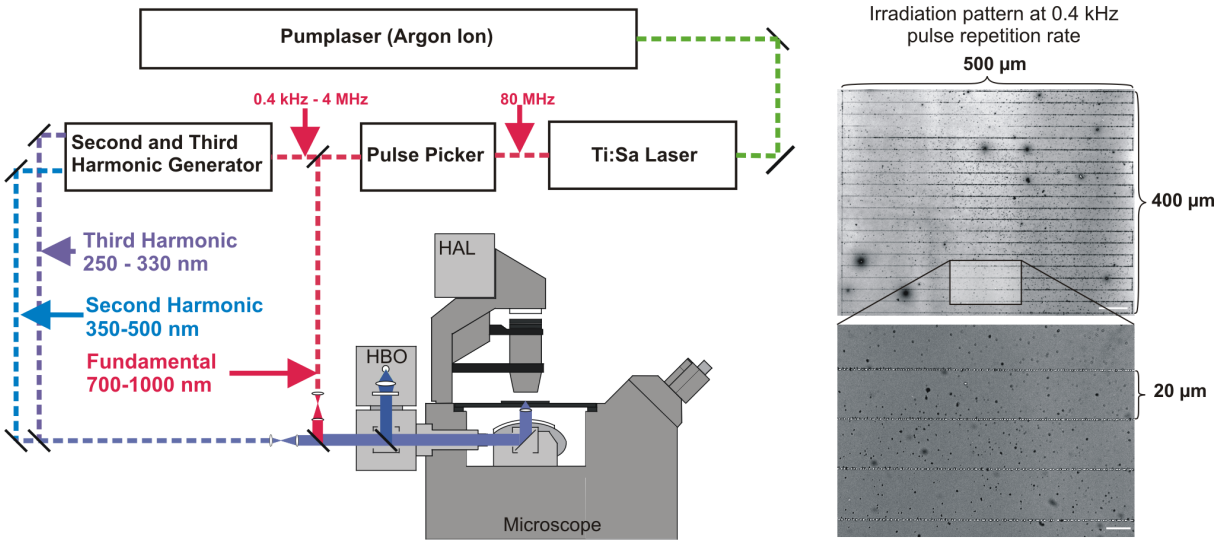

Figure 2.3 Optical setup for DNA damage induction at 420-455 nm with second harmonic of the fundamental Ti:Sa laser radiation. Left panel shows the irradiation pattern performed by using the motorised xy table. Scale bar – 10 µm.

2.9.2. Optical setup for irradiation at 350 nm during live cell imaging

For laser damage induction the pulsed UV-A laser was coupled into confocal laser scanning microscope (LSM 510) via epifluorescence illumination path (Figure 2.4 A). Laser-microbeam was focused into the middle of the field of view by a 100X, NA 1.3 Plan Neofluar oil immersion objective (Zeiss). UV-A laser is a frequency tripled Nd:YLF laser (Spectra Physics) delivering 20 ns duration pulses at 350 nm with user defined energies from 1 µJ to 200 µJ at user defined repetition rates 1 Hz - 1000 Hz. Before entering the microscope laser pulse energy was reduced around 80% with the gradient position dependent attenuator (Laseroptik) (Figure 2.4).

The cells for immunofluorescent staining were irradiated in a 500 µm × 535 µm area by moving the motorised x,y table, which was driven by an MCU 26 controller (Zeiss) at 1470 µm/s speed. For every experiment 350 Hz repetition rate with different pulse energies from 2 - 6 µJ was used. By selected irradiation options around 100 cells were irradiated in 25 seconds with single pulses hitting cell nucleus every 4 µm (Figure 2.4 B). For one kinetic measurement 8 quadrangulars were irradiated at different times during 1 hour (under optimal growing conditions described below) and finally fixed immediately after last

irradiation (Figure 2.4 C). The time points were determined by the time difference between finishing the irradiation of one quadrangular and start of the fixation.

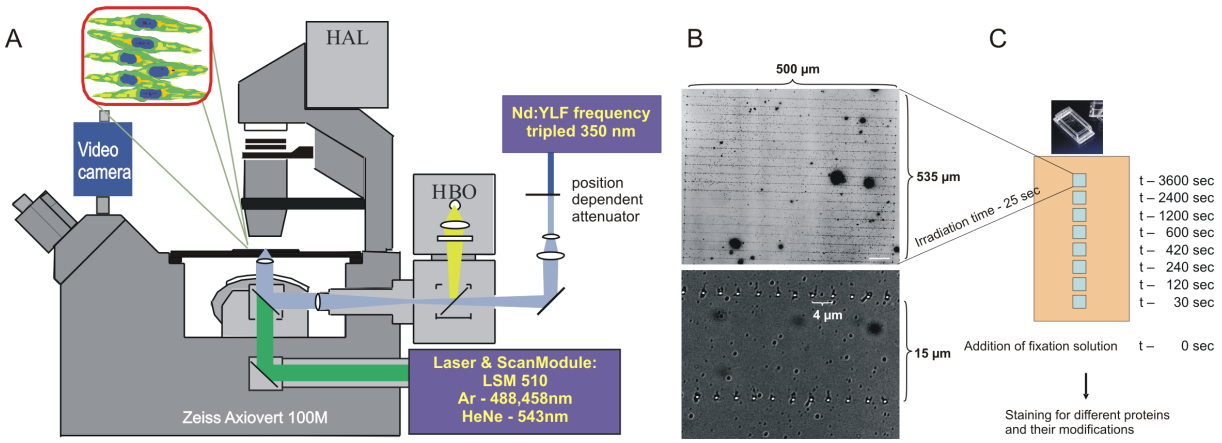

Figure 2.4 A - Optical setup for DNA damage induction at 350 nm for measuring the recruitment kinetics of different DNA repair proteins. B - the irradiation pattern performed by using the motorised xy table, used for immunofluorescent detection of endogenous proteins. C – Irradiation of cells at 8 different times for one measurement of endogenous protein recruitment kinetic.

For live cell imaging 1 Hz repetition rate was used. Subsequently one single pulse was passed through to hit the cell nucleus at 10 seconds after the start of image acquisition. To provide optimal growing conditions for the living cells, an incubation chamber was constantly supplied with a 5% CO_2, 37ºC atmosphere by a tempcontrol 37-2 digital (Zeiss) and a CTI-Controller 3700 digital (Zeiss). The temperature of the objective was additionally kept at 37ºC by a tempcontrol mini device (Zeiss).

2.10. Microscopy and image analysis

2.10.1. Live cell imaging

Confocal imaging of living cells was done using a Zeiss laser scanning microscope (LSM 510) equipped with 100X, NA 1.3 Plan Neofluar oil immersion objective, a HeNe and an Argon ion lasers and emission filter sets for the detection of FITC signals (BP530/20) as well as for Rhodamine signals (LP 580, LP 625). Scanning was controlled by the Zeiss LSM software version 3.2 and individual colour channels were recorded subsequently to

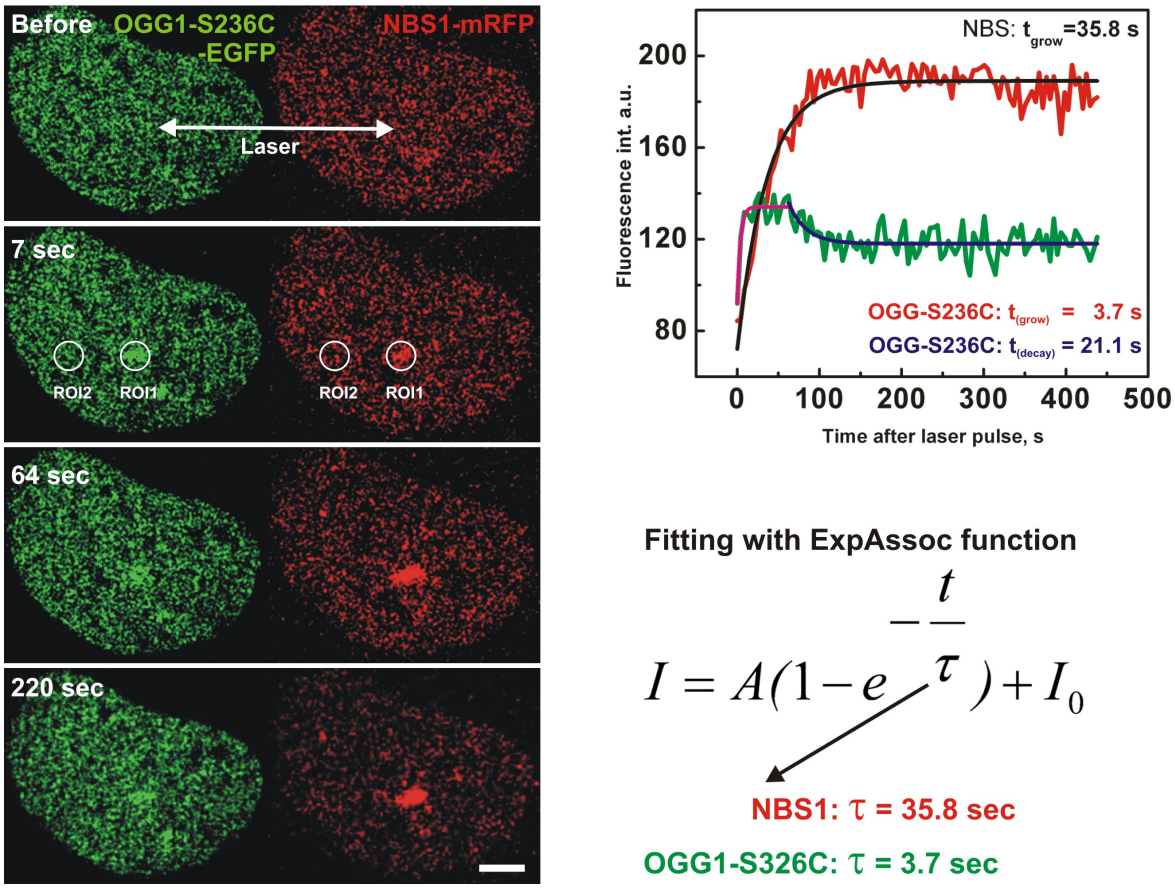

Figure 2.5 Example of recruitment kinetic measurement by using live cell imaging of OGG1-S326C-EGFP and NBS1-mRFP expressed in the same cell nucleus (human U-2 OS cells) after laser irradiation. ROI1 - region of interest at irradiated site, ROI2 – background. Scale bar – 5 µm. The left panel shows intensity changes at irradiated sites after background subtraction during observation time. Green represents OGG1-S326C, a DNA repair protein with fast recruitments kinetics, red shows NBS1, which is an order of magnitude slower. Time constants of recruitment kinetics are calculated from the fit with exponential association function as shown in the right part of the figure.

minimize cross talk. The time course of irradiated cells was recorded via time series of the LSM software. Fluorescence intensity changes in not irradiated region of the cell nucleus were subtracted from fluorescence intensity changes in damaged region for photobleaching correction due to repetitive imaging. Obtained curves were normalized to maximum. An average values and standard deviations for intensity changes were calculated from more than ten cells for every single condition (different pulse energies), if not stated otherwise in the text. The average curves were fitted by first order of exponential associate function (Figure 2.5) using instrumental weightening with a least-squares method. All mathematical procedures were performed by the OriginPro 7.0 software (OriginLab).

2.10.2. Immunofluorescence

Confocal imaging of fixed samples was performed using a microscope with structured illumination. The Apotome (Zeiss) unit is mounted in the epifluorescence illumination path of an inverted Axiovert 200 (Zeiss). Filtersets for DAPI (Zeiss No 49), FITC (Zeiss No 38 HE), Cy3 (Zeiss No 43 HE) were used. The camera (Zeiss, MRM Axiocam) as well as the structured illumination were controlled by the Axiovision software (Zeiss). For full information of the focus fluorescence intensity Z stacks containing 14 optical layers every 250 nm were recorded by using Plan-Apochromat 63x NA 1.4 oil DIC objective (Zeiss). Exposition time was set to obtain not overexposed signals for foci with the highest signal intensity. In order to be able to compare the signal intensities, exposure time was kept constant during image acquisition of one independent experiment. For each time point 3 or 4 Z-stacks were recorded. Further, 3D images were imported into ImageJ software (Abramoff et al., 2004) where the same threshold was set for all Z stacks from one experiment and finally the volume and overall intensity of every single focus was measured by using Sync 3D Measure plug in. Average focus intensity was calculated by dividing the total focus intensity by its volume. The mean of average focus intensity was obtained from around 100 – 300 foci for each time point by using the OriginPro software. For average focus intensity at time 0 sec the threshold value was taken. Normalization to maximum and curve fitting with the first order of exponential association or exponential decay functions were done as described above by using the OriginPro 7.0 software.

Images of Immunofluorescent Comet-assay samples were taken by using the the same Apotome (Zeiss) set up described above. Additional air objectives EC-Plan-Neofluar 10x NA 0.3 and Plan-Apochromat 20x NA 0.8 were used without structured illumination to record comets. Macro imaging of an ~1 cm^2 area was imaged using a Zeiss laser scanning microscope (LSM510) equipped with a HeNe and an Argon ion lasers, 10x NA 0.3 and 20x NA 0.8 Plan-Neofluar objectives and emission filter set for the detection of FITC signals (BP530/20).

3. Results

3.1. Laser induce damage with high spatial resolution

Coherent laser light can be highly focused in three dimensions to a submicrometer range. According to theoretical calculations, a laser at 750 nm can affect an ellipsoidal volume with a diameter of 667 nm and 2400 nm height, if 10% of the lasers maximum intensity is used as a cut off and one photon absorption is assumed (Meldrum et al., 2003). This affected volume can be reduced if two or three photon absorption is used: diameter – 472 nm and height 1.2 µm for two-photon and 385 nm and 847 nm respectively for three-photon effects (Meldrum et al., 2003). This allows very precise damage induction in desired regions of the cell nucleus not only in the xy-plane but also along the z axis.

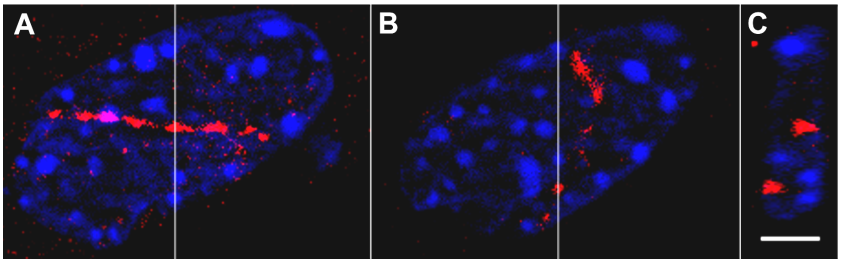

Figure 3.1 Induction of cyclobutane pyrimidine dimers (red) by a laser microbeam at 420 nm in 3T3 cell nucleus stained with DAPI (blue); big rounded structures in blue channel are heterochromatin blobs, typical for mouse cells. A and B show two optical sections of the same cell nucleus in a distance of 2.7 µm. C – cut view in the middle (shown by semi transparent lines in A and B) of the 3D reconstruction of the same nucleus. Scale bar – 5 µm.

An example is shown in Figure 3.1 where a NIH 3T3 mouse fibroblast cell nucleus was irradiated with laser light at 420 nm in two different focal planes. It is shown that laser-microbeam irradiation at this wavelength, can induce double strand breaks and also cyclobutane pyrimidine dimers (CPD). Normaly, CPD's are induced by UV-C light due to direct absorption by DNA molecules, which absorb light between 240-270 nm. In these experiments the light at 420 nm was used, which is far away from the absorbance spectrum of DNA. Thus, those highly localized CPD's are the result of two photon absorption of the 420 nm light.

Two perpendicular laser irradiation tracks are visualised by immunofluorescence staining of CPD (red color) in Figure 3.1. Since irradiation was performed in different focal planes of the same cell nucleus respectively, induced CPD's are lying in different optical sections in a 2.7 µm distance from each other (Figure 3.1 A and B). Immunofluorescence staining shows that CPD's are induced only in the laser focus where highest power density is found, but not above or below irradiated regions (Figure 3.1 C) where the laser beam power density is substantially diminished as compared to the focus. By variation of the dose and laser pulse energy, DNA damage in even smaller volumes can be achieved.

3.2. DNA damage dependency on irradiation quality

3.2.1. Different levels of DNA damage detected by γ-H2AX staining

Parameters such as dose and pulse energy of the laser-microbeam can be tuned in a very broad range. Thus, in order to perform DNA repair studies after laser irradiation, it is very important to know which effects of DNA damage can be caused by variation of different laser beam parameters. Furthermore, this question needs to be clarified as more and more different lasers are used in medicine for diagnosis and therapy.

In this section is shown that DNA double strand breaks can be induced also by blue laser light from 420 to 460 nm without an external sensitizer using doses above 10^3 J/m^2. Depending on pulse energy and irradiation dose, the morphological pattern of the immuno-stained H2AX phosphorylation can be classified into 6 categories as shown in Figure 3.2. All the immunofluorescent data were recorded after irradiation at two different wavelengths (420 nm and 455 nm) by changing dose and pulse energy in orders of magnitude: dose from 10^6 J/m^2 (1300 pulse/µm) to 10^3 J/m^2 (1.3 pulse/µm) and pulse energy from 375 pJ to 7.5 pJ per pulse.

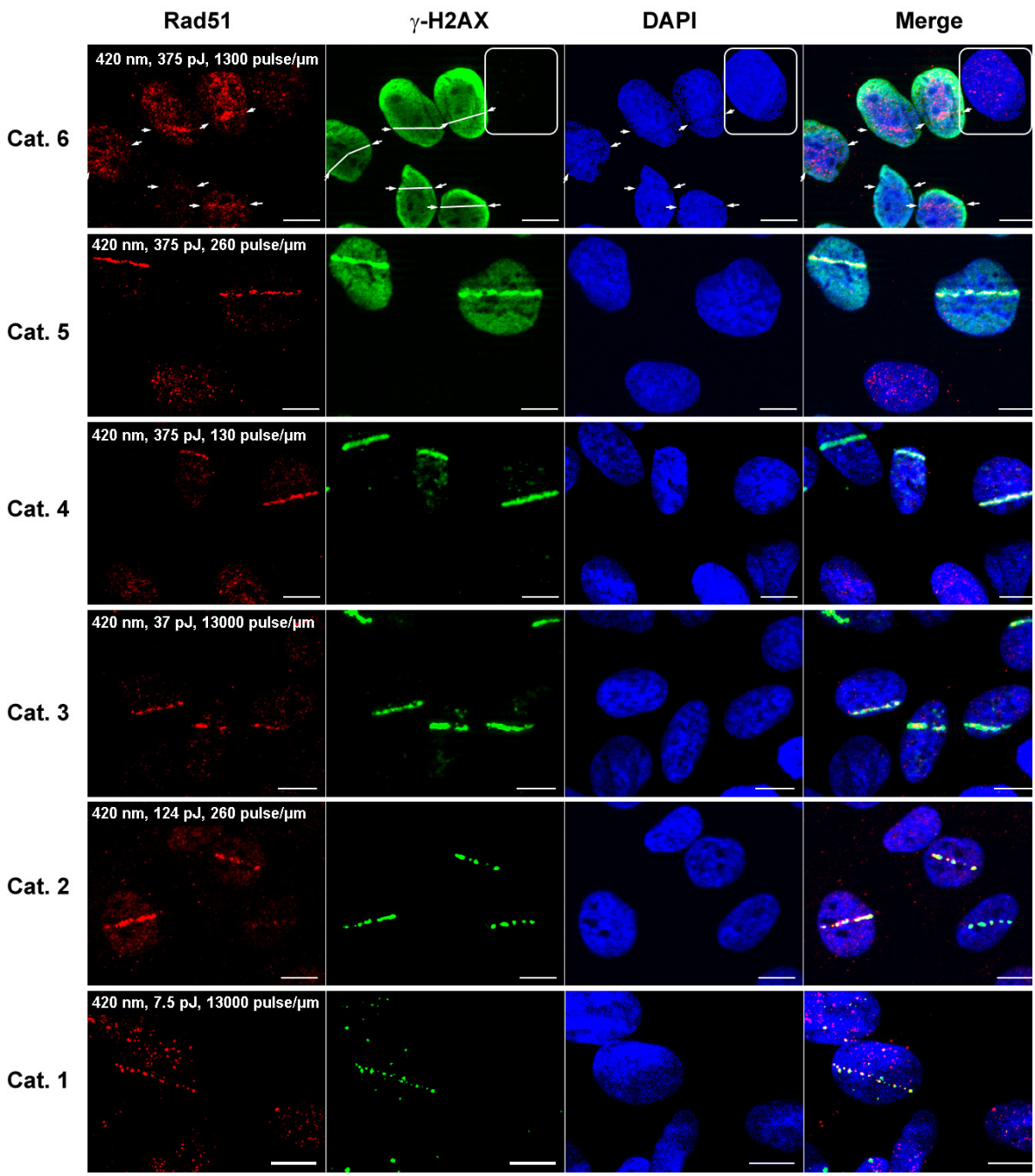

Figure 3.2 Six typical patterns of double strand breaks (γ-H2AX) one hour after induction by laser-microbeam (420 nm) with different pulse energies at different repetition rates (dose) from highest damaging level Cat.6 to the lowest Cat.1. Scale bar - 10 µm, in all figures exposure time was optimized for every single picture.

Irradiation with high dose at 420 nm (375 pJ pulses at 400 kHz ~ 1300 pulse/µm, 10^6 J/m^2) induces very intense homogeneous H2AX phosphorylation (green) in the whole cell nucleus (marked with DAPI (blue)) (Figure 3.2, Cat.6) with no or very weak Rad51 foci (Red). Even in irradiated regions, compared to the other parts of the cell nucleus, the green

fluorescence intensity is equal or even reduced. Note that one cell in Figure 3.2, Cat.6 marked with a frame has no γ-H2AX signal, although is located just few micrometers from the irradiated cell.

Additionally, DNA staining in laser track is reduced (arrows in the DAPI channel). Those facts indicate that laser-microbeam irradiation at high dose causes massive local damage of the nuclear structure. At a dose 5 times lower, such nuclear disruption is not detected anymore. However, the homogenous γ-H2AX signal is still seen in the whole cell nucleus, in this case with more intense signal in the laser track, which does colocalize with Rad51 foci (Figure 3.2 Cat.5).

The level of double strand breaks or H2AX phosphorylation around the laser track in category 4 is still higher than that of the not irradiated cells and became almost similar to that in category 3. If the dose or pulse energy of the laser beam is reduced (7.5 pJ, 13000 pulse/μm; 124 pJ, 260 pulse/μm), the H2AX phosphorylation signal in the irradiated area (tracks) becomes more inhomogeneous (Cat. 1 and 2), although hundreds or thousands of laser pulses pass each micrometer of the laser track in cell nucleus. Some empty spaces occur due to nucleoli, but even outside the nucleoli γ-H2AX signal is distributed non-homogeneously. This issue will be addressed in section 3.5. At lower doses the distinquishable γ-H2AX signal is no longer detected.

3.2.2. Pulse energy and dose dependent DNA damage induction

Irradiation dose variation by changing pulse repetition rate and thus the number of pulses hitting each volume of chromatin was found to induce different levels of double strand breaks, which were empirically evaluated by the morphology of phosphorylated H2AX foci. Also crucial changes were found to be induced by different laser pulse energies. Figure 3.3 A shows typical γ-H2AX pattern after irradiation with 375 pJ pulses at 80 kHz repetition rate.

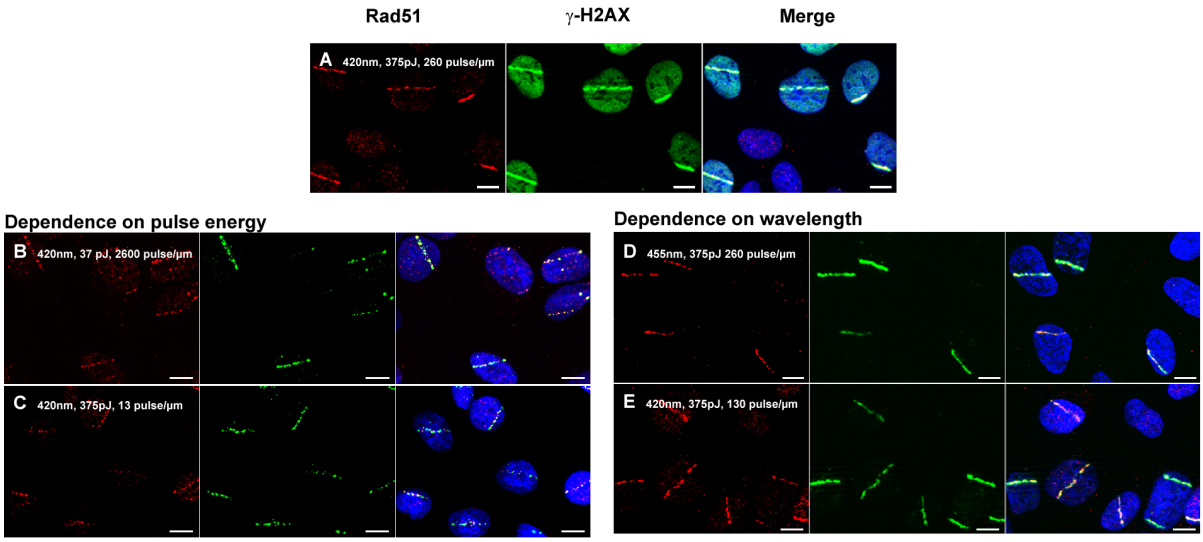

Figure 3.3 Comparison of double strand break patterns 1 hour after induction by different pulse energies (A,B,C) and wavelengths (A,D,E) . Figures A and B show differences in DSB patterns after the same overall dose but ten times lower pulse energies. The same pattern as in B can only be achieved if dose is reduced approximately 20 times using 375 pJ pulse energy (Figure C). Figures A and D show differences in DSB pattern after irradiation at two different wavelengths 420 (A) and 455 nm (D), respectively, but the same dose. In order to get the same pattern as it is presented in D the dose of the 420 nm microbeam should be reduced two times (figure E). Scale bar -10 µm. Exposure time was optimized for every single picture.

A completely different result is obtained, when the cells are irradiated with ten times lower pulse energy (37 pJ) at ten fold repetition rate, i.e. same total energy (Figure 3.3 B). DNA damage is much lower after irradiation with reduced pulse energy although the dose was kept the same. Similar morphology at high pulse energy (375 pJ) is detected only if the total energy is reduced 20 times, as shown in Figure 3.3 C. This example clearly visualizes that the level of induced DNA damage highly depends not only on the dose but even stronger on the peak power density of the pulse.

3.2.3. Wavelength dependent DNA damage induction

Above it is shown how DNA damage is dependent on two laser-microbeam parameters, dose and pulse energy. However, still there is another very important parameter left, the wavelength. Various biomolecules, dependent on their chemical structure, absorb light photons of different wavelengths. DNA itself absorbs photons up to ~280 nm with an absorption maximum at 260 nm. Therefore, ultraviolet light under 280 nm might induce

direct DNA damage, usually due to direct absorption and photochemical reaction. However, the cell contains molecules which absorb not only UV-B, or -C but also UV-A and visible light. To those belong flavins, porphyrins, and other molecules, which are very good sensitizers and can be excited even by two or three photon absorption of near infrared light (700-900 nm).

In order to find out how double strand break induction depends on the wavelength, the comparison of γ-H2AX foci morphology after irradiation at 420 and 455 nm was performed. Already a small shift (35 nm) into the red region of the spectrum caused less damage when all other microbeam parameters were kept the same (Figure 3.3 A and D). Irradiation at 420 nm with 260 pulses per μm each of 375 pJ energy cause high level of DNA damage - γ-H2AX phosphorylation all over the whole cell nucleus with a more intense signal in the irradiated region. In contrast, irradiation with the same pulse energy and dose, but with the wavelength shifted to the red about 35 nm, induced DSBs only in the laser track. No increased level of the signal was detected in other parts of the nucleus. A similar damage pattern is observed after irradiation at 420 nm only if the total dose is reduced at least 2 times (130 pulses/μm) (Figure 3.3). Even though it looks as if damage is still a bit higher than in Figure 3.3 D but in this case one can say that in order to induce the same level of DNA double strand breaks at 455 nm at least two times higher dose than at 420 nm is needed.

3.3. Immunofluorescent Comet-assay – a novel staining method of CA for comparison of DNA fragmentation levels in single cells

In the previous sections laser induced damage was visualised by γ-H2AX antibody, which is widely accepted as a marker for DSBs (Rogakou et al., 1998). However, whether it labels exclusively DSBs is still under discussion. Therefore, a novel variation of neutral Comet-assay - Immunofluorescent Comet-assay (IFCA) was used to analyse DNA fragmentation. This method serves not only for high resolution visualisation of fragments, but also helps to get more detailed insight into mechanism of neutral Comet-assay.

3.3.1. IFCA versus conventional SYBR Green staining

It is widely accepted that histone H1 is a protein strongly binding to DNA. In this section is shown that it can be detected by immunofluorescence even after lysis and electrophoresis in the neutral Comet-assay. The possibility to use antibody staining of histone H1 enables the

visualization of neutral comets with higher resolution or more details than after the conventional DNA staining with SYBR Green.

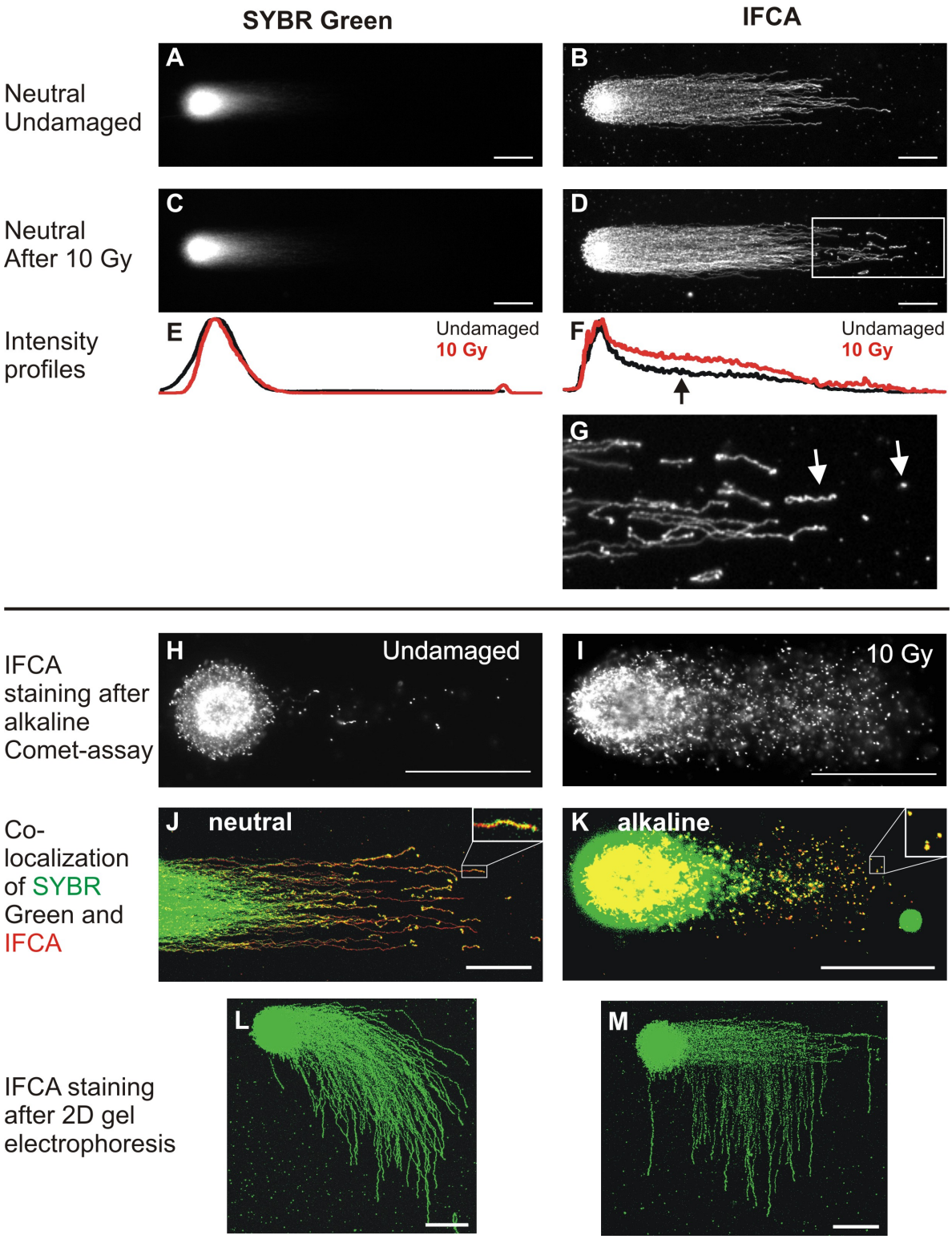

Figure 3.4 Direct comparison of IFCA and SYBR Green staining for neutral Comet-assay. A and C - SYBR Green staining of the untreated cells (A) and cells after 10 Gy irradiation (C), intensity profiles of the same cells are shown in panel E. B and D - IFCA staining of neutral Comet-assay of the untreated (B) and with 10 Gy irradiated cells (D), F represents intensity profiles. G - magnification of comet tail in D showing small dot like and fibre like fragments marked with arrows. H and I - IFCA staining after alkaline Comet-assay H - untreated and I - irradiated with 10 Gy cells. J and K - colocalization of SYBR Green (green) and Histone H1 (red) signals. IFCA signal colocolizes with SYBR Green in neutral J and alkaline K comets. L and M – Projections of Z-Stack of undamaged cells after 2D gel electrophoresis and IFCA staining. 7 min horizontal, then 7 min at 45° and 7 min at 90° – L; 10 min horizontal, then 10 min vertical – M. Scale bars - 50 μm.

Figure 3.4 directly compares conventional SYBR Green staining and IFCA for the neutral Comet-assay. The samples were double-stained by both methods. The left column of Figure 3.4 shows images taken using a FITC filterset (SYBR Green). The right column shows images of the identical cells taken with a Cy3 filterset (IFCA). During image acquisition, care was taken not to overexpose the images and subsequently the images were processed identically in order to ensure a valid comparison. Additionally the intensity profiles of the comets are shown (Figure 3.4 E and F). With the conventional comet assay (left column, Figure 3.4 A, C) at most faint tails are visible. In contrast, IFCA of the same cells reveals much more details. Long single filaments emanate from the head. They can be recognized even in the untreated cell (Figure 3.4 B), this might be due to the intrinsic damage or due to experimental procedures. In the cells irradiated with 10 Gy (^{137}Cs, photon energy 662 keV), additional filaments emanate from the head as is evident from the intensity increase in the middle part of the tail from IFCA intensity profile comparison (Figure 3.4 F, arrow). The small intensity increase at the end of the tail is due to the short fragments (Figure 3.4 D), which are detected only by IFCA. A magnified view of this region marked with a frame in Figure 3.4 is additionally shown in Figure 3.4 G.

Interestingly, the histone H1 signal could be detected using IFCA even after harsh conditions used in alkaline lysis and electrophoresis. Representative images of untreated and irradiated (10 Gy) Hela cells after alkaline Comet-assay and IFCA staining are shown in Figure 3.4 H and I respectively. It shows that immunofluorescent staining of histone H1 reveals high level of details in tails of both - neutral and alkaline comets.

An attempt to visualize these details with SYBR Green staining would require over exposure or rude processing of the images by increasing brightness and contrast. This was done in Figure 3.4 J and K, where the SYBR Green and the IFCA signal colocalization is shown in both Comet-assay versions. Green represents DNA staining by SYBR Green whereas red is IFCA detection of Histone H1. The image was processed in order to show the colocalization of signals especially at the end of the tail (insert in Figure 3.4 J and K, top right). Yellow and orange show that the signals in the neutral Comet-assay indeed do colocalise. This proves that histone H1 is still bound to DNA after the lysis and electrophoresis, and IFCA truly visualizes chromatin.

Bottom images show two dimensional IFCA of undamaged cells. In Figure 3.4 L electrophoresis was done 7 min horizontally, then 7 min at 45° angle and last 7 min at 90° angle. While Figure 3.4 M was taken of the undamaged cell electrophoresed at two different angles 0° and 90° each for 10 min. These both images are Z-stack projections on xy plane. By performing the two dimensional electrophoresis in combination with histone H1 immunofluorescent staining, single fibers can be easily separated. However, the number of fibers going out from the head is still difficult to be determined.

3.3.2. SSBs in neutral Comet-assay and fragment size estimation

According to literature, closely located SSBs in a distance up to 14 nucleotides on opposite strands make the DNA structure unstable and can be converted into DSBs at 37° C (Vispe and Satoh, 2000). Detailed *in silico* sequence analysis of chromosome #6 shows that Nt.BbvCI (nicking) can produce 49 pairs of SSBs that fulfil above mentioned requirements. This means that theoretically 49 DSBs and 50 fragments due to clustered SSBs can be generated. Chromosome #6 contains about 2.75 % of whole human diploid genome sequence. Extrapolating this to the whole genome of a diploid cells one would expect to have approximately 1764 DSBs generated by clustered SSBs; this is equal to 44 Gy if gamma irradiation induce ~ 40 DSBs/cell/Gy (Gulston et al., 2002). In contrast, after BbvCI digestion (pure DSB induction) one would expect to obtain ~2.8 10^6 DSBs and the same number of fragments (according to the whole genome *in silico* fragmentation analysis). Consequently the comets and their profile intensities representing nicking (Figure 3.5 B) and cutting (Figure 3.5 C) show very large differences in the tail. Figure 3.5 B and E show a number of fragments as a result of the action of the nicking enzyme Nt.BbvCI and

thus represent SSBs converted to DSBs. In contrast, after the digestion with BbvCI only a few fibres are still bound to the former nucleus (head) (Figure 3.5 C and F frame I). The majority of the genome is highly fragmented as predicted and is visible as a cloud of small fragments (Figure 3.5 C and F frame III). An even better insight into the fragmentation pattern can be obtained by extending the electrophoresis time up to 3h (Figure 3.5 E and F).

The damaging pattern after BbvCI treatment shows three different types of fragments. Figure 3.5 F frame I shows several long fibres emanating from the former nucleus (head), which are still connected to it. Frame II shows several tens of shorter, but still stretched fibre fragments. The majority of signal in Figure 3.5 C and F are dot like and form a big cloud at the end of the comet tail (frame III). Interestingly, a detailed analysis of all human chromosome fragmentation by the BbvCI enzyme showed that almost all fragments (>99.9%) should be in the range from 5 bp to 30 kbp. Thus, fragments with the size up to 30 kbp migrate very fast and form a big cloud of dot like fragments at the end of the tail (frame III).

Additional experiment was done to investigate how DNA molecules of similar size migrate under the same conditions. Lambda DNA with the size of 48.5 kbp was used. Figure 3.5 G shows that after 25 min of electrophoresis the 48.5 kbp sized DNA migrate approximately 540 μm from the loading pocket and are found to be located at the end of the neutral comet tail (comet tail length in insert – 520 μm). The 48.5 kbp DNA is not forming short stretched fibres but form dot like structure (not shown). This confirms that dot like fragments in IFCA are at least not larger than 50 kbp. Longer fibres (frames I and II in Figure 3.5 C) may occur because of incomplete restriction due to hardly accessible DNA.

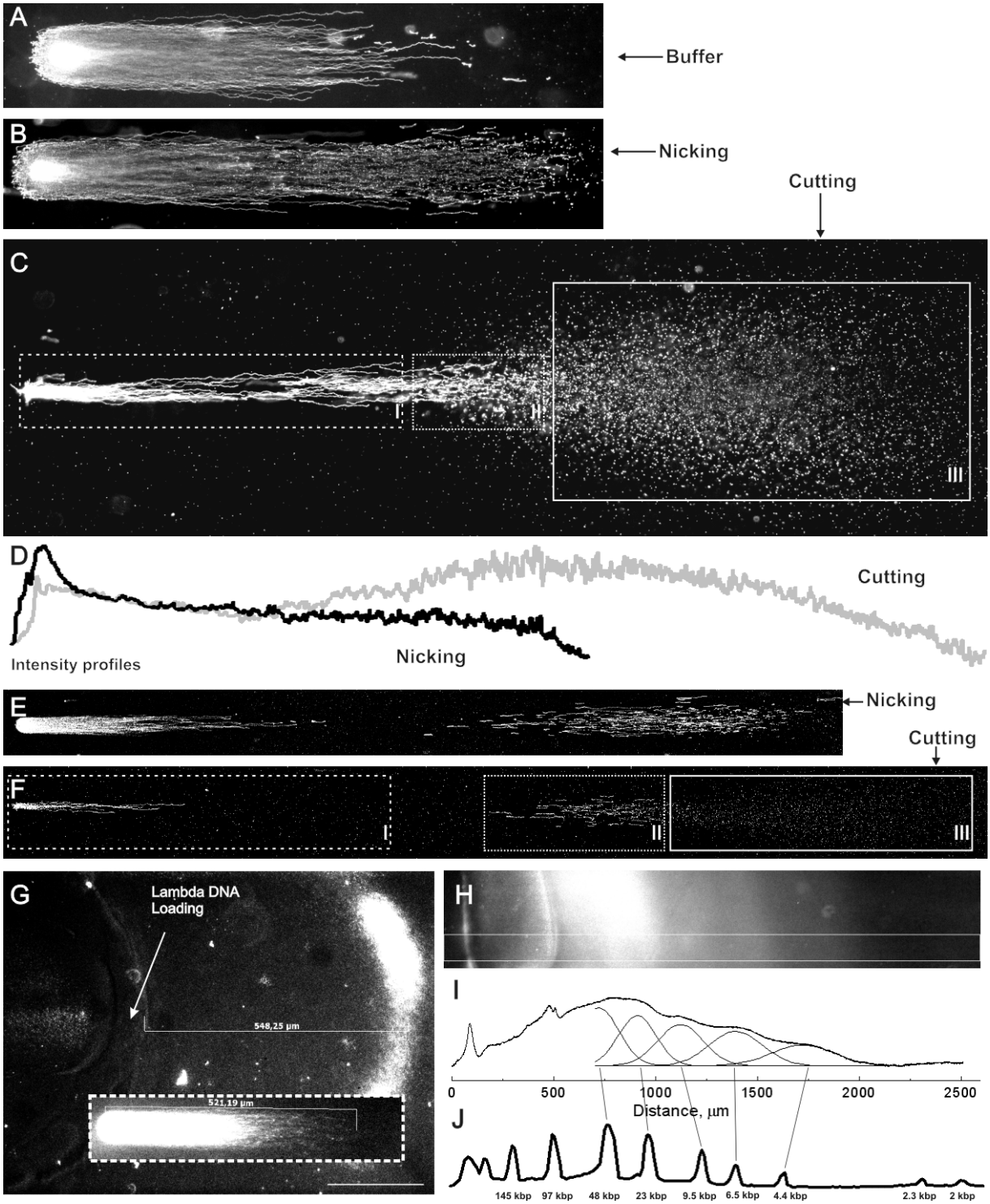
A
Buffer
B
Nicking
Cutting
C
I
II
III
D
Cutting
Nicking
Intensity profiles
E
Nicking
Cutting
F
I
II
III
G
Lambda DNA
Loading
548,25 µm
521,19 µm
H
I
0
500
1000
1500
2000
2500
Distance, µm
J
145 kbp
97 kbp
48 kbp
23 kbp
9.5 kbp
6.5 kbp
4.4 kbp
2.3 kbp
2 kbp

Figure 3.5 Single strand breaks and double strand breaks in the neutral Comet-assay. A, B and C - Representative IFCA images of cells treated with enzyme buffer NEB4 as control (A) nicking Nt.BbvCI (B) and with cutting BbvCI (C) enzymes recognizing the same DNA sequence and electrophoresed for 25 min. D - intensity profiles. E and F - Comets after the same treatment but, 3 hours of electrophoresis. G - In the single cell gel electrophoresis for 25 min lambda DNA (48.5 kbp) migrate 530 μm. This means that fragments of such size are located at the end of the comet tail (neutral comet stained with YOYO1 is shown in the insert). H - migration of low range PFGE marker in 25 min of neutral electrophoresis stained with SYBR Green. I - intensity profile of insert in J with the intensity profile modulation by using 5 Gaussian peak functions representing the distinct fragment sizes in PFGE – J. Neutral Comet-assay shows fragmentation of DNA after nicking enzyme treatment due to single strand breaks located on opposite strands close to each other (<14 nt). After cutting with BbvCI, dot like fragments in the size up to ~ 50 kbp form a big cloud at the end of the comet tail (frame III).

Furthermore, Figure 3.5 H shows the result of low range PFGE marker electrophoresis for 25 min done on the Comet-assay. The intensity profile of it was modulated by 5 Gaussian peaks representing fragments of distinct size (Figure 3.5 I and J). This indicates that also fragments even down to 4.4 kbp are not washed away but are partially separated and can be detected in the neutral Comet-assay if a highly sensitive approach is used. Fragments with the size higher than 48 kbp are not well separated firstly due to the fact that the conventional gel electrophoresis in general can not separate fragments larger than ~50 kbp and secondly, since the introduced low range PFGE marker gel piece diameter is around 500 μm. It means that the peaks representing high molecular weight molecules (143 – 50 kbp) after short migration are very broad and are located within 500 μm from the marker gel incorporation.

3.3.3. DNA fragmentation after ionizing radiation, UV-A laser-microbeam and chemical damage

The fragmentation pattern after treatment with different DNA double strand break induction mechanisms was studied using IFCA. Figure 3.6 shows typical comets after neutral IFCA of HeLa cells treated by ionizing radiation, UV-A laser-microbeam irradiation and bleomycin.

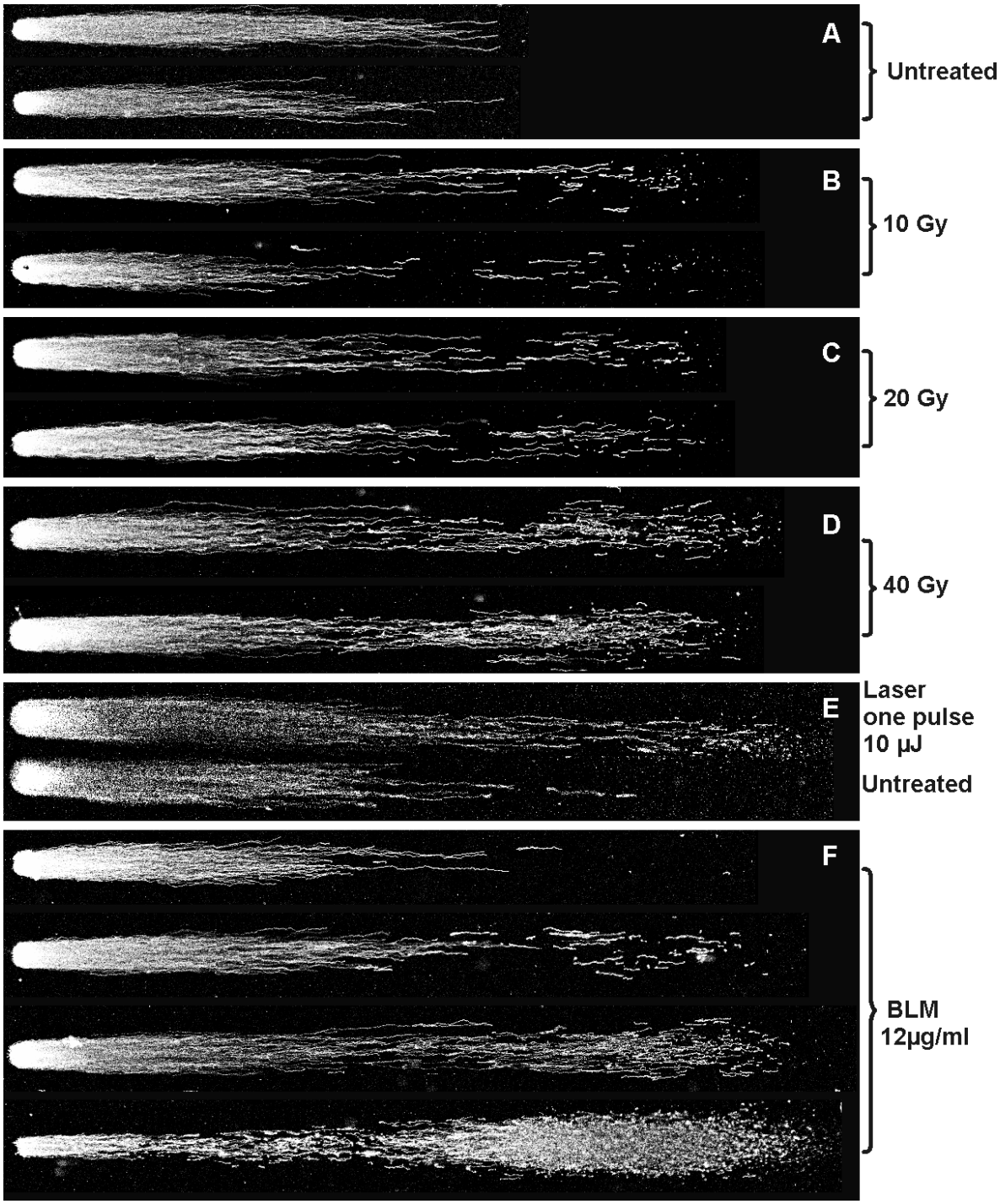

Figure 3.6 Fragmentation patterns of differently damaged cells (IR, Bleomycin, UV-A laser) after neutral lysis, 2h electrophoresis and IFCA. The damage type and dose are given on the right side. A - Untreated cells do not show any fragmentation. B, C and D represent comets after exposure to 10 Gy, 20 Gy and 40 Gy respectively. E- top comet after irradiation with one pulse of UV-A laser-microbeam; bottom untreated cell nearby. F - different fragmentation patterns after bleomycin treatment 12 µg/ml.

In Figure 3.4 it was already shown that untreated cells do not have fragments at the end of the tail. Indeed no fragmentation is detected even after 2h of electrophoresis, - all chromosomes appear to emanate out of the nucleus (Figure 3.6 A). After 10 Gy irradiation short fibre fragments as well as several dot like fragments occur (Figure 3.6 C). The number of both short and dot like fragments increases after irradiation with 20 Gy and 40 Gy (Figure 3.6 C and D).

In Figure 3.6 E DNA fragmentation after irradiation with one single 10 µJ (20 ns) pulse of a UV-A laser-microbeam is shown in direct comparison with untreated cell. Lasers induce a high number of small dot like as well as short and longer fibre fragments (Figure 3.6 E). From the intensity profiles in Figure 3.7 is seen that the fragmentation pattern is similar to that after 20 Gy irradiation. The difference is only that damage after ionizing radiation are induced in the whole cell nucleus whereas damage after laser irradiation are induced in a small volume of laser focus. It shows that irradiation with a UV-A laser does induce a high concentration of SSBs and DSBs in a small volume of the cell nucleus, without an external sensitizer.

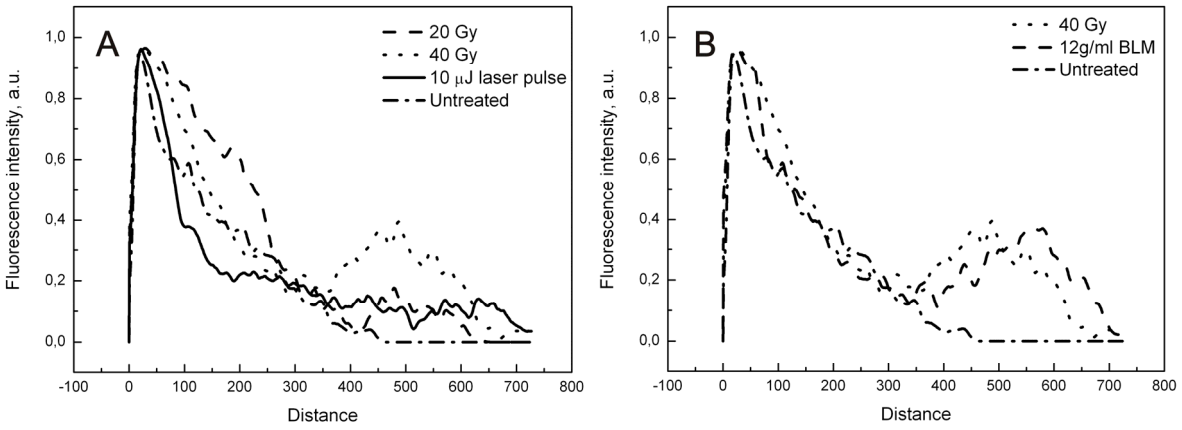

Figure 3.7 A and B - comparison of intensity profiles showing that laser microiradiation induced pattern is similar to the one induced by 20 Gy (A), when the third bleomycin comet from Figure 3.6 F has a pattern similar to that after 40 Gy (B).

After the bleomycin treatment the fragmentation level varies largely from cell to cell as it was already reported by Ostling et al. (Ostling and Johanson, 1987). In Figure 3.6 F four different types of comets detected after 12 µg/ml bleomycin treatment are depicted. Comets similar to untreated cells as well as with medium and very high fragmentation level can be found. It shows that DNA damage induction by bleomycin in asynchronous cells differs

severely. It is possible that this variation is dependent on the cell cycle phase, where bleomycin uptake and the DNA access are different.

Table 3.1 compares the parameters of treatments inducing similar fragmentation pattern. The calculation of parameters is in details described in materials and methods.

Table 3.1 Comparison of important parameters for every type of treatment.

Treatment	Photon energy	Dose	Absorbed energy	Number of photons needed	Molecules per nucleus
20 Gy (^{137}Cs)	661 keV	20 Gy or J/kg	0.6×10^{-12} J	12.5×10^{3}	
10 µJ UV-A, 350nm Laser pulse	3.5 eV	17×10^{7} J/kg	1×10^{-6} J	1×10^{12}	
BLM 12 µg/ml					1.5×10^{6}

3.4. Timing of DNA repair proteins on laser induced DSBs

In order to understand the DSB repair dynamics, the recruitment kinetics of repair proteins were measured. Damage was induced with a pulsed UV-A laser at 350 nm (section 2.9.2). In the following sections the life cell imaging was used to measure EGFP fusion proteins, while immunofluorescence analysis was used to detect the behaviour of the endogenous proteins.

3.4.1. Generation of expression constructs and U-2 OS cell lines stably expressing fusion proteins

Recruitment kinetics of Ku80-, XRCC4- and NBS1- EGFP fusion proteins were measured using U-2 OS cell lines stably expressing those exogenous proteins. Ku80-EGFP and

XRCC4-EGFP stable U-2 OS cell lines as well as plasmids were generated by the diploma student Teresa Lenser under my supervision (Lenser, 2007).

NBS1 sequence was cut out by using restriction enzymes SacII and BamHI from pIRES-NBS1 plasmid kindly provided by E.Fritz and cloned into pEGFP-C1 vector. In the final construct the sequence coding the first seven amino acids in the N-terminus of the NBS1 protein are missing. Nevertheless, the protein showed identical accumulation kinetics to laser induced damage as NBS1-2GFP construct used by Lukas et. al. (Lukas et al., 2004) (data not shown). Coding DNA sequences of Ku80 and XRCC4 were amplified from human U-2 OS cells and cloned into pEGFPC3 and pEGFPN1. The OGG1 cDNA was amplified from human keratinocytes (HaCat), cloned into pENTR4 and then through LR recombinase reaction transferred into pDEST47 plasmid containing the GFP sequence. All the constructs are summarized in Table 3.2 and corresponding maps are shown in Figure 3.8. In order to prove that the correct insert was cloned into the correct vector, the restriction analysis was performed followed by the sequencing. Sequences of the used inserts are displayed in Appendix.

Table 3.2 Overview of used vectors for expression of fusion proteins.

Expression vector	Vector Size, kbp	Fusion protein	Molecular weight of fusion protein	Molecular weight of endogenous protein
pDest47-OGG1-S326C	7215	N – OGG1 – GFP – C	66 kDa	39 kDa
pEGFP-N1-Ku80	5711	N – Ku80 – EGFP – C	110 kDa	83 kDa
pEGFP-C3-XRCC4	5704	N – EGFP – XRCC4 –C	66 kDa	38 kDa
pmRFP-C1-NBS1	6958	N – pmRFP – NBS1 –C	112 kDa	85 kDa
pEGFP-C1-NBS1	6992	N – EGFP – NBS1 –C	112 kDa	85 kDa

No mutation was found in the cDNA of Ku80, XRCC4 and NBS1. However, a point mutation, where C is replaced by C, was discovered at the position 977 of the amplified glycosylase OGG1 gene sequence. This results in the substitution of serine for cystein at

the position 326 (S326C). This is a frequent OGG1 polymorphism occurring in humans, which causes functional defects in the enzyme (Hill and Evans, 2006). OGG1-S326C tends to form dimers, has lower DNA binding affinity but still excise 8-OxoGuanine, however at rates 2 to 6 fold lower than wild type glycosylase (Hill and Evans, 2006).

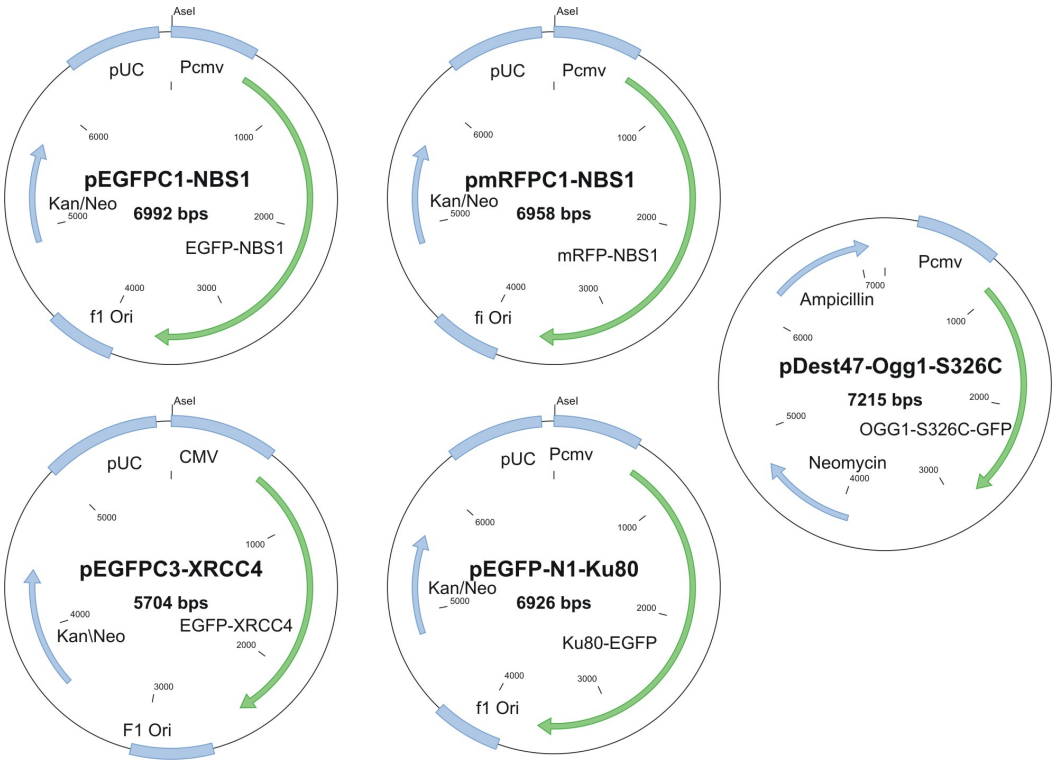

Figure 3.8 Maps of expression vectors with marked restriction site for linearization used in generation of stable cell lines.

In the Figure 3.9 localisation of fusion proteins in human U-2 OS cells is shown. OGG1-S326C-EGFP signal, as expected, colocolize with DAPI signal representing nuclear DNA and is recognized by anti-OGG1 antibody. The Ku80-EGFP is also located in the cell nucleus as expected, however with preferential localisation in the nucleoli. It was reported that only in S and G2 cell cycle phase Ku80 proteins are accumulated to nucleoli (Li and Yeh, 1992), while recent studies used Ku80-EGFP fusion proteins, which are excluded from it (Koike and Koike, 2008; Mari et al., 2006). Notably, a pEGFPC3-Ku80 construct (generated by Teresa Lenser) product, where EGFP is tagged at the N terminal of Ku80, showed very little or no signal in nucleoli. However the accumulation kinetics of pEGFPC3-Ku80 and pEGFPN1-Ku80 at the same damaging conditions were the same (data not shown).

The product of pEGFPC3-XRCC4 construct was mainly found in the nucleus and excluded from the nucleoli. Minor fluorescence was detected in the cytoplasm as well. It is in consistance with data from the literature (Mizuta et al., 1997; Yurchenko et al., 2006). Strictly nuclear localization also for NBS1-EGFP is shown in the right panel of Figure 3.9 in agreement with literature data (Lukas et al., 2003). As expected all fusion proteins showed accumulation to laser induced damages (Figure 3.11 A), with different kinetics described in the following section.

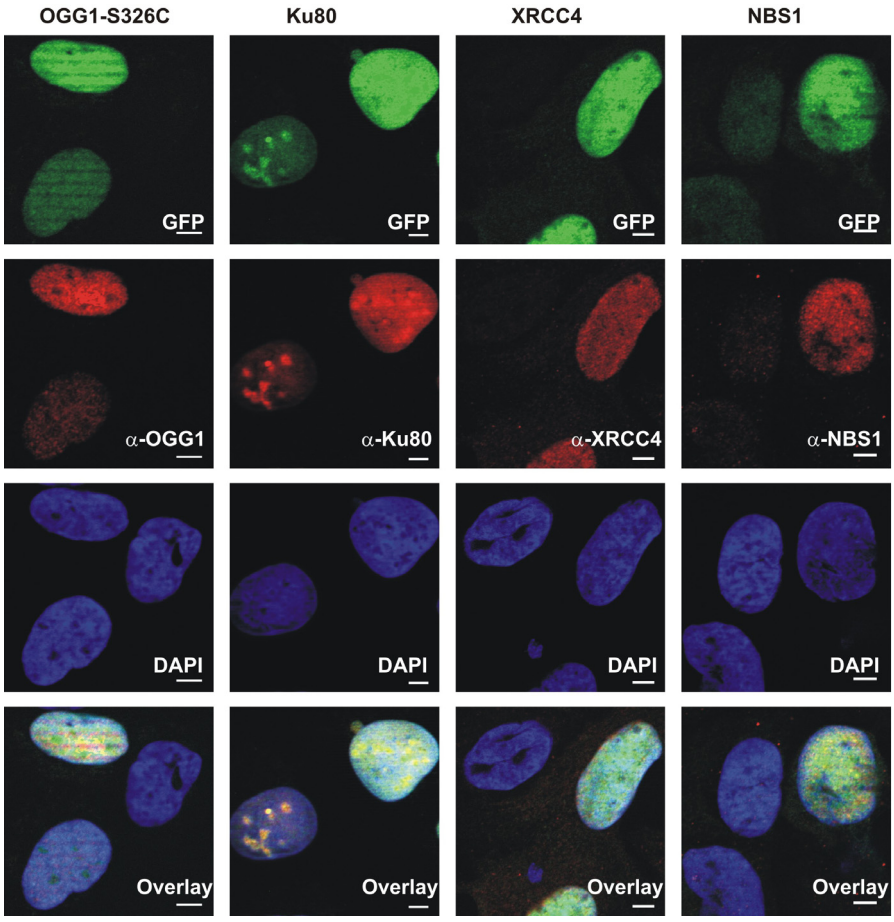

Figure 3.9 Localisation of fusion proteins in U-2 OS cells. Each column starting from above shows staining of EGFP fusion protein (green), specific antibody (red) and nuclear DNA (blue). Scale bar – 5 µm.

In order to obtain similar fusion protein expression levels in all analysed cells, the U-2 OS lines stably expressing Ku80-EGFP or XRCC4-EGFP or NBS1-EGFP were generated as described in the materials and methods. Only OGG1-S326C-GFP was used as a transient

transfection. The western blot analysis of stable cell lines indicates that the fusion (exogenous) proteins are expressed at the expected size (Figure 3.10 B). Ku80-EGFP and NBS1-EGFP expression levels are somewhat lower than those of the corresponding endogenous proteins, while XRCC4-EGFP is expressed at higher levels than endogenous XRCC4 (Figure 3.10 B).

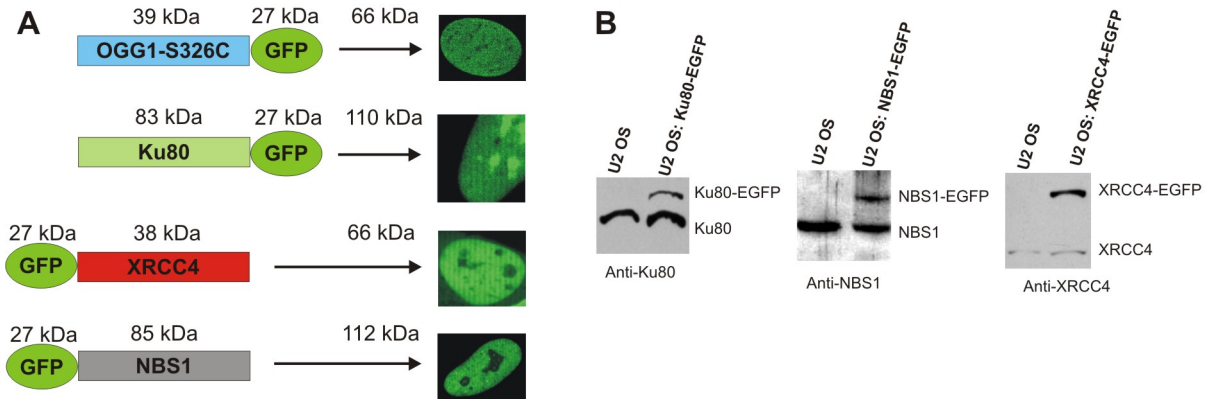

Figure 3.10 A – schematic depiction of OGG1-S326C-, Ku80-, XRCC4- and NBS1-EGFP fusion proteins and their size. B – western blot analysis of stable U-2 OS cell lines expressing Ku80-EGFP, NBS1-EGFP and XRCC4-EGFP, showing that fusion proteins are expressed at the expected size.

3.4.2. Recruitment of DSB repair proteins highly depend on the used laser pulse energy

At a single DSB only a few molecules of each of the NHEJ enzymes are recruited. Thus, the signal from proteins at a DSB can not be distinguished from the background signal and their recruitment kinetics can not be measured directly. In order to overcome this, the accumulation kinetics for human Ogg1-S326C-EGFP, Ku80-EGFP, XRCC4-EGFP and NBS1-EGFP proteins were measured after laser-microbeam irradiation, which is known to induce DSBs with high efficiency as shown in section 3.3.3 and also by others (Uematsu et al., 2007; Mari et al., 2006). Each cell was irradiated with a single pulse having a defined energy 10 seconds after image acquisition start. Spot formation for each of the above mentioned fusion proteins is shown in Figure 3.11 A, where the foci are indicated with arrows. Intensity changes at irradiated regions were normalized in order to compare recruitment kinetics. Examples of mean accumulation curves of stably expressed XRCC4-GFP in U-2 OS cells after irradiation with different laser pulse energies are shown in Figure

3.11 B. The corresponding recruitment times after fitting mean curves with the one phase exponential association function are presented in Table 3.3.

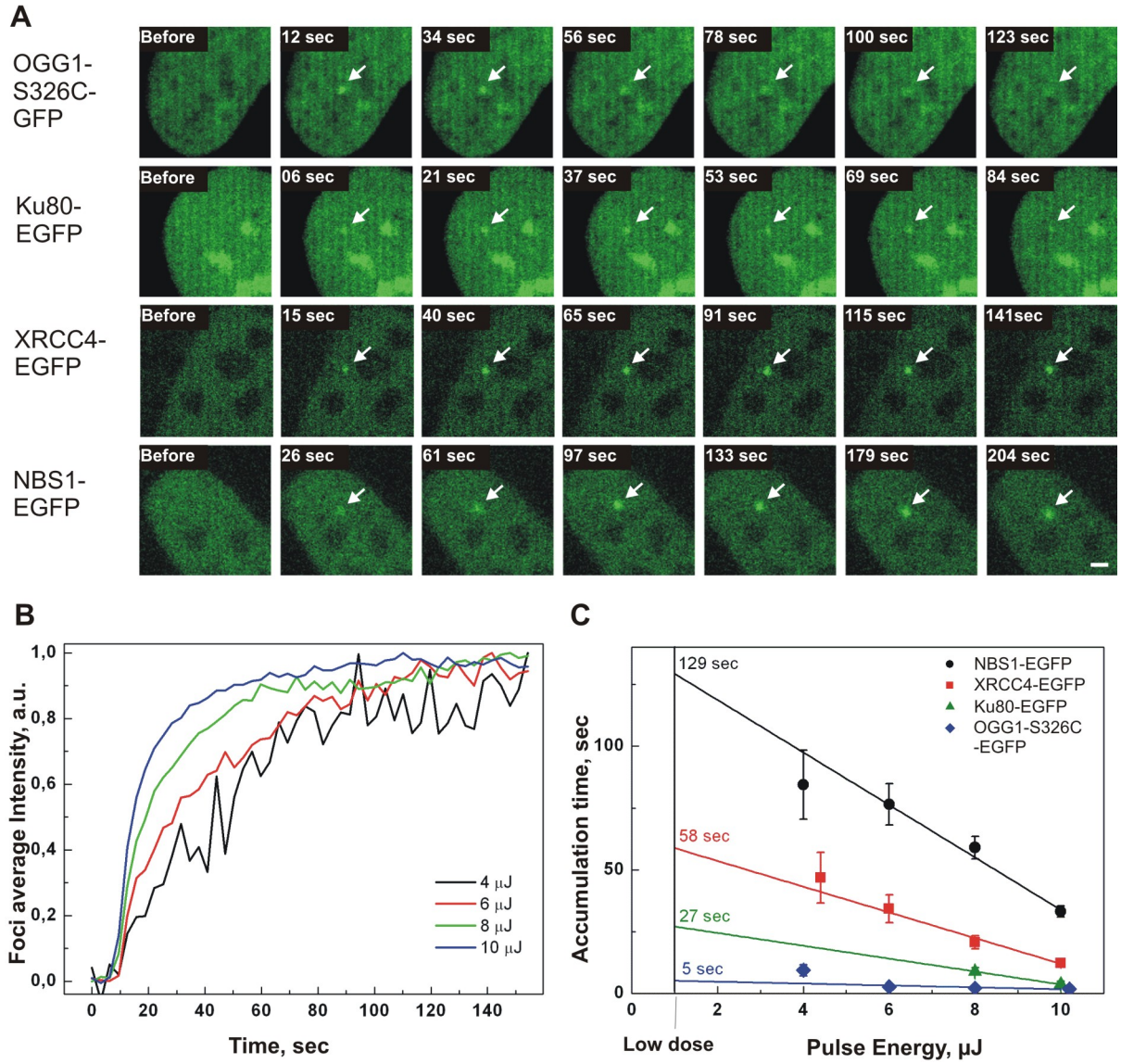

Figure 3.11 Recruitment of EFGP fusion proteins highly depend on pulse energy. A - Time laps imaging of protein recruitment to DSBs after irradiation with 6 μJ laser pulses for Ogg1-S326C, XRCC4, NBS1 and with 8μJ pulses for Ku80. Scale bar – 2 μm. B - Shows average curves (n > 10) of to maximum normalized XRCC4 accumulation kinetics after damaging with different energy laser pulses. C - Recruitment times of all measured proteins are highly dependent on pulse energy, straight lines show linear regression fits which are used to extrapolate data points to low dose conditions in order to estimate recruitment times at biologically relevant situation.

Table 3.3 Recruitment times of EGFP fusion proteins to damage sites induced by pulses of different energies.

OGG1-S326C		Ku80		XRCC4		NBS1	
Pulse energy, μJ	τ_A, sec	Pulse energy, μJ	τ_A, sec	Pulse energy, μJ	τ_A, sec	Pulse energy, μJ	τ_A, sec
4	9.4 ± 2.2			4.4	46.8 ± 10.3	4	84.4 ± 13.9
6	2.8 ± 0.8			6	34.2 ± 5.6	6	76.5 ± 8.3
8	2.2 ± 0.4	8	8.9 ± 1.5	8	20.7 ± 2.7	8	59.0 ± 4.5
10.2	1.9 ± 0.5	10	3.7 ± 1.3	10	12.2 ± 1.1	10	33.2 ± 2.2

Estimated recruitment times at low dose after linear extrapolation

5.1 ± 1.4 sec	27.1 ± 0 sec	58.8 ± 8.0 sec	129.3 ± 12.0 sec

The same procedure was applied also for OGG1-S326C-, Ku80- and NBS1-EGFP fusion proteins. Results are summarized in Table 3.3 and graphically presented in Figure 3.11 E. As mentioned, every data point is a result of more then 10 experiments, only OGG1-S326C at 4 μJ and XRCC4 at 4.4 μJ were measured 3 and 4 times respectively. The accumulation time (τ_A) inversely depends on the laser pulse energy for all proteins. By decreasing the pulse energy and thus the damage level, recruitment of the measured proteins slows down. The data can be easily fitted by linear regression, shown as the straight line in Figure 3.11 C. This allows to extrapolate recruitment times to low dose, which reflect the biologically more relevant situation. For NBS1 the estimated recruitment time is 129 ± 12 sec which is close to the value of 177 ± 41 sec measured after laser irradiation of BrdU sensitized cells (Lukas et al., 2004). These authors used laser irradiation, which has been found to be comparable to 3 Gy of the ionizing radiation (Bekker-Jensen et al., 2006). This indicates that the extrapolation strategy is valid and can be used to calculate the accumulation of NHEJ proteins at conditions comparable to ionizing radiation.

Although the polymorphic OGG1-S326C is known to cleave 8-OxoGuanine at rates from 2 to 6 fold slower than wilde type protein, it is recruited to damage site very rapidly. It is the first recruited protein (τ = 5 ± 1 sec) indicating that with the UV-A laser-microbeam considerable oxidative damage is induced (Lan et al., 2005), which due to base excision repair machinery (BER) is converted into SSBs. If the SSBs are located on opposite strands very close to each other, in a distance lower than 14 nucleotides, the DNA structure becomes unstable and finally two SSBs are converted into one DSB (Vispe and Satoh, 2000). Apparently, concentrated UV-A laser light induces large amount of oxidative damage in a small region and thus induces DSBs via SSBs.

Further, by following the extrapolation to zero in Figure 3.11 C laser induced DSBs are detected by Ku80 with the time constant of 27.1 seconds. The late NHEJ enzyme XRCC4 is recruited with the time constant of 58.8 ± 8 sec. It was shown that XRCC4 is basically recruited by Ku80 and does not require DNA-PKcs (Mari et al., 2006), which seems to improve the stability of the NHEJ complex (Yano and Chen, 2008). The latest protein recruited to the laser induced DSBs is NBS1-EGFP with an accumulation time of 129 ± 12.0 seconds.

3.4.3. Late NHEJ factor XRCC4 is recruited earlier than NBS1 from the MRN complex

The above described data show that under the measured conditions XRCC4-EGFP molecules are recruited earlier than NBS1. This is surprising since XRCC4 is in a complex with Ligase IV and thus is involved in the latest NHEJ step, while generally NBS1 is believed to be a key player in the choice of the pathway and is thought to be involved in sensing of DSB and chromatin modification around the DSB. In Figure 3.12 A a direct comparison of the mean accumulation curves of NBS1 and XRCC4 is depicted. Those curves were measured by live cell imaging after irradiation with a 6 µJ laser pulse. Foci fluorescence intensity of XRCC4-EGFP reaches plateau at around 120 sec after the laser pulse, while the NBS1-EGFP signal reaches plateau only at around 200 sec. A fit of those curves gives accumulation times of 34.2 and 76.5 seconds respectively (Table 3.3), indicating that XRCC4 is recruited two times faster than NBS1.

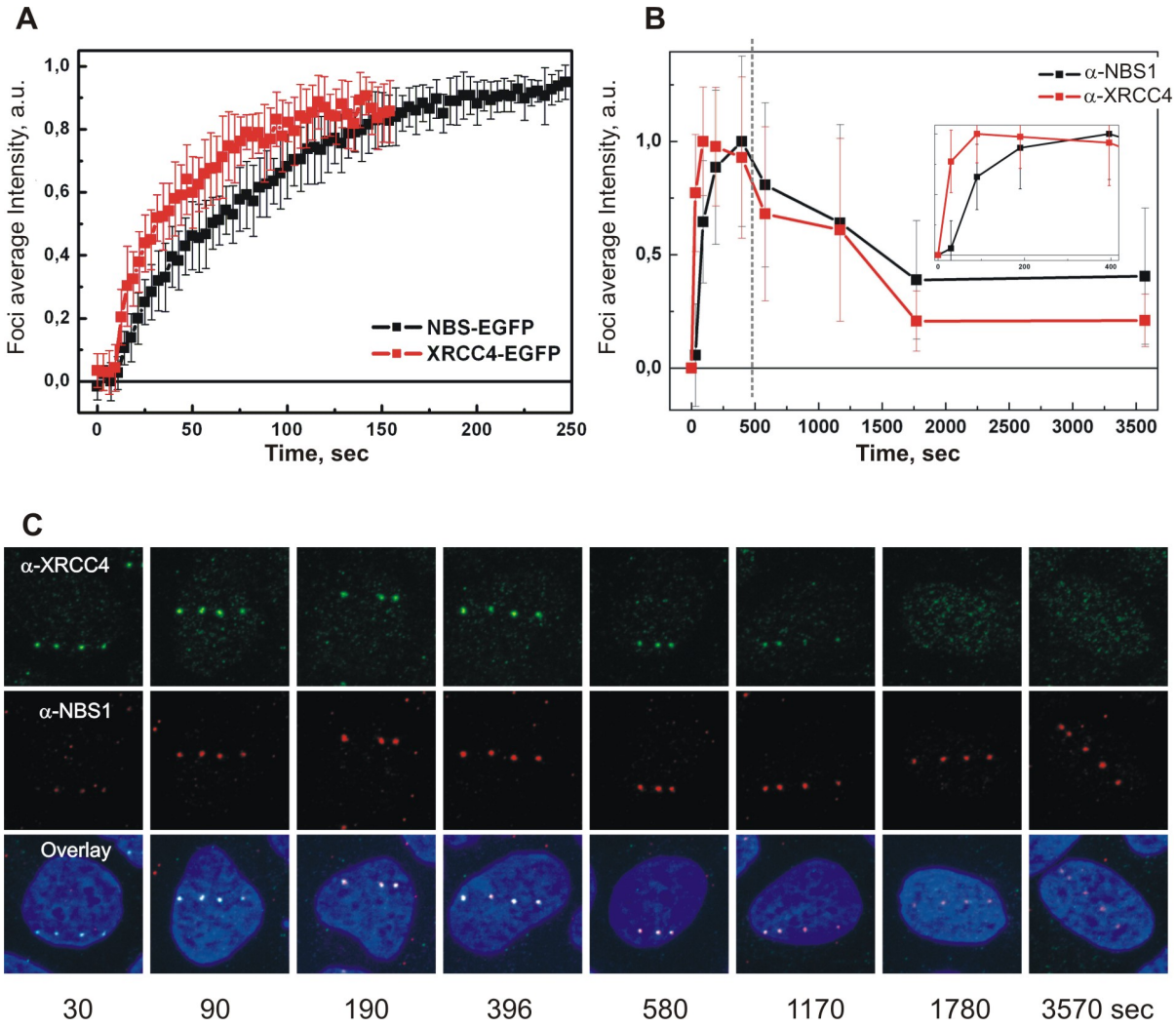

Figure 3.12 Exogenous and endogenous XRCC4 are recruited earlier or not later than NBS1. A – average (n = 14) of normalized focus intensity changes of XRCC4-EGFP (red) and NBS1-EGFP (black) after laser irradiation with 6 µJ pulse measured by live cell imaging. B - representative recruitment kinetics of endogenous XRCC4 (red) and NBS1 (black) over 1 h normalized to maximum. Each point represents a mean of average foci intensity in 3D of around 200 foci (~ 50 cells). Error bars represent standard deviations. C – representative images of projections of 14 optical slices for every cell nucleus at different times after laser-microbeam irradiation over 1h (correspond to B).

In order to exclude artefacts possible in live cell imaging experiments, especially due to the higher expression levels of XRCC4-EGFP (Figure 3.10 B), the recruitments of endogenous DSB repair enzymes were measured by using the immunofluorescence staining after the UV-A laser-microbeam irradiation with pulse energy of 4 µJ. This energy was chosen due to the fact that at lower pulse energies XRCC4 signal could not be detected or properly

evaluated anymore. Although the fixation procedure decreases the temporal resolution, it was found that fast processes still can be detected after antibody staining. Representative images of foci formation of XRCC4 and NBS1 over 1 h in double stained samples are shown in Figure 3.12 C. For each time point the mean of measured average focus intensity of around 200 foci was calculated. The result is shown in Figure 3.12 B. Curves were normalized to their maximum in order to obtain the direct comparison of temporal dynamics. XRCC4 represented in red colour reaches the maximum at 90 sec after irradiation while the NBS1 signal reaches the maximum only at 390 sec (Figure 3.12 B). The same behaviour pattern of both endogenous proteins was reproduced in six experiments out of six shown in Figure 3.13.

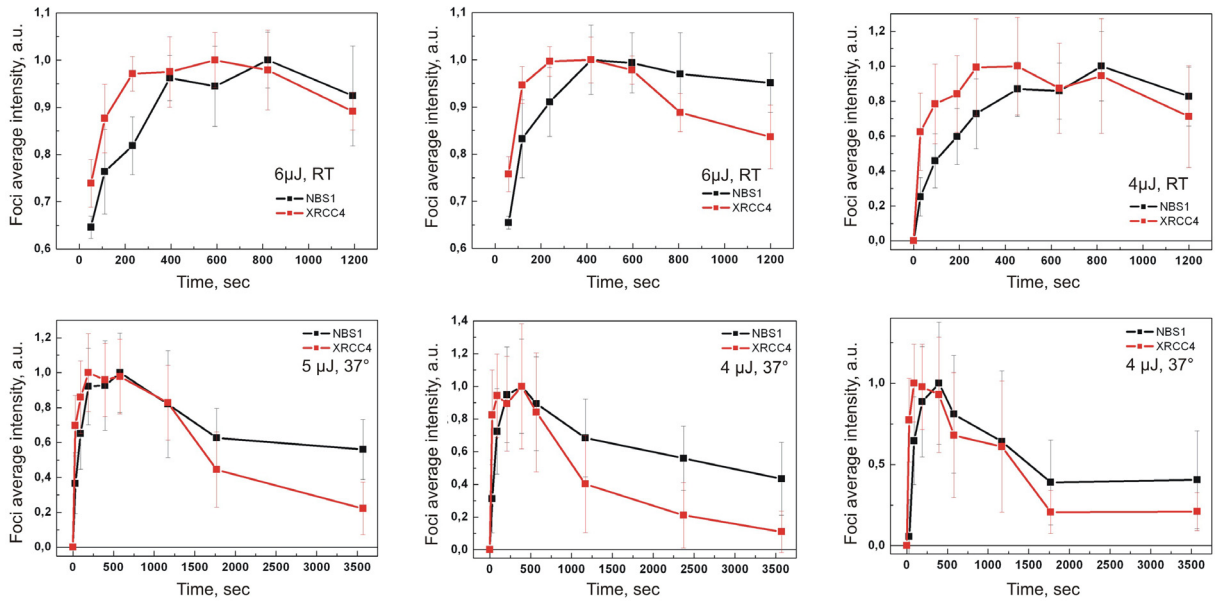

Figure 3.13 Recruitment kinetics of endogenous XRCC4 and NBS1 measured in doubly stained samples. Label 37ºC means that experiments were performed under optimal cell growing conditions. Whereas RT - means that experiment were performed at room temperature without CO_2 supply. In all cases XRCC4 (red) reaches maximum faster than NBS1 (black).

Additionally, the average recruitment time values from four (XRCC4) and two (NBS1) independent experiments after fitting the curves with an exponential association function are presented in Table 3.4, showing very fast XRCC4 (~ 16 sec) and slower NBS1 (~ 87 sec) recruitment. Standard deviations of calculated recruitment times are very high due to the fact that fit was done only on first 5 points, having already high standard deviations.

Endogenous protein accumulation confirms the data obtained from live cell imaging of fusion proteins. It shows that endogenous XRCC4 is recruited faster or at least not later than endogenous NBS1. Especially, significant differences can be seen in the insert of Figure 3.12 B where comparison of data points 30 sec after irradiation is depicted. At this time point the average intensity of XRCC4 foci is very close to the maximum intensity, while for NBS1 it is close to the background value. The same is observed also for all endogenous XRCC4 accumulation kinetics shown in Figure 3.13

Table 3.4 Recruitment kinetics of endogenous proteins and kinetics of DNA-PKcs phosphorylation.

XRCC4	16 ± 19 sec; n = 4
XRCC4 decay after 390 sec	625 ± 748 sec; n = 4
NBS1	87± 64.5 sec; n = 2
Phosphorylation of DNA-PKcs at Ser2056	158 ± 81 sec; n = 2
Phosphorylation of DNA-PKcs at Thr2609	304 ± 110 sec; n = 2
Rad51 (fit after 390 sec)	445 ± 663 sec; n = 2

3.4.4. XRCC4 recruitment time does not depend on the NBS1

It was earlier described that NBS1 is believed to be a molecule mediating pathway choice as well as it is also thought to be involved in DSB sensing. In contrast the results above show very early XRCC4 recruitment to laser induced DSBs even before NBS1. In order to confirm this data and also to clarify whether NBS1 regulates recruitment of enzymes involved in late NHEJ, the focus formation of XRCC4 in NBS1 null cells was analysed.

Immunofluorescent staining in Figure 3.14 A shows that endogenous XRCC4 form focus in wilde type and NBS1 null mouse embryonic fibroblasts. The same is observed when both cell lines are transfected with plasmid for transient XRCC4-EGFP expression. Moreover, in

both cell lines normalized accumulation kinetics after laser irradiation are identical (Figure 3.14 B). Note, that here only information whether foci are formed and how fast are they formed is available. Possible slight differences in total foci intensity should be elucidated by further experiments. In MEF cells without Ku80 protein that is responsible for recruitment of XRCC4 (Mari et al., 2006) no XRCC4 foci could be detected at different times, whereas 53BP1 is clearly detectable (Figure 3.14 C). Live cell imaging of the same Ku80 deficient MEF's transfected with the XRCC4-EGFP also didn't show any formation of focus (data not shown). These results indicate that NBS1, in contrast to Ku80, is not directly involved in recruitment of XRCC4.

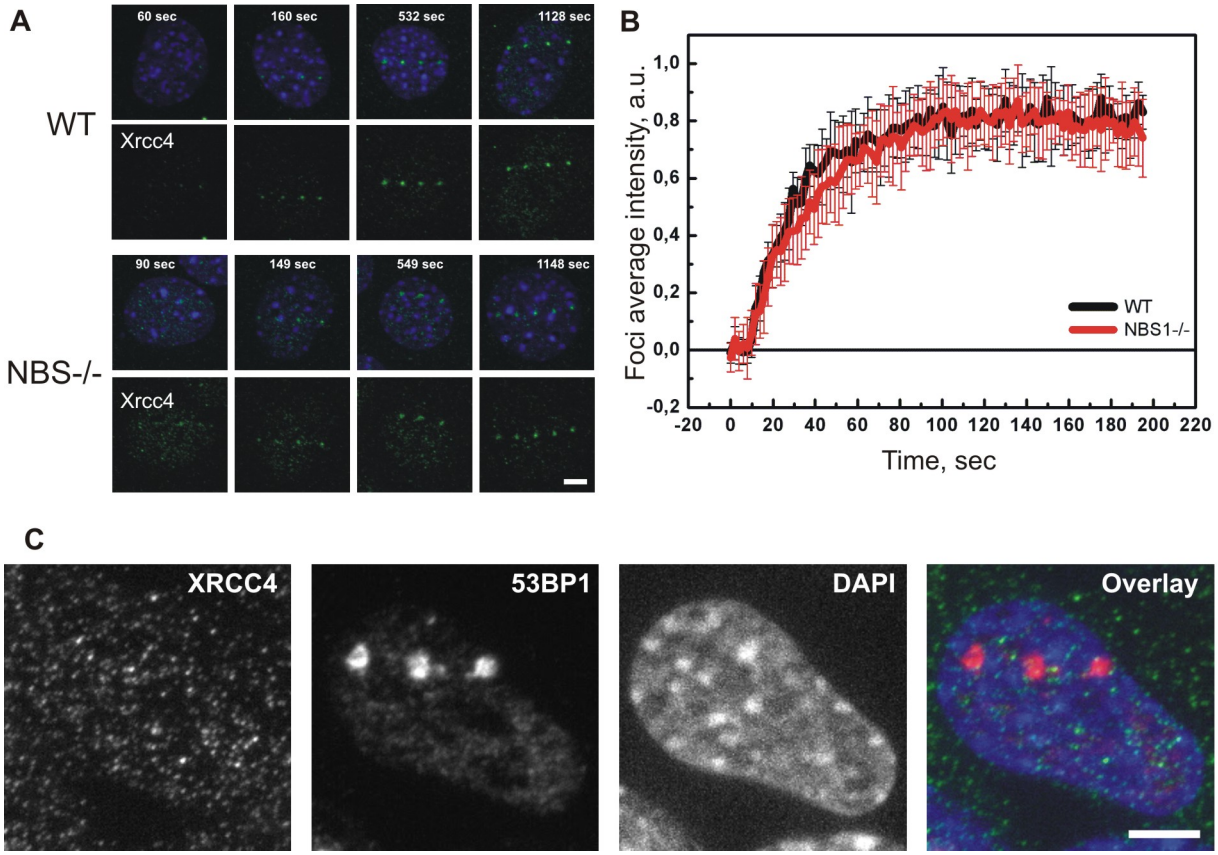

Figure 3.14 XRCC4 accumulation time is not affected by presence or absence of NBS1. A - immunofluorescene of endogenous protein shows efficient endogenous XRCC4 foci formation in NBS1 proficient and null MEF's (pulse energy 4 µJ). B - shows that XRCC4-EGFP fusion protein reaches plateau in wilde type and NBS1-/- cells within the same time (Pusle energy 8 µJ). C – in Ku80 deficient cells after 390 seconds endogenous XRCC4 is not accumulated to laser induced damage marked by 53BP1. Scale bar – 5 µm.

3.4.5. XRCC4 is replaced by Rad51

For direct comparison of NHEJ and HRR timing, the double staining of endogenous XRCC4 and Rad51 was performed in cells irradiated with laser microbeam at different times. In Figure 3.15 A the XRCC4 foci average intensity (red) shows typical behaviour by reaching the maximum few minutes after treatment when Rad51 foci can not be detected yet. This experiment was performed two times, the outcome was the same, the mean curve of those two experiments is shown in Figure 3.16.

After residence at DSBs till 400 sec (indicated with vertical line) XRCC4 signal starts to decrease. Simultaneously, at the same time (400 sec) Rad51 signal starts to grow dramatically with the similar kinetics of XRCC4 signal decay (Table 3.4; Rad51 $\tau_A = 445 \pm 663$ while XRCC4 $\tau_D = 625 \pm 748$). Interestingly, XRCC4 foci are observed in every cell nucleus at the accumulation stage (0 – 400 sec). As shown in the Figure 3.15 C, 90 seconds after irradiation XRCC4 foci are formed in cells with high level of Rad51 expression as well as in those cells, which do not have Rad51 protein, marked with frames. At the dissociation stage (400 - 2400 sec post irradiation) only several cells show foci. Figure 3.15 C shows an example where four cells with different Rad51 expression levels are depicted 1170 seconds after irradiation. One dark cell nucleus in the red channel was labelled with the frame in Figure 3.15. It shows that Rad51 expression level is very low and consequently no foci formation of Rad51 at laser irradiated sites can be observed, while XRCC4 foci are highly intense. In contrast, the neighbouring cell marked with an arrow shows opposite effect. It has high expression level of Rad51 and therefore intense foci at DSBs while XRCC4 foci intensity is dramatically reduced compared to the cell in frame. This can clearly be compared in depicted profile intensity curves for both time points. These results indicate that HRR machinery after 400 seconds start to exchange NHEJ at laser induced DSBs in cells with high Rad51 expression (representing cells in late S, G2 cell cycle phase). While in cells with low Rad51 level (representing cells in G1 phase) XRCC4 foci persist longer. It can clearly be seen in the plot, where correlation between the focus average intensities of Rad51 and XRCC4 are shown at 1170 sec after irradiation (Figure 3.15 B). The linear regression line with negative slope can be fitted through all data points, indicating that foci with high Rad51 intensity have low intensity of XRCC4 and vice versa.

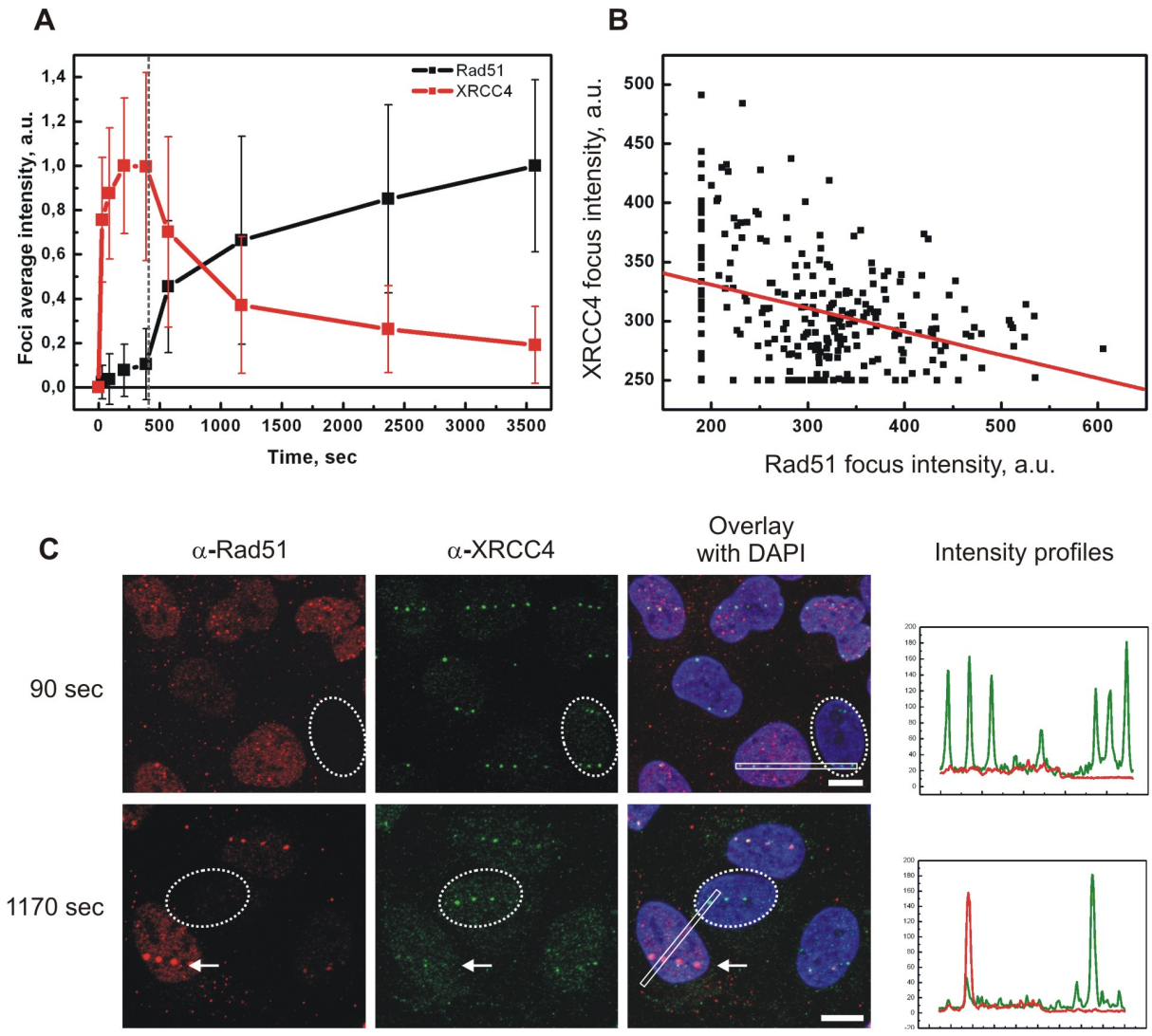

Figure 3.15 XRCC4 exchange by Rad51 molecules. A - Focus average intensity changes during 1h at laser induced DSBs, normalized to maximum, visualised by double staining of XRCC4 and Rad51 (C). B - XRCC4 and Rad51 average focus intensity correlation at 20 min after irradiation. Fit by linear regression function shows that cells with higher Rad51 foci signal has lower intensity XRCC4 foci. C - comparison of double staining at 90 and 1170 sec after irradiation. Frames show cells with low Rad51 expression levels where XRCC4 foci are detectable longer than in cells with high Rad51 levels shown with arrow. Rectangles in overlay images show the location where intensity profiles (right panel) were measured. Scale bar - 10 μm.

3.4.6. DNA-PKcs is phosphorylated after NHEJ and before HRR are recruited

Since phosphorylation of DNA PKcs also was shown to be very important for DNA repair, in the following the immunofluorescence method was applied to measure also the phosphorylation kinetics of DNA-PKcs at Ser2056 and Thr2609 sites with the specific antibodies.

The recruitment times, obtained from fitting the curves shown in Figure 3.16 with the exponential association function, are summarized in Table 3.4 (see above in section 3.4.3). Both sites of the DNA-PKcs kinase are phosphorylated slower than NBS1 is accumulated, and most interestingly, with different kinetics. The serine 2056 is modified two fold faster than threonine 2609 with the time constants of 158 ± 81 and 304 ± 110 seconds, respectively. This suggests that those sites are involved in different processes. This is in agreement with Uematsu et al. who reported that the Ser2056 site is a result of the autophosphorylation (Uematsu et al., 2007; Chen et al., 2007), while the threonine 2609 is most probably phosphorylated by ATM or even may be by ATR. One can suggest, that faster autophosphorylation at the Ser2056 site is responsible for DNA-PKcs structure changes, which does liberate DNA ends, allowing them for enzymatic processing. In contrast, the DNA-PKcs phosphorylation by ATM at the Thr2609 could be probably responsible for release of NHEJ complex?

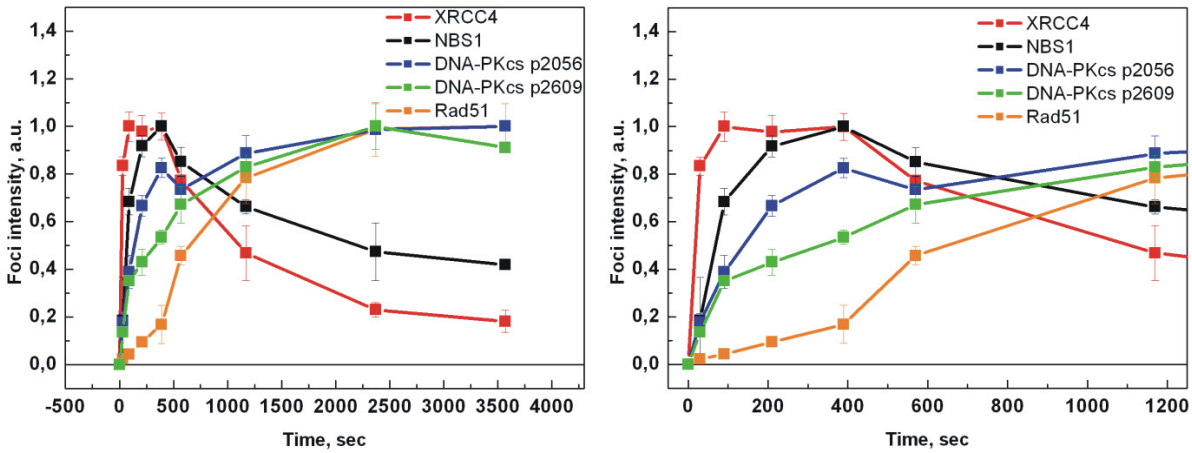

Figure 3.16 DNA-PKcs is phosphorylated after recruitment of XRCC4 and NBS1, but before Rad51. Recruitment kinetics of XRCC4 (red), NBS1 (black), Rad51 (orange) and phosphorylation dynamics of DNA-PKcs at sites Ser2056 (blue) and Thr2609 (green). Right panel shows time course of first 20 min.

Interestingly, the time constants for phosphorylations are between the NBS1 and Rad51 recruitment, i.e., modifications of those sites are slower than NBS1, but still faster than Rad51 recruitment. This can be obviously recognized in Figure 3.16 where mean kinetics of all measured endogenous protein recruitments and phosphorylations are shown.

3.5. Spatial dynamics of laser induced damage

In the following section spatial dynamics of damaged site will be analysed. Again live cell imaging and immunofluorescence analysis are used for that purpose.

3.5.1. Quasi continuous laser irradiation induce different levels of DSBs on laser track

Low pulse energies of 37.5 pJ at quasi continuous irradiation with 520 pulses per µm were delivered to the cell nuclei by Ti:Sa laser system. In Figure 3.17 an U-2 OS cell nucleus was irradiated twice at different sites with about 520 pulses per µm i.e. in a quasi continuous manner, since the distance between pulses is below the resolution limit of a microscope. Hence, one would expect that damage would be induced continuously along the track. In contrast to expectation, immunofluorescence staining against γ-H2AX and Rad51 shows different results. Phase contrast image merged with the green channel (γ-H2AX) in Figure 3.17 demonstrates that non-homogeneity in the γ-H2AX signal is not caused by the presence of nucleoli, which are located in this case outside of the laser track.

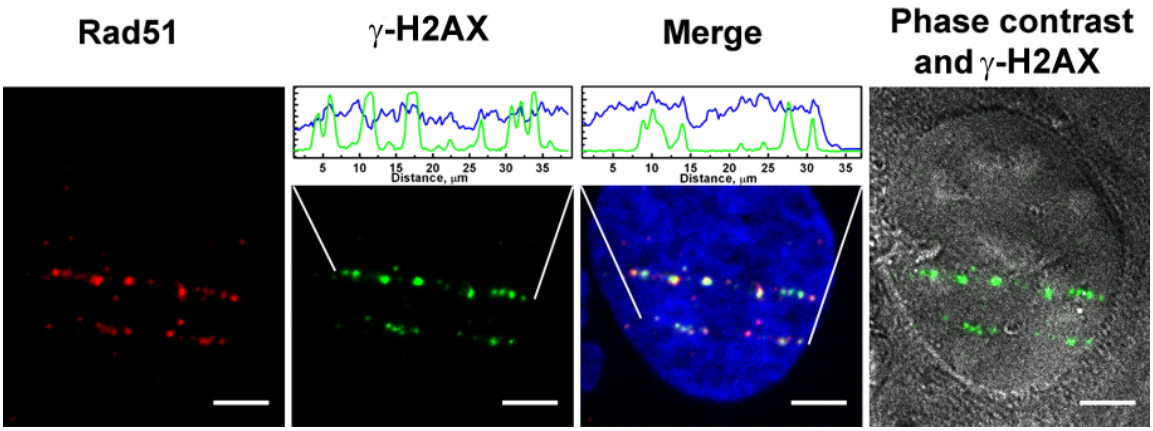

Figure 3.17 Double strand break induction in U-2 OS cells after irradiation with 520 low energy (37.5 pJ at 420 nm) pulses per 1 µm. Inserts represent intensity profile of γ-H2AX and DAPI signals in first irradiated regions. Phase contrast is depicted in order to annotate nucleoli influence in discontinuously induced DSBs. Scale bar - 5 µm.

One explanation for the occurrence of non-homogeneously distributed DNA damage foci may be that firstly chromatin and secondly endogenous photosensitizers are distributed non-homogeneously in the cell nucleus. However, the graph in Figure 3.17 with the intensity profile curves, taken from irradiated region, shows that there is no strong correlation between γ-H2AX foci (green) and DAPI staining (blue). Thus, it can be speculated that other factors like the DNA repair machinery also may play a crucial role in such inhomogeneous distribution of foci, however this has to be elucidated in further experiments.

3.5.2. Laser induced foci fuse ~ 20 minutes after irradiation

Aten and co-authors have already reported another type of clustering (Aten et al., 2004) that appears after alpha particle irradiation in some G1 phase cells. Between 3 to 5 big γ-H2AX clusters are formed with a distance of ~2 μm from each other. The same effect is observed also in this study after Ti:Sa laser irradiation at 420 nm.

In Figure 3.18 A seven cell nuclei are shown. Six cells show more or less continuous γ-H2AX signal. Whereas one nucleus, marked with an arrow, has 5 large foci distributed approximately 2 μm from each other without Rad51 signal. Absence of Rad51 signal discloses that cell is in G1 cell cycle phase. Phase contrast image overlay with γ-H2AX signal indicates that signal empty spaces appear not due to nucleoli.

Furthermore, foci clustering dynamics in living cells after irradiation with UV-A laser (350 nm) was detected. U-2 OS cells transiently expressing NBS1-EGFP fusion protein were irradiated with laser-microbeam at four different locations. Spatial dynamics of those four NBS1-EGFP foci is depicted in Figure 3.18 B, where pictures of one single plane were taken every 2 minutes. It can be clearly recognized that the second focus is moving towards the first one and merges after ~ 20 min. The same type of damaged DNA fusion was detected in nine of ten observed cells. Furthermore, only damage that were close to each other (in a distance not longer that 2μm) were able to merge. In order to confirm that this fusion of several damaged sites is not a consequence of natural chromatin dynamics, three foci at different directions but still close to each other were induced in cells stably expressing NBS1-EGFP fusion protein. After 1h only one focus could be observed (Figure 3.19).

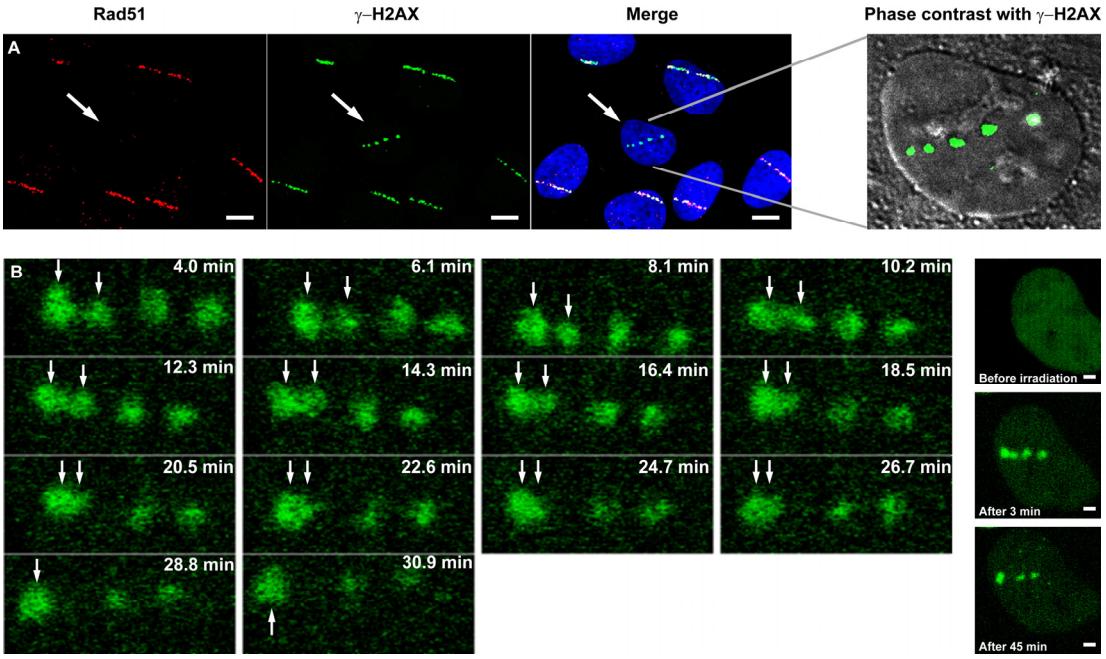

Figure 3.18 A- Clustering of DSB foci. The cell marked with an arrow one hour after irradiation has five distinct big γ-H2AX foci, which do not colocalize with Rad51 and thus, possibly are in G1 cell cycle phase. Phase contrast picture shows that empty spaces in γ-H2AX signal are not due to nucleoli. In this experiment irradiation with laser-microbeam at 420 nm, 50 pulse/µm, 185 pJ was done. Scale bar – 10 µm. B – Fusion of GFP-NBS1 foci in living cells induced by UV-A laser (350nm). Two neighbouring foci are fused approximately in ~20 min after irradiation. Time laps starting at 3 min after irradiation are shown. In the right panel pictures the same cell are shown before, 3 min and 45 min after irradiation. Scale bar – 2 µm.

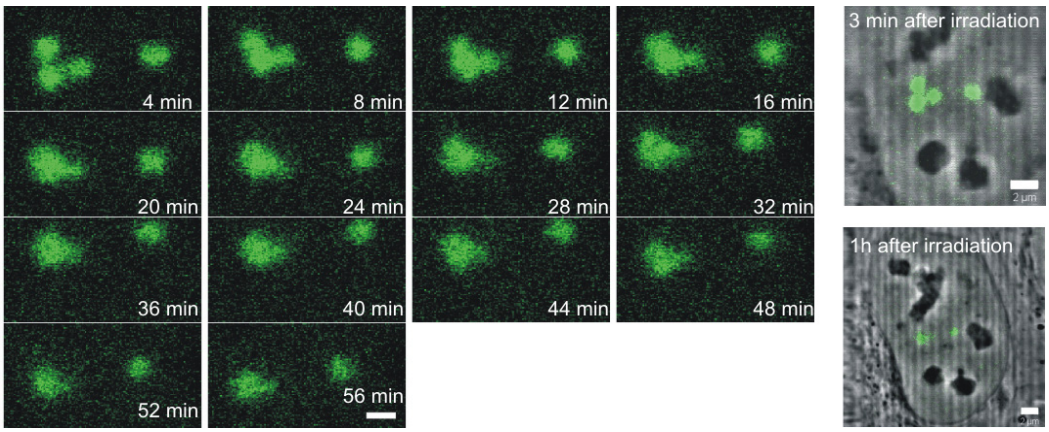

Figure 3.19 Fusion of GFP-NBS1 foci induced in three directions. Time laps starting at 4 min after irradiation show that three foci induced in three directions also coalesce. Right panel shows foci in overlay with phase contrast. Scale bar – 2 µm.

4. Discussion

4.1. DNA double strand break induction depends on a subtle combination of pulse peak power, dose and wavelength of the laser-microbeam

Among all known experimental techniques for DNA damage induction, the laser-microbeam is the most versatile in terms of spatial and temporal accuracy, in terms of compatibility with the microscopic techniques required to directly observe the repair process and in terms of flexibility of beam parameters. Here it is shown, that induced DNA damages are neither solely dependent on the wavelength, nor on pulse peak power nor on dose but on a subtle combination of all three parameters.

Unlike in the most other studies on laser induced DNA damage repair in the present work the laser damaging approach was applied without pre-sensitization. In this case the biological system is not disturbed by exogenous elements such as BrdU or DNA intercalating dye Hoechst, which directly influence the environment of the DNA backbone and therefore might have an effect on the physical DNA properties. Notably, avoiding the pre-sensitization still allows inducing different levels of double strand breaks. Figure 3.2 Cat. 1 and Figure 3.17 show that low pulse energy applied at a high repetition rate, induces just several discrete DSB foci in the laser track, although quasi continuous irradiation is performed. By higher energy pulses even a destruction of DNA can be induced, indicated by reduced DAPI staining in the laser track (Cat 6 in Figure 3.2). In this case the γ-H2AX staining is observed in the entire cell nucleus.

The phenomenon of H2AX phosphorylation covering the whole cell nucleus is still not understood. One explanation for this could be that high energy pulses activate a large number of ATM molecules at the irradiated site, which spread over the entire cell nucleus and phosphorylate H2AX even in the intact chromatin. Such a hyperactivation of ATM

possibly can be achieved not only due to DNA ends occurring in DSBs but also due to the dramatic change in the chromatin structure (Bakkenist and Kastan, 2003) caused by high energy laser pulses.

4.2. Fusion of laser induced damage

Formation of large distinct foci after quasi continuous irradiation with higher pulse energies was described in the section 3.5.2. Large γ-H2AX clusters are detected after one hour by immunofluorescent detection. The same phenomenon was seen also after damage induction with alpha particles (Aten et al., 2004). The authors concluded that several neighbouring damage sites coalesce with time. However, microscopy of fixed samples could not definitely confirm whether the fusion is responsible for the formation of large γ-H2AX clusters. It is possible that chromatin heterogeneity might cause heterogeneous γ-H2AX pattern. On the other hand Kruhlak et al. (Kruhlak et al., 2006) have reported that ionizing irradiation induced foci in mammals fuse only transiently and two neighbouring foci induced by low energy of UV-A laser do not coalesce within 10 min. In the present study, the cells expressing NBS1-EGFP were observed up to one hour after UV-A laser irradiation, showing for the first time, that the laser induced damages really fuse if located near to each other. The time needed for such coalescence is about ~ 20 min, thus it is not surprising that Kruhlak et al. couldn't observe it within 10 min. Furthermore, a fusion of three damaged sites induced at different directions indicates that this process is not caused by natural chromatin dynamics, but most probably is driven by some mechanism indeed related to DNA repair. It is thought that the MRN complex could be involved in this process (Aten et al., 2004). Interestingly, in agreement with the shown data, repair centres were detected in yeast (Lisby et al., 2003). In this case only two or three Rad52 foci were observed after whole cell treatment with ionizing radiation at a dose equivalent to 80 DSBs. So far, DNA damage foci after quasi-continuous irradiation represent an interesting observation, however its molecular origin still has to be elucidated.

4.3. IFCA for high resolution visualisation of DNA fragmentation

For a more direct view on DNA damages, as compared to indirect visualization by repair proteins, in the present work the immunofluorescent Comet-assay (IFCA) was established. This is a highly sensitive method for the visualisation of single chromatin fibers and chromatin fragments with high resolution in the alkaline and the neutral Comet-assays.

IFCA uses immunofluorescent detection of the linker histone H1 protein instead of the standard DNA binding dyes used in the conventional Comet-assays. Conventional staining provides quite blurred comet tails where the fine structure of the fragmented DNA can be resolved only after overexposure or harsh image processing by increasing brightness and contrast. Even then, details of the comet tail can not be recorded with such resolution as by using IFCA, which now can be complementarily used for direct visualisation of DSBs.

In the tail of the neutral and alkaline Comet-assays IFCA clear signals of histone H1 are detected that completely colocalize with the SYBR Green signal (conventional Comet assay). This documents that histone H1 is a strongly DNA binding protein and still can be detected even after neutral and alkaline Comet-assay procedures. This is relatively surprising, since the alkaline lysis buffer uses 2.5 M NaCl, which should strip all non-covalently bound proteins from the DNA (Levin et al., 1978). Only in the middle part of the comet the green signal over - shines the red one coming from antibody staining (Figure 3.4 J and K). It can be that the high number of chromatin fibres enter the neighbouring agarose pores and thus form a structure with high density, which restricts chromatin access by large antibody molecules, while the small SYBR Green molecules still stain DNA. Therefore, the better accessible single fibres in the periphery of the tail are stained more intensively by IFCA. This fact might limit the use of IFCA for a large dose range. However, it in turn might allow studying low dose effects with higher sensitivity than conventional dye based staining. One could speculate, that in ideal case the undamaged cell will not have any tail while the cell with one DSB (for example induced by nuclease) will show two chromatin fiber ends, stretched out of the head. However, the method still has to be optimized in order to get such a high sensitivity.

The IFCA experiments show, that long chromatin fibers are emanating also from untreated cells. In the literature, such stretching was described to occur only after induction of DNA double strand breaks (Klaude et al., 1996; Singh and Stephens, 1997; Rivero et al., 2003). Singh et al. (Singh and Stephens, 1997) have demonstrated that DNA stretching is different at various electrophoresis conditions. No stretched fibres are detected when electrophoresis is performed at 0.5 V/cm (Singh and Stephens, 1997). For IFCA experiments 1 V/cm is used thus, probably, it causes stretching of chromatin fibres. The origin of these long filaments is still not clearly understood. Collins et al. claim that the comet tail, especially in the alkaline version is formed of relaxed loops (formed after strand break induction) (Collins et al., 1997; Collins, 2004). Others predict that chromosome ends are moving out

of the nucleus in the neutral and alkaline Comet-assay (Singh and Stephens, 1997; Singh et al., 1999a; Rivero et al., 2003). Singh et al, utilizing the comet assay in combination with the fluorescence in situ hybridisation technique (Comet-FISH) have shown that one fibre belongs to one chromosome. However, they couldn't prove that it is a chromosome end and not a stretched loop containing two chromatin fibres (Rivero et al., 2003). In the present work no reliable evidences could be provided either for DNA loop or chromosome end hypotheses. However, the presented data, especially the 2D IFCA experiments of undamaged cells (Figure 3.4 L and M) at least support the conclusion that each filament observed in comet tail is the end of a one intact chromosome, containing one chromatin fibre.

4.4. Fragment size calibration and direct comparison of fragmentation patterns after different damaging treatments

For the first time the fragment size distribution in the neutral Comet-assay is shown. From the lambda DNA (48 kbp) migration pattern one can assume that double stranded fragments with the size of 48 kbp migrate 540 µm within 25 min of electrophoresis and are located at the end of the comet tail as dot like structures (Figure 3.5 G). A similar result is predicted from the comparison of the *in silico* fragmentation analysis of the cutting/restriction enzyme BbvCI with its fragmentation pattern in the comet tail. This reveals that fragments up to 30 kbp are forming dot like fragments at the end of the tail.

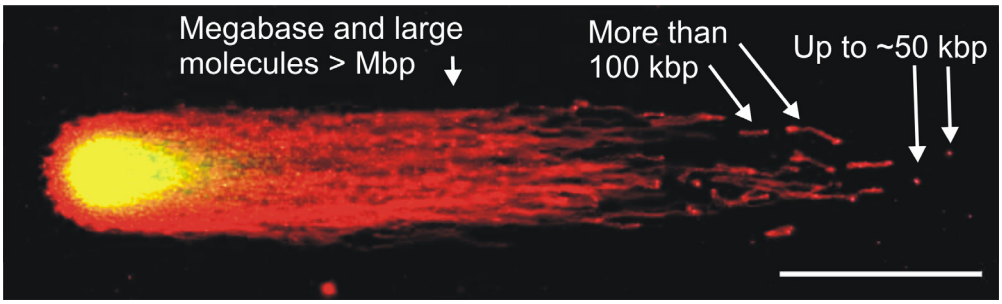

Figure 4.1 Fragment size distribution in the neutral Comet-assay. HeLa cell after 10 Gy irradiation and 25 minutes of electrophoresis. Red – IFCA signal, green – SYBR Green signal representing DNA. Scale bar – 100 µm.

General conclusion can be drawn, suggesting that chromatin fragments up to ~50 kbp are forming dot like fragments at the end of the comet tail (Frame III in Figure 3.5 C). Larger fragments with the size of several hundreds of kbp form short and longer fibres (Frame II in Figure 3.5 C). Finally, long fibres connected to the head are megabase DNA molecules, obviously representing single chromosomes (Frame III in Figure 3.5 C) (Figure 4.1).

Comparison of fragmentation patterns with different noxes reveals that after bleomycin treatment the damaging level highly differs from cell to cell (Ostling and Johanson, 1987). A treatment with 12 μg/ml bleomycin for 30 min results in a fragmentation pattern similar to that of 40 Gy of ^{137}Cs exposure (Figure 3.6 B). For this damage millions of molecules in one cell nucleus are needed (Table 4.1).

The DNA damage patterns after ionizing and UV-A radiation are surprisingly similar to each other. In particular, ionizing radiation of 20 Gy (photon energy 662 000 eV) induces a similar fragmentation pattern as 10 μJ laser irradiation (3.5 eV). This means that the photon number required to induce the same fragmentation pattern is approximately 10^8 times higher for UV-A laser treatment although the energies of photons differs only 2×10^5 times (Table 4.1). Thus the gamma photons induce damage 500 times more efficiently than UV-A photons (350 nm) although the overall absorbed energy is the same (Table 4.1).

Table 4.1 DNA fragmentation efficiency of treatments.

Treatment	Number of photons or molecules	Relative break efficiency
20 Gy (^{137}Cs)	1.25×10^4	500
10 μJ UV-A, 350nm Laser pulse	1×10^{12}	1
BLM, 12 μg/ml	1.5×10^6	n.d.

The 500 times higher efficiency of gamma irradiation compared to UV-A is probably due to physical, but not biological effects. A significant difference in irradiation protocols is that a small number of ionising photons affects the whole cell nucleus. In contrast, the UV-

A laser-microbeam induces highly localized damage. It delivers 10^{13} UV-A photons into a small volume of 3 μm^3 during a short time period of 20 nsec. It means 10^6 photons per femtosecond – approximately one optical cycle. This probably causes the saturation of molecules in the excited state and many following photons can not be absorbed. Consequently the factor of 500 has to be taken as an empirical value and can be used for the comparison of UV-A and ionizing irradiation induced effects in terms of double strand breaks. Here, the comparison of fragmentation after irradiation with the same geometries is necessary.

It is worth noting, that, by keeping in mind the theory that chromosomes in the interphase cell nucleus form chromosome territories (Cremer and Cremer, 2001), the fragments at the end of the Comet-assay after one pulse of spatially resolved laser-microbeam irradiation should originate from one or at least few chromosomes. In contrast, after entire nucleus gamma irradiation, various fragments should be generated from (all) different chromosomes.

4.5. Inverse relationship of DSB repair protein recruitment time with pulse energy

Changing the pulse energy, thus dose and pulse peak power simultaneously, the recruitment kinetics of the DSB repair proteins change their characteristics: accumulation time increases linearly with decreasing energy of the laser pulses. This allows extrapolating the dependency curves to zero in order to estimate the protein dynamics at low dose conditions. This is extremely important for NHEJ proteins, since only several molecules of each NHEJ factor are known to bind to DSBs. Therefore, due to low signal to noise ratio these enzymes can not be visualised as foci after ionizing radiation. Interestingly, the NBS1 recruitment time estimated by extrapolation (129 ± 12 sec) is very close to the value reported by Lukas et al (Lukas et al., 2004), (177 ± 41 sec) who applied local UV-A laser irradiation on cells pre-sensitized with BrdU. After comparison of the RPA foci appearance in the laser track to that one after ionizing radiation they claimed that laser damaging used in their setup is equivalent to 3 Gy of ionizing radiation (Bekker-Jensen et al., 2006). This shows that the extrapolation strategy used in the present work is valid and can be applied to calculate recruitment of DNA repair proteins fused to EGFP at biologically relevant conditions.

The inverse linear recruitment time dependency on pulse energy is quite intriguing. One could expect that the accumulation of proteins at high pulse energies would be slower due

to the limited number of proteins in the cell and a high amount of induced DNA damage. In contrast, the observed effect is opposite to this expectation and can be explained by the following. It is known that UV-A laser light at low doses induces single strand breaks (Lan et al., 2005). If the dose given at the same time point is increased, additionally double strand breaks are induced, thus different repair pathways are activated simultaneously (Dinant et al., 2007). Important is that those DSBs most probably are secondary damages, generated due to the clustered SSBs. The requirement for such an event is two SSBs on the opposite strands in a distance less than 14 base pairs (Vispe and Satoh, 2000). This makes the DNA structure unstable and thus a DSB is generated. The conversion of two closely located SSBs into one DSB requires time, therefore at low pulse energies recruitment of DSB repair proteins is delayed due to slowly generated DSBs. By elevating the pulse energy, the power density increases and direct destruction of DNA backbone becomes possible. Therefore, primary DSBs are induced in higher amounts. This means, that DSBs are generated immediately. Subsequently DSB repair can be performed without a delay. In conclusion, it can be stated that the inverse recruitment time dependency is due to the change in ratio of primary and secondary induced DSBs. Presently this is a working hypothesis, which should be confirmed experimentally in the future work.

4.6. Early NHEJ is followed by recruitment of the MRN complex, DNA-PKcs autophosphorylation and late HRR

The most intriguing result of this study is that the late NHEJ factor XRCC4 is recruited to laser induced damage earlier than NBS1. This was demonstrated by two methods: the live cell imaging of EGFP fusion proteins as well as by the immunofluorescent staining for detection of the endogenous proteins. This finding is very surprising, since XRCC4 is generally thought to be involved in the latest NHEJ step in complex with Lig4, which ligates DNA ends. So far, NBS1 was believed to be on the top of both the NHEJ and the HRR pathways and therefore would be one of the key molecules for pathway choice (Yang et al., 2006). Notably, NBS1 absence does not inhibit XRCC4 focus formation as shown in section 3.4.4, indicating that XRCC4 assembly to DSBs is not directly dependent on NBS1. It rather requires Ku80 in agreement with the literature (Mari et al., 2006).

In *Saccharomyces cerevisiae* it was demonstrated that for the Dnl4 (homologue of human Lig4) recruitment at DSBs, induced by HO-endonuclease, the Ku70/80 heterodimer is required but not MRX complex (MRN in humans), which seems to be more important for

dissociation of Dnl4 (Wu et al., 2008). This publication reported that Dnl4 assembly at endonuclease induced DSBs in *Saccharomyces cerevisiae* is delayed around 10 min compared to MRX complex. Additionally, in mammals it was shown that XRCC4 is present at PPOI endonuclease induced damage several hours later than ATM (Berkovich et al., 2007). This is in contrast to data shown in the present study (section 3.4.3) and can be explained by several facts. First of all those two publications apply a damage induction method using endonucleases, which is a method with low temporal resolution (at least several tens of minutes). Secondly, both groups use the Chromatin Immuno Precipitation (ChIP) technique to measure the protein presence at one DNA site close to the DSB whereas the present study uses the evaluation of average focus intensity. Thus proteins bound directly to damage as well as to the surrounding chromatin are detected. Here the behaviour of NBS1 and XRCC4 proteins is known to be different. XRCC4 is known to bind directly to damage site (DNA ends) through Ku70/80 and DNA-PKcs. In contrast, NBS1 is involved in the sensing of the DSBs through the Mre11 binding to DNA ends and additionally is involved in chromatin modification around the DSBs in range of megabase pairs. Therefore, the measured kinetics of NBS1 accumulation as a focus signal increase, represents proteins involved in both functions.

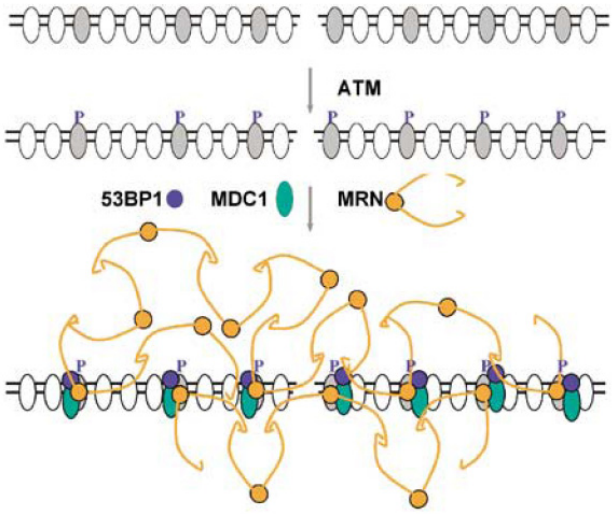

Figure 4.2 Possible model for DSB stabilization in surrounding chromatin through MRN complex. Adapted from (van Gent and Van der Burg, 2007).

Following this, it is worth to notice the finding demonstrating that XRCC4 recruitment time is not affected by absence of NBS1. This shows that those proteins are recruited to DSBs

most probably independently. As was proposed by several groups, NHEJ is responsible for the stability of DNA ends (Soutoglou et al., 2007; van Gent and Van der Burg, 2007) in close proximity, binding directly to them, while the MRN complex (Mre11-Rad50-NBS1) is stabilising DNA ends on the larger scale, by managing the interaction network in surrounding chromatin through γ-H2AX and MDC1 (Figure 4.2).

In the following, timing events measured in this work will be discussed. Ku80 is the fastest molecule found to be at DSBs with a recruitment time of 27 seconds. It rapidly recruits DNA-PKcs and all other NHEJ factors such as XLF and XRCC4/Lig4, before the assembly of NBS1 and chromatin modifications such as γ-H2AX are achieved. DNA-PKcs is known to inhibit access to DNA ends until it is autophosphorylated. Thus, no repair can take place (Weterings and Chen, 2007) although the ligation machinery is already in the vicinity of the lesion. Lou et al. has reported that autophosphorylation of DNA-PKcs at Ser2056 is mediated by the MDC1 protein (Lou et al., 2004), which has a very similar recruitment behaviour as NBS1 (Lukas et al., 2004). In agreement, phosphorylation at this site of DNA-PKcs is done after the NBS1 (Figure 3.14 and Table 3.4) is recruited. Therefore MDC1 mediated autophosphorylation of DNA-PKcs indicates conformational changes of DNA-PK that allow the processing machinery to perform its task. Obviously, this happens only after assembly of all NHEJ factors to the damaged site. This is supported by a recent publication, showing that efficient DNA end processing by endonucleases or polymerases requires the presence of XRCC4/Lig4 complex (Budman et al., 2007).

Figure 3.15 and Figure 3.16 show that XRCC4 persists at DSBs approximately 400 seconds after irradiation and then starts to go away exactly in that moment when the Rad51 focus intensity starts to increase dramatically. The kinetics of XRCC4 signal decay and Rad51 accumulation are complementary (Table 3.4) suggesting that Rad51 replaces XRCC4. Furthermore, phosphorylation at both DNA-PKcs sites (Ser2056 and Thr2609) occurs exactly between the accumulation of those two molecules (Figure 3.16). Therefore, depending on the DNA end processing, which obviously depends on the cell cycle phase and DNA damage type, the pathway finally is chosen. In the G2 phase, Rad51, representing the action of HRR, starts to accumulate rapidly and replaces the NHEJ machinery. In contrast, in the G1 phase XRCC4 persists longer at DBSs and therefore, Lig4 ligates DNA ends (Figure 3.15). This experimentally corroborates an earlier suggestion that DNA-PKcs might be a molecule regulating the pathway choice (Allen et al., 2003; Allen et al., 2002; Shrivastav et al., 2008) and shows the timing of events.

The described model is shown in Figure 4.3 and explains how HRR repair can be initiated in the G2 cell cycle phase since it is well known that Ku70/80 molecules have a high affinity to DNA ends (Walker et al., 2001) and thus, if bound to them, would initiate NHEJ without allowing the HRR to proceed to G2. According to the model in Figure 4.3, early as well as late NHEJ factors are in fact recruited rapidly to DSBs and are inactive (therefore black colour in Figure 4.3), till DNA-PKcs is phosphorylated and DNA end processing is started. Only then either NHEJ join the DNA ends or gives access to the HRR pathway.

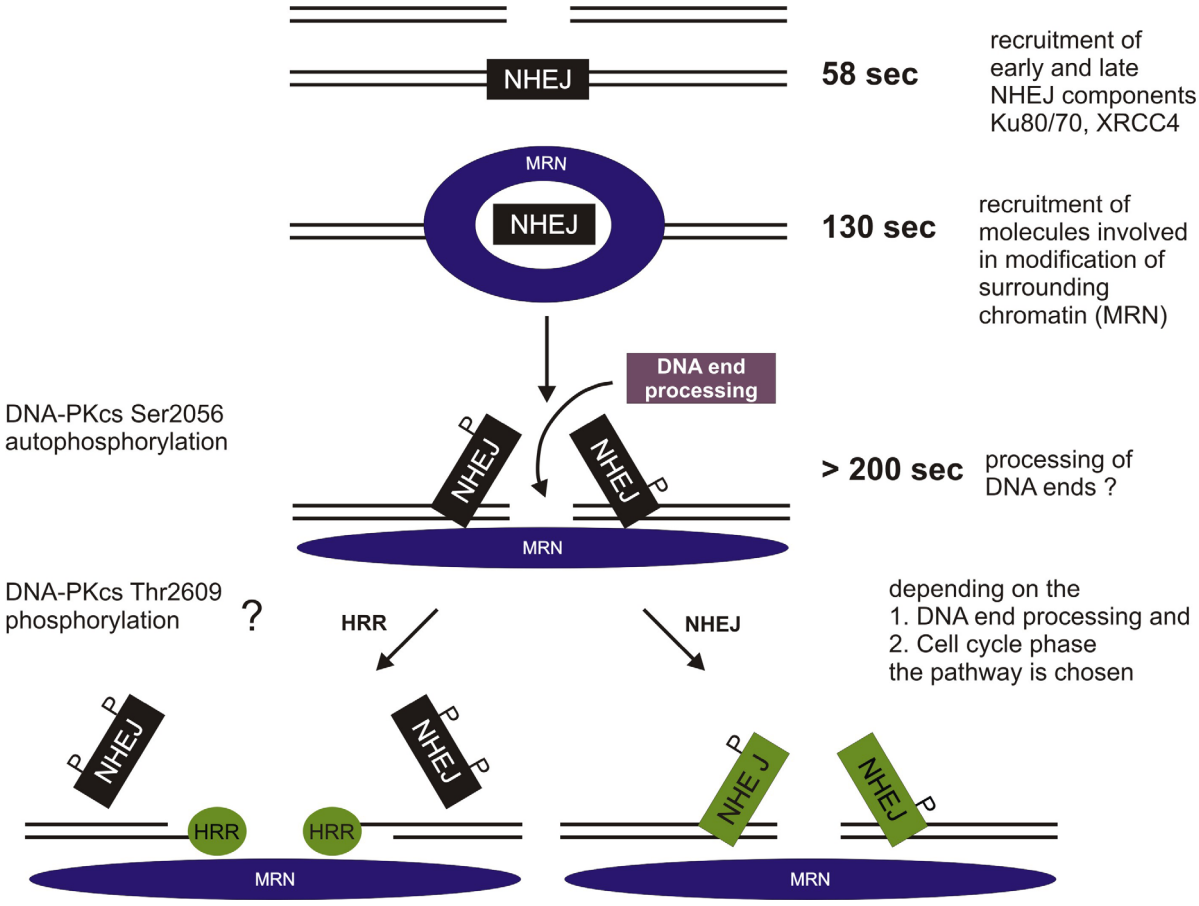

Figure 4.3 Model showing early recruitment of all NHEJ factors that are exchanged by HRR molecules after the DNA end processing when the choice of repair pathway is done.

This hypothesis is also supported by the fact that ubiquitinylation of histones occurs at the onset of HRR (Mailand et al., 2007). Recently it was shown that ubiquitinylation of Ku80 is needed for its release (Postow et al., 2008). One could speculate that those both facts are

related to each other, suggesting that after ubiquitinylation the NHEJ machinery is released (Ku80) and HRR is recruited. Alternatively it could be that the simple DSBs are repaired by NHEJ immediately without choosing the pathway and only complex DSBs requires resection and thus HRR.

In conclusion, double strand break repair starts with the assembly of NHEJ enzymes. The pathway choice is made during the DNA processing until 400 sec after irradiation. After this time point, XRCC4/Lig4 either further ligates DNA ends in G1 cells and thus remains longer visible, or it starts to detach from the damaged site and is replaced by Rad51 in G2 cells where HRR is possible. This supports the hypothesis that NHEJ factors and the MRN complex is initially recruited to the laser induced damage independent of each other. And gives an explanation how NHEJ and HRR pathways can cooperate on one DSB.

4.7. Final conclusions/theses

From this work the following conclusions can be drawn:

1. Early and late NHEJ factors are recruited very early (within 1 min) to the DSBs, even earlier than NBS1.
2. Recruitment time of XRCC4 is not directly influenced by NBS1.
3. HRR machinery (Rad51) is replacing NHEJ proteins at laser induced DSBs in G2 cell cycle phase after the decision of pathway choice is done ~ 400 sec after DNA damaging.
4. DNA-PKcs is phosphorylated at Ser2056 and Thr2609 with different kinetics. With time constants between recruitment of NHEJ and HRR.
5. Timing model of cooperation of NHEJ, HRR pathways and MRN complex at laser induced DSBs is presented.
6. Recruitment kinetics of DNA repair proteins inversely depend on used laser pulse energy.
7. This dependency can be extrapolated to zero, allowing the estimation of the protein recruitment time at biologically relevant conditions.
8. This inverse dependency could be due to the different ratio of DSBs generated due to clustered SSBs and directly induced DSB by high energy pulses (DSB_{SSB} :DSB_{Cut}). Low energy induce more DSBs via clustered SSBs and therefore more time is needed for DSB formation, while at higher energies fraction of primary DSBs increases.
9. The new method for visualisation of Comet-assay was developed and named as Immunofluorescent Comet-assay (IFCA). It enables visualisation of comet tails with high resolution. It allows visualising details, hardly detectable by conventional staining methods.
10. IFCA detects single fragments at high resolution and possibly will be able to detect single DSBs when optimized.
11. The size of fragments at the end of the neutral comet tail was determined, showing that small dot like fragments are of the size up to ~ 50 kbp. Larger fragments form filaments of different length.

12. Laser-microbeam induced γ-H2AX and NBS1 foci do coalesce in 20 min after irradiation if induced close to each other.
13. The level of laser induced damage highly depends on combination of used laser-microbeam wavelength, pulse power density (defined by energy and pulse duration) and dose (repetition rate).

5. References

Abramoff, M.D., P.J.Magelhaes, and S.J.Ram. 2004. Image Processing with ImageJ. *Biophotonics International* 11:36-42.

Ahnesorg, P., P.Smith, and S.P.Jackson. 2006. XLF interacts with the XRCC4-DNA ligase IV complex to promote DNA nonhomologous end-joining. *Cell* 124:301-313.

Allen, C., J.Halbrook, and J.A.Nickoloff. 2003. Interactive competition between homologous recombination and non-homologous end joining. *Molecular Cancer Research* 1:913-920.

Allen, C., A.Kurimasa, M.A.Brenneman, D.J.Chen, and J.A.Nickoloff. 2002. DNA-dependent protein kinase suppresses double-strand break-induced and spontaneous homologous recombination. *Proc. Natl. Acad. Sci. U. S. A* 99:3758-3763.

Aten, J.A., J.Stap, P.M.Krawczyk, C.H.van Oven, R.A.Hoebe, J.Essers, and R.Kanaar. 2004. Dynamics of DNA double-strand breaks revealed by clustering of damaged chromosome domains. *Science* 303:92-95.

Ayoub, N., A.D.Jeyasekharan, J.A.Bernal, and A.R.Venkitaraman. 2008. HP1-beta mobilization promotes chromatin changes that initiate the DNA damage response. *Nature* 453:682-U14.

Bakkenist, C.J. and M.B.Kastan. 2003. DNA damage activates ATM through intermolecular autophosphorylation and dimer dissociation. *Nature* 421:499-506.

Bekker-Jensen, S., C.Lukas, R.Kitagawa, F.Melander, M.B.Kastan, J.Bartek, and J.Lukas. 2006. Spatial organization of the mammalian genome surveillance machinery in response to DNA strand breaks. *Journal of Cell Biology* 173:195-206.

Berkovich, E., R.J.Monnat, and M.B.Kastan. 2007. Roles of ATM and NBS1 in chromatin structure modulation and DNA double-strand break repair. *Nature Cell Biology* 9:683-U137.

Berns, M.W. and K.O.Greulich. 2007. Methods in Cell Biology: Laser Manipulation of Cells and Tissues. Elsevier/Academic Press, New York.

Block, W.D., Y.P.Yu, D.Merkle, J.L.Gifford, Q.Ding, K.Meek, and S.P.Lees-Miller. 2004. Autophosphorylation-dependent remodeling of the DNA-dependent protein kinase catalytic subunit regulates ligation of DNA ends. *Nucleic Acids Research* 32:4351-4357.

Bradshaw, P.S., D.J.Stavropoulos, and M.S.Meyn. 2005. Human telomeric protein TRF2 associates with genomic double-strand breaks as an early response to DNA damage. *Nature Genetics* 37:193-197.

Budman, J., S.A.Kim, and G.Chu. 2007. Processing of DNA for nonhomologous end-joining is controlled by kinase activity and XRCC4/Ligase IV. *Journal of Biological Chemistry* 282:11950-11959.

Buis, J., Y.P.Wu, Y.B.Deng, J.Leddon, G.Westfield, M.Eckersdorff, J.M.Sekiguchi, S.Chang, and D.O.Ferguson. 2008b. Mre11 nuclease activity has essential roles in DNA repair and genomic stability distinct from ATM activation. *Cell* 135:85-96.

Buis, J., Y.P.Wu, Y.B.Deng, J.Leddon, G.Westfield, M.Eckersdorff, J.M.Sekiguchi, S.Chang, and D.O.Ferguson. 2008a. Mre11 nuclease activity has essential roles in DNA repair and genomic stability distinct from ATM activation. *Cell* 135:85-96.

Burma, S., B.P.C.Chen, and D.J.Chen. 2006. Role of non-homologous end joining (NHEJ) in maintaining genomic integrity. *Dna Repair* 5:1042-1048.

Celeste, A., O.Fernandez-Capetillo, M.J.Kruhlak, D.R.Pilch, D.W.Staudt, A.Lee, R.F.Bonner, W.M.Bonner, and A.Nussenzweig. 2003. Histone H2AX phosphorylation is dispensable for the initial recognition of DNA breaks. *Nat. Cell Biol.* 5:675-679.

Chen, B.P.C., N.Uematsu, J.Kobayashi, Y.Lerenthal, A.Krempler, H.Yajima, M.Lobrich, Y.Shiloh, and D.J.Chen. 2007. Ataxia telangiectasia mutated (ATM) is essential for DNA-PKcs phosphorylations at the Thr-2609 cluster upon DNA double strand break. *Journal of Biological Chemistry* 282:6582-6587.

Collins, A.R. 2004. The comet assay for DNA damage and repair - Principles, applications, and limitations. *Mol. Biotechnol.* 26:249-261.

Collins, A.R., V.L.Dobson, M.Dusinska, G.Kennedy, and R.Stetina. 1997. The comet assay: What can it really tell us? *Mutat. Res.* 375:183-193.

Collins, A.R., A.A.Oscoz, G.Brunborg, I.Gaivao, L.Giovannelli, M.Kruszewski, C.C.Smith, and R.Stetina. 2008. The comet assay: topical issues. *Mutagenesis* 23:143-151.

Cremer, T. and C.Cremer. 2001. Chromosome territories, nuclear architecture and gene regulation in mammalian cells. *Nat. Rev. Genet.* 2:292-301.

Cui, X.P., Y.P.Yu, S.Gupta, Y.M.Cho, S.P.Lees-Miller, and K.Meek. 2005. Autophosphorylation of DNA-dependent protein kinase regulates DNA end processing and may also alter double-strand break repair pathway choice. *Molecular and Cellular Biology* 25:10842-10852.

de With, A. and K.O.Greulich. 1995. Wavelength dependence of laser-induced DNA damage in lymphocytes observed by single-cell gel electrophoresis. *J. Photochem. Photobiol. B* 30:71-76.

Desai, N., E.Davis, P.O'Neill, M.Durante, E.A.Cucinotta, and H.Wu. 2005. Immunofluorescence detection of clustered gamma-H2AX foci induced by HZE-particle radiation. *Radiation Research* 164:518-522.

Dinant, C., M.de Jager, J.Essers, W.A.van Cappellen, R.Kanaar, A.B.Houtsmuller, and W.Vermeulen. 2007. Activation of multiple DNA repair pathways by sub-nuclear damage induction methods. *J. Cell Sci.* 120:2731-2740.

Ding, Q., Y.V.R.Reddy, W.Wang, T.Woods, P.Douglas, D.A.Ramsden, S.P.Lees-Miller, and K.Meek. 2003. Autophosphorylation of the catalytic subunit of the DNA-dependent protein kinase is required for efficient end processing during DNA double-strand break repair. *Molecular and Cellular Biology* 23:5836-5848.

Dynan, W.S. and S.Yoo. 1998. Interaction of Ku protein and DNA-dependent protein kinase catalytic subunit with nucleic acids. *Nucleic Acids Research* 26:1551-1559.

Essers, J., W.Vermeulen, and A.B.Houtsmuller. 2006. DNA damage repair: anytime, anywhere? *Curr. Opin. Cell Biol.* 18:240-246.

Greubel, C., V.Hable, G.A.Drexler, A.Hauptner, S.Dietzel, H.Strickfaden, I.Baur, R.Krucken, T.Cremer, G.Dollinger, and A.A.Friedl. 2008. Competition effect in DNA damage response. *Radiation and Environmental Biophysics* 47:423-429.

Greulich, K.O. 1999. Micromanipulation by Light in Biology and Medicine - The laser microbeam and optical tweezers. Birkhaeuser, Basel, Switzerland.

Gulston, M., J.Fulford, T.Jenner, C.de Lara, and P.O'Neill. 2002. Clustered DNA damage induced by radiation in human fibroblasts (HF19), hamster (V79-4) cells and plasmid DNA is revealed as Fpg and Nth sensitive sites. *Nucleic Acids Res.* 30:3464-3472.

Hamada, N., G.Schettino, G.Kashino, M.Vaid, K.Suzuki, S.Kodama, B.Vojnovic, M.Folkard, M.Watanabe, B.D.Michael, and K.M.Prise. 2006. Histone H2AX phosphorylation in normal human cells irradiated with focused ultrasoft X rays: Evidence for chromatin movement during repair. *Radiation Research* 166:31-38.

Hauptner, A., T.Cremer, M.Deutsch, S.Dietzel, G.A.Drexler, C.Greubel, V.Hable, R.Krucken, R.Lowe, H.Strickfaden, G.Dollinger, and A.A.Friedl. 2006. Irradiation of living cells with single ions at the ion microprobe SNAKE. *Acta Physica Polonica A* 109:273-278.

Heiss, M., B.E.Fischer, B.Jakob, C.Fournier, G.Becker, and G.Taucher-Scholz. 2006. Targeted irradiation of Mammalian cells using a heavy-ion microprobe. *Radiat. Res.* 165:231-239.

Hill, J.W. and M.K.Evans. 2006. Dimerization and opposite base-dependent catalytic impairment of polymorphic S326COGG1 glycosylase. *Nucleic Acids Research* 34:1620-1632.

Hoeijmakers, J.H. 2001. Genome maintenance mechanisms for preventing cancer. *Nature* 411:366-374.

Huen, M.S. and J.Chen. 2008. The DNA damage response pathways: at the crossroad of protein modifications. *Cell Research* 18:8-16.

Jakob, B., J.H.Rudolph, N.Gueven, M.E.Lavin, and G.Taucher-Scholz. 2005. Live cell imaging of heavy-ion-induced radiation responses by beamline microscopy. *Radiation Research* 163:681-690.

Karagiannis, T.C. and A.El Osta. 2007. Chromatin modifications and DNA double-strand breaks: the current state of play. *Leukemia* 21:195-200.

Kim, J.S., T.B.Krasieva, H.Kurumizaka, D.J.Chen, A.M.Taylor, and K.Yokomori. 2005. Independent and sequential recruitment of NHEJ and HR factors to DNA damage sites in mammalian cells. *J. Cell Biol.* 170:341-347.

Klaude, M., S.Eriksson, J.Nygren, and G.Ahnstrom. 1996. The comet assay: Mechanisms and technical considerations. *Mutat. Res.* 363:89-96.

Koike, M. and A.Koike. 2008. Accumulation of Ku80 proteins at DNA double-strand breaks in living cells. *Experimental Cell Research* 314:1061-1070.

Konig, K., I.Riemann, P.Fischer, and K.J.Halbhuber. 1999. Intracellular nanosurgery with near infrared femtosecond laser pulses. *Cell Mol. Biol. (Noisy. -le-grand)* 45:195-201.

Kruhlak, M.J., A.Celeste, G.Dellaire, O.Fernandez-Capetillo, W.G.Muller, J.G.McNally, D.P.Bazett-Jones, and A.Nussenzweig. 2006. Changes in chromatin structure and mobility in living cells at sites of DNA double-strand breaks. *Journal of Cell Biology* 172:823-834.

Lan, L., S.Nakajima, K.Komatsu, A.Nussenzweig, A.Shimamoto, J.Oshima, and A.Yasui. 2005. Accumulation of Werner protein at DNA double-strand breaks in human cells. *J. Cell Sci.* 118:4153-4162.

Lavin, M.F. 2007. ATM and the Mre11 complex combine to recognize and signal DNA double-strand breaks. *Oncogene* 26:7749-7758.

Lee, J.H. and T.T.Paull. 2007. Activation and regulation of ATM kinase activity in response to DNA double-strand breaks. *Oncogene* 26:7741-7748.

Lee, K.J., J.R.Huang, Y.Takeda, and W.S.Dynan. 2000. DNA ligase IV and XRCC4 form a stable mixed tetramer that functions synergistically with other repair factors in a cell-free end-joining system. *Journal of Biological Chemistry* 275:34787-34796.

Lenser,T. Early Birds in DNA-Repair: Aspects of Real-Time Accumulation Kinetics of Ku80 and XRCC4. 2007. Friedrich-Schiller-Universität Jena.

Ref Type: Thesis/Dissertation

Levin, J.M., E.Jost, and P.R.Cook. 1978. Dissociation of Nuclear Proteins from Superhelical Dna. *J. Cell. Sci.* 29:103-116.

Li, L.L. and N.H.Yeh. 1992. Cell Cycle-Dependent Migration of the Dna-Binding Protein Ku80 Into Nucleoli. *Experimental Cell Research* 199:262-268.

Li, X. and W.D.Heyer. 2008. Homologous recombination in DNA repair and DNA damage tolerance. *Cell Research* 18:99-113.

Lisby, M., U.H.Mortensen, and R.Rothstein. 2003. Colocalization of multiple DNA double-strand breaks at a single Rad52 repair centre. *Nature Cell Biology* 5:572-577.

Lou, Z.K., B.P.C.Chen, A.Asaithamby, K.Minter-Dykhouse, D.J.Chen, and J.J.Chen. 2004. MDC1 regulates DNA-PK autophosphorylation in response to DNA damage. *Journal of Biological Chemistry* 279:46359-46362.

Lukas, C., J.Bartek, and J.Lukas. 2005. Imaging of protein movement induced by chromosomal breakage: tiny 'local' lesions pose great 'global' challenges. *Chromosoma* 114:146-154.

Lukas, C., J.Falck, J.Bartkova, J.Bartek, and J.Lukas. 2003. Distinct spatiotemporal dynamics of mammalian checkpoint regulators induced by DNA damage. *Nature Cell Biology* 5:255-U12.

Lukas, C., F.Melander, M.Stucki, J.Falck, S.Bekker-Jensen, M.Goldberg, Y.Lerenthal, S.P.Jackson, J.Bartek, and J.Lukas. 2004. Mdc1 couples DNA double-strand break recognition by Nbs1 with its H2AX-dependent chromatin retention. *Embo Journal* 23:2674-2683.

Ma, Y.M., U.Pannicke, H.H.Lu, D.Niewolik, K.Schwarz, and M.R.Lieber. 2005. The DNA-dependent protein kinase catalytic subunit phosphorylation sites in human artemis. *Journal of Biological Chemistry* 280:33839-33846.

Mailand, N., S.Bekker-Jensen, H.Faustrup, F.Melander, J.Bartek, C.Lukas, and J.Lukas. 2007. RNF8 ubiquitylates histones at DNA double-strand breaks and promotes assembly of repair proteins. *Cell* 131:887-900.

Mari, P.O., B.I.Florea, S.P.Persengiev, N.S.Verkaik, H.T.Brueggenwirth, M.Modesti, G.Giglia-Mari, K.Bezstarosti, J.A.A.Demmers, T.M.Luider, A.B.Houtsmuller, and D.C.van Gent. 2006. Dynamic assembly of end-joining complexes requires interaction between Ku70/80 and XRCC4. *Proceedings of the National Academy of Sciences of the United States of America* 103:18597-18602.

Meldrum, R.A., S.W.Botchway, C.W.Wharton, and G.J.Hirst. 2003. Nanoscale spatial induction of ultraviolet photoproducts in cellular DNA by three-photon near-infrared absorption. *EMBO Rep.* 4:1144-1149.

Miyazaki, T., D.A.Bressan, M.Shinohara, J.E.Haber, and A.Shinohara. 2004. In vivo assembly and disassembly of Rad51 and Rad52 complexes during double-strand break repair. *Embo Journal* 23:939-949.

Mizuta, R., H.L.Cheng, Y.J.Gao, and F.W.Alt. 1997. Molecular genetic characterization of XRCC4 function. *International Immunology* 9:1607-1613.

Mohanty, S.K., A.Rapp, S.Monajembashi, P.K.Gupta, and K.O.Greulich. 2002. Comet assay measurements of DNA damage in cells by laser microbeams and trapping beams with wavelengths spanning a range of 308 nm to 1064 nm. *Radiat. Res.* 157:378-385.

Mortusewicz, O., L.Schermelleh, J.Walter, M.C.Cardoso, and H.Leonhardt. 2005. Recruitment of DNA methyltransferase I to DNA repair sites. *Proceedings of the National Academy of Sciences of the United States of America* 102:8905-8909.

Olive, P.L., D.Wlodek, R.E.Durand, and J.P.Banath. 1992. Factors influencing DNA migration from individual cells subjected to gel electrophoresis. *Exp. Cell Res.* 198:259-267.

Ostling, O. and K.J.Johanson. 1984. Microelectrophoretic study of radiation-induced DNA damages in individual mammalian cells. *Biochem. Biophys. Res. Commun.* 123:291-298.

Ostling, O. and K.J.Johanson. 1987. Bleomycin, in Contrast to Gamma-Irradiation, Induces Extreme Variation of Dna Strand Breakage from Cell to Cell. *International Journal of Radiation Biology* 52:683-691.

Postow, L., C.Ghenoiu, E.M.Woo, A.N.Krutchinsky, B.T.Chait, and H.Funabiki. 2008. Ku80 removal from DNA through double strand break-induced ubiquitylation. *Journal of Cell Biology* 182:467-479.

Prise, K.M., O.V.Belyakov, M.Folkard, and B.D.Michael. 1998. Studies of bystander effects in human fibroblasts using a charged particle microbeam. *Int. J. Radiat. Biol.* 74:793-798.

Rapp, A. and K.O.Greulich. 2004. After double-strand break induction by UV-A, homologous recombination and nonhomologous end joining cooperate at the same DSB if both systems are available. *Journal of Cell Science* 117:4935-4945.

Rivero, M.T., F.Vazquez-Gundin, L.Muriel, V.Goyanes, J.Gosalvez, and J.L.Fernandez. 2003. Patterns of DNA migration in two-dimensional single-cell gel electrophoresis analyzed by DNA breakage detection-fluorescence in situ hybridization. *Environ. Mol. Mutagen.* 42:223-227.

Rodrigue, A., M.Lafrance, M.C.Gauthier, D.McDonald, M.Hendzel, S.C.West, M.Jasin, and J.Y.Masson. 2006. Interplay between human DNA repair proteins at a unique double-strand break in vivo. *Embo Journal* 25:222-231.

Rogakou, E.P., C.Boon, C.Redon, and W.M.Bonner. 1999. Megabase chromatin domains involved in DNA double-strand breaks in vivo. *J. Cell Biol.* 146:905-916.

Rogakou, E.P., D.R.Pilch, A.H.Orr, V.S.Ivanova, and W.M.Bonner. 1998. DNA double-stranded breaks induce histone H2AX phosphorylation on serine 139. *J. Biol. Chem.* 273:5858-5868.

Sartori, A.A., C.Lukas, J.Coates, M.Mistrik, S.Fu, J.Bartek, R.Baer, J.Lukas, and S.P.Jackson. 2007. Human CtIP promotes DNA end resection. *Nature* 450:509-5U6.

Shiloh, Y. 2003. ATM and related protein kinases: Safeguarding genome integrity. *Nature Reviews Cancer* 3:155-168.

Shrivastav, M., L.P.De Haro, and J.A.Nickoloff. 2008. Regulation of DNA double-strand break repair pathway choice. *Cell Research* 18:134-147.

Singh, N.P. and R.E.Stephens. 1997. Microgel electrophoresis: sensitivity, mechanisms, and DNA electrostretching. *Mutat. Res.* 383:167-175.

Singh, N.P., R.E.Stephens, H.Singh, and H.Lai. 1999a. Visual quantification of DNA double-strand breaks in bacteria. *Mutat. Res.* 429:159-168.

Singh, N.P., R.E.Stephens, H.Singh, and H.Lai. 1999b. Visual quantification of DNA double-strand breaks in bacteria. *Mutat. Res.* 429:159-168.

Soutoglou, E., J.F.Dorn, K.Sengupta, M.Jasin, A.Nussenzweig, T.Ried, G.Danuser, and T.Misteli. 2007. Positional stability of single double-strand breaks in mammalian cells. *Nature Cell Biology* 9:675-U121.

Stucki, M. and S.P.Jackson. 2006. gamma H2AX and MDC1: Anchoring the DNA-damage-response machinery to broken chromosomes. *Dna Repair* 5:534-543.

Sung, P. and H.Klein. 2006. Mechanism of homologous recombination: mediators and helicases take on regulatory functions. *Nature Reviews Molecular Cell Biology* 7:739-750.

Tartier, L., C.Spenlehauer, H.C.Newman, M.Folkard, K.M.Prise, B.D.Michael, J.Menissier-de Murcia, and G.de Murcia. 2003. Local DNA damage by proton microbeam irradiation induces poly(ADP-ribose) synthesis in mammalian cells. *Mutagenesis* 18:411-416.

Tashiro, S., J.Walter, A.Shinohara, N.Kamada, and T.Cremer. 2000. Rad51 accumulation at sites of DNA damage and in postreplicative chromatin. *J. Cell Biol.* 150:283-291.

Uematsu, N., E.Weterings, K.Yano, K.Morotomi-Yano, B.Jakob, G.Taucher-Scholz, P.O.Mari, D.C.van Gent, B.P.C.Chen, and D.J.Chen. 2007. Autophosphorylation of DNA-PKCS regulates its dynamics at DNA double-strand breaks. *Journal of Cell Biology* 177:219-229.

van Gent, D.C. and M.Van der Burg. 2007. Non-homologous end-joining, a sticky affair. *Oncogene* 26:7731-7740.

Vispe, S. and M.S.Satoh. 2000. DNA repair patch-mediated double strand DNA break formation in human cells. *J. Biol. Chem.* 275:27386-27392.

Walker, J.R., R.A.Corpina, and J.Goldberg. 2001. Structure of the Ku heterodimer bound to DNA and its implications for double-strand break repair. *Nature* 412:607-614.

Walter, J., T.Cremer, K.Miyagawa, and S.Tashiro. 2003. A new system for laser-UVA-microirradiation of living cells. *J. Microsc.* 209:71-75.

Werner, D. and C.Petzelt. 1981. Alkali-Stably Bound Proteins in Eukaryotic and Prokaryotic Dnas Show Common Characteristics. *J. Mol. Biol.* 150:297-302.

Weterings, E. and D.J.Chen. 2007. DNA-dependent protein kinase in nonhomologous end joining: a lock with multiple keys? *Journal of Cell Biology* 179:183-186.

Weterings, E. and D.J.Chen. 2008. The endless tale of non-homologous end-joining. *Cell Research* 18:114-124.

Weterings, E. and D.C.van Gent. 2004. The mechanism of non-homologous end-joining: a synopsis of synapsis. *Dna Repair* 3:1425-1435.

Weterings, E., N.S.Verkaik, H.T.Bruggenwirth, J.H.J.Hoeijmakers, and D.C.van Gent. 2003. The role of DNA dependent protein kinase in synapsis of DNA ends. *Nucleic Acids Research* 31:7238-7246.

Williams, R.S., G.Moncalian, J.S.Williams, Y.Yamada, O.Limbo, D.S.Shin, L.M.Groocock, D.Cahill, C.Hitomi, G.Guenther, D.Moiani, J.P.Carney, P.Russell, and J.A.Tainer. 2008. Mre11 dimers coordinate DNA end bridging and nuclease processing in double-strand-break repair. *Cell* 135:97-109.

Williams, R.S., J.S.Williams, and J.A.Tainer. 2007. Mre11-Rad50-Nbs1 is a keystone complex connecting DNA repair machinery, double-strand break signaling, and the chromatin template. *Biochemistry and Cell Biology-Biochimie et Biologie Cellulaire* 85:509-520.

Wood, R.D., M.Mitchell, and T.Lindahl. 2005. Human DNA repair genes, 2005. *Mutation Research-Fundamental and Molecular Mechanisms of Mutagenesis* 577:275-283.

Wood, R.D., M.Mitchell, J.Sgouros, and T.Lindahl. 2001. Human DNA repair genes. *Science* 291:1284-1289.

Wu, D.L., L.M.Topper, and T.E.Wilson. 2008. Recruitment and dissociation of nonhomologous end joining proteins at a DNA double-strand break in Saccharomyces cerevisiae. *Genetics* 178:1237-1249.

Wyman, C. and R.Kanaar. 2006. DNA double-strand break repair: All's well that ends well. *Annual Review of Genetics* 40:363-383.

Yajima, H., K.J.Lee, and B.P.C.Chen. 2006. ATR-dependent phosphorylation of DNA-dependent protein kinase catalytic subunit in response to UV-induced replication stress. *Molecular and Cellular Biology* 26:7520-7528.

Yang, Y.G., A.Saidi, P.O.Frappart, W.Min, C.Barrucand, V.Dumon-Jones, J.Michelon, Z.Herceg, and Z.Q.Wang. 2006. Conditional deletion of Nbs1 in murine cells reveals its role in branching repair pathways of DNA double-strand breaks. *Embo Journal* 25:5527-5538.

Yano, K. and D.J.Chen. 2008. Live cell imaging of XLF and XRCC4 reveals a novel view of protein assembly in the non-homologous end-joining pathway. *Cell Cycle* 7:1321-1325.

Yano, K.I., K.Morotomi-Yano, S.Y.Wang, N.Uematsu, K.J.Lee, A.Asaithamby, E.Weterings, and D.J.Chen. 2008. Ku recruits XLF to DNA double-strand breaks. *Embo Reports* 9:91-96.

Yurchenko, V., Z.Xue, and M.J.Sadofsky. 2006. SUMO modification of human XRCC4 regulates its localization and function in DNA double-strand break repair. *Molecular and Cellular Biology* 26:1786-1794.

6. Appendix

6.1. Abbreviations

ATM	Ataxia Telangiectasia Mutated
ATR	Ataxia-Telangiectasia and Rad3-related
(E)GFP	(Enhanced) Green Fluorescent Protein
BLM	Bleomycin
BP	Band Pass
bp	Base Pair
BSA	Bovine Serum Albumin
CA	Comet-Assay
Cat.	Category
cDNA	Coding DNA
CPD	Cyclobutane Pyrimidine Dimers
CW	Continous Wave
DABCO	1,4-diazabicyclo[2.2.2]octane
DAPI	4',6-diamidino-2-phenylindole
DMEM	Dulbecco´S Modified Eagle Medium
DNA	Deoxyribo-Nucleic Acid
DNA-PKcs	DNA Dependent Protein Kinase Catalytic Subunit
DSB	Double Strand Break
DTT	Dithiothreitol
E.coli	*Escherichia Coli*
EDTA	Ethylenediaminetetraacetic Acid
FCS	Fetal Calf Serum
G418	Geneticin
H2AX	H2A Histone, Member X

γ-H2AX	Phosphorylated Histone H2AX
Gy	Gray
HeNe	Helium-Neon
HRP	Horseradish Peroxidase
HRR	Homologous Recombination Repair
IFCA	Immunofluorescent Comet-Assay
kb	Kilobase
K_d	Dissociation Constant
Ku80	X-ray Repair, Complementing Defective, in Chinese Hamster, 5
Lig4	Ligase 4
LP	Long Pass
LSM	Laser Scanning Microscope
mRFP	Monomeric Red Fluorescent Protein
MDC1	Mediator of DNA Damage Checkpoint Protein 1
MRE11	Meiotic Recombination 11
MRN complex	Mre11/Rad50/Nbs1 Complex
NA	Numeric Aperture
NBS1	Nijmegen Breakage Syndrome
Nd:YAG	Neodymium-Doped Yttrium Aluminium Garnet
Nd:YLF	Neodymium-Doped Yttrium Lithium Fluoride
NHEJ	Non-Homologous End Joining
PAGE	Polyacrylamide Gel Electrophoresis
PBS	Phosphate Buffered Saline
PCR	Polymerase Chain Reaction
PFGE	Pulsed Field Gel Electrophoresis
RNA	Ribonucleic Acid
RNase	Ribonuclease
ROI	Region Of Interest
ROS	Reactive Oxygen Species
rpm	Rotations per Minute
RPMI	Cell Culture Medium (Roswell Park Memorial Institute)
RT-PCR	Reverse Transcriptase PCR
SDS	Sodium Dodecyl Sulfate
SSB	Single Strand Break

TEMED	Tetramethyl-1,2-Diaminoethane
Ti:Sa	Titanium:Sapphire
Tris	Tris(Hydroxymethyl)Aminomethane
Triton X-100	Octylphenoldecaethylenglycolether
Tween 20	Polyoxyethylensorbitanmonolaurat
U-2 OS	Human Osteosarcoma Cell Line
UV-A	Ultraviolet Light (320 - 400 Nm)
XLF	Xrcc4-like Factor
XRCC4	X-ray Repair, Complementing Defective, in Chinese Hamster, 4

6.2. Buffers and solutions

BUFFER	SUBSTANCE	END CONCEN-TRATION	AMOUNT
6x DNA Loading Buffer	Tris HCl, 0.5 M, pH 7.5	20 mM	400 µl
	Glyerol	20%	3 ml
	Bromphenol Blue	0.25%	25 mg
	Xylene cyanol	0.25%	25 mg
	dH_2O	-	up to 10 ml
10x FA Gel-Buffer, pH 7.0	MOPS	200 mM	41.8 g
	Natrium acetate	50 mM	6.8 g
	EDTA	10 mM	3.7 g
	DEPC water	-	up to 1000 ml
1x FA Running-Buffer	10x FA Gel-Buffer	1x	100 ml
	Formaldehyde 37%	0.75%	20 ml
	DEPC water	-	up to 1000 ml
Fixation Solution	Formaldehyde	3.7%	37 µl
	Triton X-100 1% Stock	0.1%	100 µl
	PBS	-	up to 1 ml
10x PBS, pH 7.4	NaCl	137 mM	80.0 g
	KCl	2.7 mM	2.0 g
	Na_2HPO_4	10 mM	17.8 g
	KH_2PO_4	2 mM	2.73 g
	dH_2O	-	up to 1000 ml
1x PBS	10x PBS, pH7.4	1x	100 ml
	dH_2O	-	up to 1000 ml
1x PBS-T 0.05%	10x PBS, pH7.4	1x	100 ml
	Tween 20	0.05%	500 µl
	dH_2O	-	900 ml
1x PBS-T 0.1%	10x PBS, pH7.4	1x	100 ml
	Tween 20	0.1%	1000 µl
	dH_2O	-	900 ml
DABCO Antifade	DABCO	2 mM	223 mg
	1M tris-HCl (pH8)	2 %	0.2 ml
	Glycerol	90 %	9 ml
	dH_2O	8 %	0.8 ml
Permeabilization Solution	Saponine 1%Stock (10 mg in 1 ml PBS)	0.01%	10 µl
	Triton X-100 1% Stock	0.7%	700 µl

	PBS	-	up to 1 ml
10x RNA Loading Buffer	Bromphenol Blue Solution	0.002%	20 mg
	EDTA 500 mM, pH 8.0	4 mM	80 µl
	Formaldehyde 37%	2.7%	720 µl
	Glyerol	20%	2 ml
	Formamide	30%	3.084 ml
	10x FA Gel Buffer	4x	4 ml
	DEPC water	-	up to 10 ml
RPMI Medium	RPMI Medium	88.5%	177 ml
	FCS	10%	20 ml
	2 Mercaptoethanol 10 mM	0.05 mM	1 ml
	Penicillin/Streptomycin	1%	2 ml
1x SDS Gel Destaining Buffer for Commassie	Acetic Acid	10%	100 ml
	Ethanol	10%	200 ml
	dH_2O	-	up to 1000 ml
1x SDS Gel Drying Buffer	Glycerin	10%	100 ml
	Methanol	20%	200 ml
	dH_2O	-	up to 1000 ml
6x SDS Loading Buffer	Tris HCl, pH6.8	0.27 M	425 mg
	Glycerol	60%	6 ml
	SDS	6%	0.6 g
	Bromphenolblau	0.12%	12 mg
	DTT	0.3 M	Fresh 46 mg/ml
	dH_2O	-	4 ml
5x SDS Running Buffer, pH 8.8	Tris-Base	500 mM	60.6 g
	Glycin	1.52 M	114 g
	SDS	1%	10 g
	dH_2O	-	up to 1000 ml
Separating Gel (for 4 gels 10%)	Acryl-Bisacrylamid (29:1) 40%	13.3%	6.7 ml
	Tris HCl 3 M, pH 8.8	0.38 M	2.5 ml
	SDS 10%	0.1%	0.2 ml
	dH_2O	-	9.6 ml
	Ammonium persulphate 1.5%	0.075%	1 ml
	TEMED	0.05%	10 µl
Stacking Gel (for 4 gels)	Acryl-Bisacrylamid (29:1) 40%	6.4%	1.6 ml
	Tris HCl 0.5 M, pH 6.8	0.125 M	2.5 ml
	SDS 10%	0.1%	0.1 ml
	dH_2O	-	5 ml
	Ammonium persulphate 1.5%	0.12%	0.8 ml

	TEMED	0.1%	10 µl
50x TAE Buffer	Tris Base	2 M	242 g
	Acetic Acid	2 M	57.1 ml
	EDTA 0.5 M pH 8.0	50 mM	100 ml
	dH_2O	-	up to 1000 ml
1x TAE Buffer	50x TAE Buffer	1x	25 ml
	dH_2O	-	up to 1000 ml
10x Transfer Buffer, pH 8.8	Tris Base	250 mM	30.3 g
	Glycine	1.92 M	144.1 g
	dH_2O	-	up to 1000 ml
1x Transfer Buffer, pH 8.8	10x Tranfer Buffer	1x	100 ml
	Methanol	10%	100 ml
	dH_2O	-	up to 1000 ml
1x Whole Cell Protein Extraction Buffer Stock Solution	Tris-HCl 1 M pH 7.4	20 mM	4 ml
	$MgCl_2$ 0.5 M	1 mM	0.4 ml
	NaCl 5 M	500 mM	20 ml
	Glycerol 0.1 M	20 mM	40 ml
	NP40 0.1 M	0.5 mM	1 ml
	EDTA 0.5 M	1 mM	0.4 ml
	EGTA 0.2 M	1 mM	1 ml
	dH_2O	-	up to 200 ml
1x Whole Cell Protein Extraction Buffer	1x Whole Cell Protein Extraction Buffer Stock Solution	1x	1 ml
	DTT 1 M	1 mM	1 µl
	PMSF 0.5 M	1 mM	2 µl
	NaF 0.5 M	2.5 mM	5 µl
	Na_3VO4 0,1 M	0.2 mM	5 µl
	B-glycerolphosphate 1 M	1 mM	1 µl
Neutral lysis, pH8	EDTA	33 mM	10.7 g
	SDS	0.5 %	5 g
	dH_2O		Up to 1000 ml
Alkaline lysis	Tris, pH10 100 mM stock	10 mM	100 ml
	EDTA, 500 mM Stock	100 mM	200 ml
	NaCl	2.4 M	140.4 g
	N-Lauroylsarcosine Sodium salt	1 %	10 g
	NaOH	77.5 mM	3.1 g
	dH_2O		Up to 890 ml
	10% DMSO, and 1% Triton X-100 have to be added shortly before use		
1x TBE Buffer	Tris-base	90 mM	10.9 g
	Boric acid	90 mM	5.56 g

	EDTA	0.2 mM	0.74 g
	dH_2O		Up to 1000 ml
Alkaline electrophoresis pH13.1	NaOH, 1M stock	333 mM	300 ml
	EDTA, 500 mM stock	1 mM	2 ml
	dH_2O		Up to 1000 ml
Neutralisation 0.4 M tris, pH7.5	Tris-HCl	320 mM	50.8 g
	Tris-base	80 mM	9.44 g
	dH_2O		Up to 1000 ml
Tris 100 mM, pH10	Tris-base	100 mM	12.1 g
	dH2O		Up to 1000 ml
TE, pH7.4	Tris-HCl	10 mM	1.57 g
	EDTA	1 mM	0.37 g
	dH_2O		Up to 1000 ml
SYBR Green staining solution	DABCO-Antifadel	49.9 %	4990 ml
	TE-buffer(filtrated)	49.9 %	4990 ml
	SYBR Green (10,000x)	20x	20 µl
1× restriction reaction pH7.9	Potassium acetate	50 mM	
	Tris acetate	20 mM	
	Magnesium acetate	10 mM	
	DTT	1 mM	

6.3. Materials and Manufacturers

Antibodies

Primary Antibodies

53BP1 (NB-100-305)	Novus Biologicals, Littleton, USA
Cyclobutane pyrimidine dimers (mc-062)	Kamiya, Seattle, USA
DNA-PKcs (phospho Ser2056)	Abcam, Cambridge, UK
DNA-PKcs (phospho Ser2609)	Abcam, Cambridge, UK
GFP (sc-8334)	Santa Cruz Biotechnology, Santa Cruz, USA
Histone H1 (sc-8030)	Santa Cruz Biotechnology, Santa Cruz, USA
Ku80 (MS-285-P0)	Lab Vision, Suffolk
NBS1 (NB-100-143)	Novus Biologicals, Littleton, USA
OGG1 (915-020)	Biomol, Hamburg, GER
Rad51 (PC-130)	Calbiochem,
Rad51 (sc-8349)	Santa Cruz Biotechnology, Santa Cruz, USA
Tubulin-alpha (sc-5286)	Santa Cruz Biotechnology, Santa Cruz, USA
XRCC4 (ab2857)	Abcam, Cambridge, UK
γH2AX (05-636)	Upstate, Temecula, USA

Secondary Antibodies

anti-mouse IgG Alexa Fluor 488 (donkey, A21202)	Invitrogen, Karlsruhe, GER
anti-mouse IgG Alexa Fluor 594 (donkey, A21203)	Invitrogen, Karlsruhe, GER
anti-mouse IgG HRP (NA 931)	GE Healthcare, Buckinghamshire, UK
anti-rabbit IgG Alexa Fluor 488 (donkey, A21206)	Invitrogen, Karlsruhe, GER
anti-rabbit IgG Alexa Fluor 555 (donkey, A31572)	Invitrogen, Karlsruhe, GER
anti-rabbit IgG Alexa Fluor 494 (donkey, A11053)	Invitrogen, Karlsruhe, GER
anti-rabbit IgG HRP (goat, P0448)	DAKO, Hamburg, GER

Chemicals and Kits

AccuPrime™ *Pfx* DNA Polymerase Kit	Invitrogen, Karlsruhe, GER
Acetic acid	Roth, Karlsruhe, GER
Acetone	Roth, Karlsruhe, GER
Acryl-Bisacrylamid (29:1)	Roth, Karlsruhe, GER
Agarose type II	Sigma-Aldrich, Munich, GER
Agarose type VII	Sigma-Aldrich, Munich, GER
Ammonium persulphate	Sigma-Aldrich, Munich, GER
Bacto-Agar	Beckton Dickinson, Heidelberg, GER
B-glycerolphosphate	Sigma-Aldrich, Munich, GER
Boric acid	Roth, Karlsruhe, GER
Bovine Serum Albumine (Fraction V)	Sigma-Aldrich, Munich, GER
Bromphenol Blue	Sigma-Aldrich, Munich, GER
Butanol	Roth, Karlsruhe, GER
DABCO	Sigma-Aldrich, Munich, GER
DMSO	Roth, Karlsruhe, GER
DNA Standard Marker	Eurogentec, Seraing, Belgium
DTT	Sigma-Aldrich, Munich, GER
ECL Pierce Western Blotting Substrate	Perbio Science, Bonn, GER
ECL Plus Amersham Western Blotting Detection System	GE Healthcare, Buckinghamshire, GBR
EDTA	Roth, Karlsruhe, GER
EGTA	Sigma-Aldrich, Munich, GER
Ethanol	Roth, Karlsruhe, GER
Ethidium Bromide	SERVA, Heidelberg, GER
Fetal calf serum	PAA Laboratories, Pasching, AUT
Formaldehyde 37%	Sigma-Aldrich, Munich, GER
Formamide	Sigma-Aldrich, Munich, GER
FuGENE HD Transfection Reagent	Roche, Mannheim, GER
FuGENE 6 Transfection Reagent	Roche, Mannheim, GER
G418	Sigma-Aldrich, Munich, GER
Giemsa stain, Modified solution	Sigma-Aldrich, Munich, GER
Glycerol/ glycerine	Roth, Karlsruhe, GER
HiSpeed Plasmid Purification Midi and Mini Kits	QIAGEN, Hilden, GER
Hybond-ECL Nitrocellulose Membrane	GE Healthcare, Buckinghamshire, GBR
Hyperfilm ECL Amersham	GE Healthcare, Buckinghamshire, GBR
Isopropanol	Roth, Karlsruhe, GER
Kanamycin	Sigma-Aldrich, Munich, GER
Ampicillin	Sigma-Aldrich, Munich, GER

KCl	Sigma-Aldrich, Munich, GER
KH_2PO_4	Merck, Darmstadt, GER
Lambda DNA	New England Biolabs, Frankfurt a.M., GER
LB-medium capsules	Q-BIOgene, Morgane-Irvine, USA
Methanol	Roth, Karlsruhe, GER
2-mercaptoethanol	Merck, Darmstadt, GER
$MgCl_2$	Sigma-Aldrich, Munich, GER
MOPS	Roth, Karlsruhe, GER
Na Acetate	Sigma-Aldrich, Munich, GER
NaCl	Roth, Karlsruhe, GER
NaF	Roth, Karlsruhe, GER
Na_2HPO_4	Merck, Darmstadt, GER
NaH_2PO_4	Roth, Karlsruhe, GER
NaOH	Roth, Karlsruhe, GER
Na_3VO_4	Sigma-Aldrich, Munich, GER
N-Lauroylsarcosine Sodium salt solution	Fluka, Steinheim, GER
Nonfat dried milk powder	AppliChem, Darmstadt, GER
NP40	Sigma-Aldrich, Munich, GER
Top10 *E.coli* cells	Invitrogen, Karlsruhe, GER
OptiMEM 1 medium	Invitrogen, Karlsruhe, GER
PageRuler Prestainded Protein Ladder Plus	Fermentas, Vilniuse, LT
PCR Primers	Eurofins MWG Operon, Ebersberg, GER
pEGFP-C3/C1/N1, mammalian expression vectors	Clontech, Saint-Germain-en-Laye, Dann
Penicillin/Streptomycin Solution	Sigma-Aldrich, Munich, GER
PFGE marker, low range	New England Biolabs, Frankfurt a.M., GER
PMSF	Sigma-Aldrich, Munich, GER
PonceauS Concentrate	Roth, Karlsruhe, GER
ProLong Gold antifade reagent with DAPI	Invitrogen, Karlsruhe, GER
Protease Inhibitor Cocktail	Roche, Mannheim, GER
QIAprep Spin Miniprep Kit	QIAGEN, Hilden, GER
QIAquick Gel Extraction Kit	QIAGEN, Hilden, GER
Rneasy® Mini Kit	QIAGEN, Hilden, GER
Rotiphorese blauR brilliant blue concentrate	Roth, Karlsruhe, GER
RPMI 1640 Medium	Biochrom AG, Berlin, GER
Saponine	Sigma-Aldrich, Munich, GER
SDS	SERVA, Heidelberg, GER
Smart Ladder (Dann Standard)	Eurogentec, Köln, GER
Smart Ladder Small Fragment	Eurogentec, Köln, GER
Sodium Azide	Sigma-Aldrich, Munich, GER
SYBR Green	Invitrogen, Karlsruhe, GER

TEMED	Roth, Karlsruhe, GER
ThermoScript™ Reverse Transcriptase	Invitrogen, Karlsruhe, GER
Tris acetate	Roth, Karlsruhe, GER
Tris Base	Sigma-Aldrich, Munich, GER
Tris HCl	Roth, Karlsruhe, GER
Triton X-100	Sigma-Aldrich, Munich, GER
Trypsin/ EDTA Solution	Biochrom AG, Berlin, GER
Tween 20	Roth, Karlsruhe, GER
Xylene cyanol	Sigma-Aldrich, Munich, GER
YOYO-1	Invitrogen, Karlsruhe, GER

Technical Equipment and Materials

6-well plates	Greiner Bio-One, Frickehausen, GER
96-well plates	Thermo Fisher Scientific (Nalgene Nunc), Langenselbold, GER
Achromat objective	Zeiss, Jena, GER
Argus XI Version 5.0.10	biostep, Jahnsdorf, GER
AxioVert 135M	Zeiss, Jena, GER
AxioVert 100M	Zeiss, Jena, GER
AxioVert 200 ApoTome, ApoTome Slider module, Axiocam MRm	Zeiss, Jena, GER
Axiovision Software	Zeiss, Jena, GER
Bio-Imager DH-30132	biostep, Jahnsdorf, GER
BioPhotometer (Spectrophotometer)	Eppendorf, Hamburg, GER
Blot Paper extra thick	Bio-Rad Laboratories, Munich, GER
Cell culture incubator	Heraeus Instruments GmbH, Düsseldorf
Centrifuge Tubes 15ml, 50ml	Greiner Bio-One, Frickenhausen, GER
Clone Manager Professional Version 8	Sci-Ed Software, Cary, USA
Chambered Coverglasses with 1-8 chambers	Nunc, Lab-Tek™, Wiesbaden, GER
Coverslips round 12mm	Roth, Karlsruhe, GER
CTI-Controller 3700 *digital*	ReCon, Erbach, GER
Culture dishes	Greiner Bio-One GmbH, Solingen, GER
Culture flasks	Greiner Bio-One GmbH, Solingen, GER
Electrophoresis Chamber and Power Supply PAC 3000	Bio-Rad Laboratories, Munich, GER
Electrophoresis Chamber	ThermoFisher Scientific, OWL Separation Systems, Waltham, USA

Gammacell GC40 (CS^{137})	MDS Nordion, Kanata, CAN
Gradient attenuator	Laseroptik
ImageJ Version 1.40	Wayne Rasband, National Institutes of Health, USA
Lab-Shaker	Gerhardt, Königswinter, GER
Lab-Shaker Lab Therm	Adolf-Kühler AG, SUI
LSM 510	Zeiss, Jena, GER
LSM 510 Software	Zeiss, Jena, GER
L-Win Triton Control	Newport Spectra-Physics, Darmstadt, GER
Mastercycler Gradient	Eppendorf, Hamburg, GER
Microcentrifuge 5415C	Eppendorf, Hamburg, GER
Microplate Reader Model 3550	Bio-Rad Laboratories, Munich, GER
Microscope Slides, SuperFrost Plus	Menzel Gläser, Braunschweig, GER
Microscope Telaval 31	Zeiss, Jena, GER
Mini centrifuge C-1200	Labnet International, Windsor, GBR
Mini Protean® Sytem Western Blot	Bio-Rad Laboratories, Munich, GER
Mixer magnetic, heatable, RCT basic	Kika Labortechnik, Köln, GER
OriginPro 7.0	OriginLab Corporation, Northampton, USA
Parafilm „M“ Laboratory Film	American National Can™, Chicago, USA
pH-Meter CG837	Schott, Mainz, GER
Pipettes cell star (1-50ml)	Greiner Bio-One, Frickenhausen, GER
Pipettes Pipetman (P2-P5000)	Gilson, Limburg-Offheim, GER
Pipette tips (10-1000µl)	Roth, Karlsruhe, GER
Pipettes Research (10-1000µl)	Eppendorf, Hamburg, GER
Pipetus-akku	Hirschmann Laborgeräte, Eberstadt, GER
Plan-Neofluar objectives	Zeiss, Jena, GER
Processor Classic E.O.S.	AGFA Healthcare, Köln, GER
Pulse Picker	Newport Spectra-Physics, Darmstadt, GER
Reaction tubes (0.5-2ml)	Roth, Karlsruhe, GER
Sonificator Sonoplus HD70	Bandelin electronic, Berlin, GER
Steril Hood “Steril Gard Hood”	Baker Company Inc, Sanford, USA
tempcontrol 37-2 digital	PeCon, Erbach, GER
tempcontrol mini	PeCon, Erbach, GER
Thermomixer 5437	Eppendorf, Hamburg, GER
Thermocycler gradient	Eppendorf, Hamburg, GER
Trans-Blot SD Semi-Dry Transfer Cell	Bio-Rad Laboratories, Munich, GER
Triton UV Laser System (Nd:YLF, frequency tripled, 350nm)	Newport Spectra-Physics, Darmstadt, GER
Ti:Sapphire laser, Tsunami	Newport Spectra-Physics, Darmstadt, GER
Uvette (cuvettes)	Eppendorf, Hamburg, GER
VarioCam	PCO Computer Optics, Kelheim, GER

Vortex-Genie 2	Scientific Industries, Bohemia, USA
Waterbath, GFL	GFL Gesellschaft für Labortechnik mbH, Burgwedel, GER
Waterbath JulaboVC 12B	JULABO Labortechnik, Seelbach, GER

Restriction Enzymes and Reagents

AgeI (R0552S)	New England Biolabs, Frankfurt a.M., GER
AseI (R0526S)	New England Biolabs, Frankfurt a.M., GER
BamHI (10220612001)	Boehringer, Mannheim, GER
BbvCI (R0601S)	New England Biolabs, Frankfurt a.M., GER
BglI (404101)	Boehringer, Mannheim, GER
BglII (R0144S)	New England Biolabs, Frankfurt a.M., GER
BsrGI (R0575L)	New England Biolabs, Frankfurt a.M., GER
BstBI (R0519S)	New England Biolabs, Frankfurt a.M., GER
EcoRI (R101L)	New England Biolabs, Frankfurt a.M., GER
HaeII (693 928)	Boehringer, Mannheim, GER
HindIII (R0104S)	New England Biolabs, Frankfurt a.M., GER
NdeI (R0111S)	New England Biolabs, Frankfurt a.M., GER
NotI (R0189S)	New England Biolabs, Frankfurt a.M., GER
Nt.BbvCI (R0632S)	New England Biolabs, Frankfurt a.M., GER
PciI (V0275S)	SibEnzyme, RUS
PstI (621633)	Boehringer, Mannheim, GER
PvuII (642703)	Boehringer, Mannheim, GER
SacI (669806)	Boehringer, Mannheim, GER
SacII (R0156L)	New England Biolabs, Frankfurt a.M., GER
SalI (R0138L)	New England Biolabs, Frankfurt a.M., GER
SfiI (R0123S)	New England Biolabs, Frankfurt a.M., GER
SspI (10972967001)	Boehringer, Mannheim, GER
XbaI (10674257001)	Boehringer, Mannheim, GER
XhoI (R0146S)	New England Biolabs, Frankfurt a.M., GER
NEB Buffer 1 (B7002S)	New England Biolabs, Frankfurt a.M., GER
NEB Buffer 2 (B7002S)	New England Biolabs, Frankfurt a.M., GER
NEB Buffer 3 (B7002S)	New England Biolabs, Frankfurt a.M., GER
NEB Buffer 4 (B7004S)	New England Biolabs, Frankfurt a.M., GER
Puffer A (141 7959)	Boehringer, Mannheim, GER
Puffer H (141 7991)	Boehringer, Mannheim, GER

Puffer M (141 7983)	Boehringer, Mannheim, GER
100x BSA (B9001S)	New England Biolabs, Frankfurt a.M., GER
T4 DNA Ligase and Buffer	Invitrogen, Karlsruhe, GER

6.4. Sequencing

Here, the sequencing results of plasmids used in this work are presented. In all cases beginning and end of the coding sequence of protein of interest are given.

pEntr-OGG1

Mutation at position 1113 (977 in cDNA of gene) G is instead of C, marked with red background. This point mutation cause a change of amino acid in the protein from Serine to Cysteine at 326 site (S326C).

```
   1  GCAGGCTCCA CCATGGGAAC CAATTCAGTC GACGAAATGC CTGCCCGCGC GCTTCTGCCC
                 > START OGG1
  61  AGGCGCATGG GGCATCGTAC TCTAGCCTCC ACTCCTGCCC TGTGGGCCTC CATCCCGTGC
 121  CCTCGCTCTG AGCTGCGCCT GGACCTGGTT CTGCCTTCTG GACAATCTTT CCGGTGGAGG
 181  GAGCAAAGTC CTGCACACTG GAGTGGTGTA CTAGCGGATC AAGTATGGAC ACTGACTCAG
 241  ACTGAGGAGC AGCTCCACTG CACTGTGTAC CGAGGAGACA AGAGCCAGGC TAGCAGGCCC
 301  ACACCAGACG AGCTTGAGGC CGTGCGCAAG TACTTCCAGC TAGATGTTAC CCTGGCTCAA
 361  CTGTATCACC ACTGGGGTTC CGTGGACTCC CACTTCCAAG AGGTGGCTCA GAAATTCCAA
 421  GGTGTGCGAC TGCTGCGACA AGACCCCATC GAATGCCTTT TCTCTTTTAT CTGTTCCTCC
 481  AACAACAACA TCGCCCGCAT CACTGGCATG GTGGAGCGGC TGTGCCAGGC TTTTGGACCT
 541  CGGCTCATCC AGCTTGATGA TGTCACCTAC CATGGCTTCC CCAGCCTGCA GGCCCTGGCT
 601  GGGCCAGAGG TGGAGGCTCA TCTCAGGAAG CTGGGCCTGG GCTATCGTGC CCGTTACGTG
 661  AGTGCCAGTG CCCGAGCCAT CCTGGAAGAA CAGGGCGGGC TAGCCTGGCT GCAGCAGCTA
 721  CGAGAGTCCT CATATGAGGA GGCCCACAAG GCCCTCTGCA TCCTGCCTGG AGTGGGCACC
 781  AAGGTGGCTG ACTGCATCTG CCTGATGGCC CTAGACAAGC CCCAGGCTGT GCCCGTGGAT
 841  GTCCATATGT GGCACATTGC CCAACGTGAC TACAGCTGGC ACCCTACCAC GTCCCAGGCG
 901  AAGGGACCGA GCCCCCAGAC CAACAAGGAA CTGGGAAACT TTTTCCGGAG CCTGTGGGGA
 961  CCTTATGCTG GCTGGGCCCA AGCGGTGCTG TTCAGTGCCG ACCTGCGCCA ATGCCGCCAT
1021  GCTCAGGAGC CACCAGCAAA GCGCAGAAAG GGTTCCAAAG GGCCGGAAGG CTTGCGGCCG
                                                      END OGG1 >
1081  CACTCGAGAT ATCTAGACCC AGCTTTCTTG
```

pEGFPC3-XRCC4

```
   1  AGATCTCGAG CTCATGGAGA GAAAAATAAG CAGAATCCAC CTTGTTTCTG AACCCAGTAT
                    > START XRCC4
  61  AACTCATTTT CTACAAGTAT CTTGGGAGAA AACACTGGAA TCTGGTTTTG TTATTACACT
 121  TACTGATGGT CATTCAGCAT GGACTGGGAC AGTTTCTGAA TCAGAGATTT CCCAAGAAGC
 181  TGATGACATG GCAATGGAAA AAGGGAAATA TGTTGGTGAA CTGAGAAAAG CATTGTTGTC
 241  AGGAGCAGGA CCAGCTGATG TATACACGTT TAATTTTTCT AAAGAGTCTT GTTATTTCTT
 301  CTTTGAGAAA AACCTGAAAG ATGTCTCATT CAGACTTGGT TCCTTCAACC TAGAGAAAGT
 361  TGAAAACCCA GCTGAAGTCA TTAGAGAACT TATTTGTTAT TGCTTGGACA CCATTGCAGA
 421  AAATCAAGCC AAAAATGAGC ACCTGCAGAA AGAAAATGAA AGGCTTCTGA GAGATTGGAA
 481  TGATGTTCAA GGACGATTTG AAAAATGTGT GAGTGCTAAG GAAGCTTTGG AGACTGATCT
 541  TTATAAGCGG TTTATTCTGG TGTTGAATGA GAAGAAAACA AAAATCAGAA GTTTGCATAA
 601  TAAATTATTA AATGCAGCTC AAGAACGAGA AAAGGACATC AAACAAGAAG GGGAAACTGC
 661  AATCTGTTCT GAAATGACTG CTGACCGAGA TCCAGTCTAT GATGAGAGTA CTGATGAGGA
 721  AAGTGAAAAC CAAACTGATC TCTCTGGGTT GGCTTCAGCT GCTGTAAGTA AAGATGATTC
 781  CATTATTTCA AGTCTTGATG TCACTGATAT TGCACCAAGT AGAAAAAGGA GACAGCGAAT
 841  GCAAAGAAAT CTTGGGACAG AACCTAAAAT GGCTCCTCAG GAGAATCAGC TTCAAGAAAA
 901  GGAAAATTCT AGGCCTGATT CTTCACTACC TGAGACGTCT AAAAAGGAGC ACATCTCAGC
 961  TGAAAACATG TCTTTAGAAA CTCTGAGAAA CAGCAGCCCA GAAGACCTCT TTGATGAGAT
1021  TTTCCGCGGG CCCGGGATC
       > END XRCC4
```

pEGFPN1-Ku80

```
   1  GGCGTGTACG GTGGGAGGTC TATATAAGCA GAGCTGGTTT AGTGAACCGT CAGATCCGCT
  61  AGCGCTACCG GACTCAGATC TCGAGCTCAA GCTTCGAATT CTGCAGTCGA CGGTACCGCG
 121  GATGGTGCGG TCGGGGAATA AGGCAGCTGT TGTGCTGTGT ATGGACGTGG GCTTTACCAT
       > START KU80
 181  GAGTAACTCC ATTCCTGGTA TAGAATCCCC ATTTGAACAA GCAAAGAAGG TGATAACCAT
 241  GTTTGTACAG CGACAGGTGT TTGCTGAGAA CAAGGATGAG ATTGCTTTAG TCCTGTTTGG
 301  TACAGATGGC ACTGACAATC CCCTTTCTGG TGGGGATCAG TATCAGAACA TCACAGTGCA
 361  CAGACATCTG ATGCTACCAG ATTTTGATTT GCTGGAGGAC ATTGAAAGCA AAATCCAACC
 421  AGGTTCTCAA CAGGCTGACT TCCTGGATGC ACTAATCGTG AGCATGGATG TGATTCAACA
 481  TGAAACAATA GGAAAGAAGT TTGAGAAGAG GCATATTGAA ATATTCACTG ACCTCAGCAG
 541  CCGATTCAGC AAAAGTCAGC TGGATATTAT AATTCATAGC TTGAAGAAAT GTGACATCTC
 601  CCTGCAATTC TTCTTGCCTT TCTCACTTGG CAAGGAAGAT GGAAGTGGGG ACAGAGGAGA
 661  TGGCCCCTTT CGCTTAGGTG GCCATGGGCC TTCCTTTCCA CTAAAAGGAA TTACCGAACA
 721  GCAAAAAGAA GGTCTTGAGA TAGTGAAAAT GGTGATGATA TCTTTAGAAG GTGAAGATGG
 781  GTTGGATGAA ATTTATTCAT TCAGTGAGAG TCTGAGAAAA CTGTGCGTCT TCAAGAAAAT
 841  TGAGAGGCAT TCCATTCACT GGCCCTGCCG ACTGACCATT GGCTCCAATT TGTCTATAAG
 901  GATTGCAGCC TATAAATCGA TTCTACAGGA GAGAGTTAAA AAGACTTGGA CAGTTGTGGA
 961  TGCAAAAACC CTAAAAAAAG AAGATATACA AAAAGAAACA GTTTATTGCT TAAATGATGA
1021  TGATGAAACT GAAGTTTTAA AAGAGGATAT TATTCAAGGG TTCCGCTATG GAAGTGATAT
```

```
1081  AGTTCCTTTC TCTAAAGTGG ATGAGGAACA AATGAAATAT AAATCGGAGG GGAAGTGCTT
1141  CTCTGTTTTG GGATTTTGTA AATCTTCTCA GGTTCAGAGA AGATTCTTCA TGGGAAATCA
1201  AGTTCTAAAG GTCTTTGCAG CAAGAGATGA TGAGGCAGCT GCAGTTGCAC TTTCCTCCCT
1261  GATTCATGCT TTGGATGACT TAGACATGGT GGCCATAGTT CGATATGCTT ATGACAAAAG
1321  AGCTAATCCT CAAGTCGGCG TGGCTTTTCC TCATATCAAG CATAACTATG AGTGTTTAGT
1381  GTATGTGCAG CTGCCTTTCA TGGAAGACTT GCGGCAATAC ATGTTTTCAT CCTTGAAAAA
1441  CAGTAAGAAA TATGCTCCCA CCGAGGCACA GTTGAATGCT GTTGATGCTT TGATTGACTC
1501  CATGAGCTTG GCAAAGAAAG ATGAGAAGAC AGACACCCTT GAAGACTTGT TTCCAACCAC
1561  CAAAATCCCA AATCCTCGAT TTCAGAGATT ATTTCAGTGT CTGCTGCACA GAGCTTTACA
1621  TCCCCGGGAG CCTCTACCCC CAATTCAGCA GCATATTTGG AATATGCTGA ATCCTCCCGC
1681  TGAGGTGACA ACAAAAAGTC AGATTCCTCT CTCTAAAATA AAGACCCTTT TTCCTCTGAT
1741  TGAAGCCAAG AAAAAGGATC AAGTGACTGC TCAGGAAATT TTCCAAGACA ACCATGAAGA
1801  TGGACCTACA GCTAAAAAAT TAAAGACTGA GCAAGGGGGA GCCCACTTCA GCGTCTCCAG
1861  TCTGGCTGAA GGCAGTGTCA CCTCTGTTGG AAGTGTGAAT CCTGCTGAAA ACTTCCGTGT
1921  TCTAGTGAAA CAGAAGAAGG CCAGCTTTGA GGAAGCGAGT AACCAGCTCA TAAATCACAT
1981  CGAACAGTTT TTGGATACTA ATGAAACACC GTATTTTATG AAGAGCATAG ACTGCATCCG
2041  AGCCTTCCGG GAAGAAGCCA TTAAGTTTTC AGAAGAGCAG CGCTTTAACA ACTTCCTGAA
2101  AGCCCTTCAA GAGAAAGTGG AAATTAAACA ATTAAATCAT TTCTGGGAAA TTGTTGTCCA
2161  GGATGGAATT ACTCTGATCA CCAAAGAGGA AGCCTCTGGA AGTTCTGTCA CAGCTGAGGA
2221  AGCCAAAAAG TTTCTGGCCC CCAAAGACAA ACCAAGTGGA GACACAGCAG CTGTATTTGA
2281  AGAAGGTGGT GATGTGGACG ATTTATTGGA CATGATATTG GATCCACCGG TCGCCACCAT
                                        END KU80 >
```

pEGFPC3-NBS1

Sequencing is not complete. Not sequenced part is shown in red colour.

```
   1  ATTCTGCAGT CGACGGTACC GCGGGCCCGG CAGGAGGAGA ACCATACAGA CTTTTGACTG
                            < Start NBS1
  61  GCGTTGAGTA CGTTGTTGGA AGGAAAAACT GTGCCATTCT GATTGAAAAT GATCAGTCGA
 121  TCAGCCGAAA TCATGCTGTG TTAACTGCTA ACTTTTCTGT AACCAACCTG AGTCAAACAG
 181  ATGAAATCCC TGTATTGACA TTAAAAGATA ATTCTAAGTA TGGTACCTTT GTTAATGAGG
 241  AAAAAATGCA GAATGGCTTT TCCCGAACTT TGAAGTCGGG GGATGGTATT ACTTTTGGAG
 301  TGTTTGGAAG TAAATTCAGA ATAGAGTATG AGCCTTTGGT TGCATGCTCT TCTTGTTTAG
 361  ATGTCTCTGG GAAAACTGCT TTAAATCAAG CTATATTGCA ACTTGGAGGA TTTACTGTAA
 421  ACAATTGGAC AGAAGAATGC ACTCACCTTG TCATGGTATC AGTGAAAGTT ACCATTAAAA
 481  CAATATGTGC ACTCATTTGT GGACGTCCAA TTGTAAAGCC AGAATATTTT ACTGAATTCC
 541  TGAAAGCAGT TGAGTCCAAG AAGCAGCCTC CACAAATTGA AAGTTTTTAC CCACCTCTTG
 601  ATGAACCATC TATTGGAAGT AAAAATGTTG ATCTGTCAGG ACGGCAGGAA AGAAAACAAA
 661  TCTTCAAAGG GAAAACATTT ATATTTTTGA ATGCCAAACA GCATAAGAAA TTGAGTTCCG
 721  CAGTTGTCTT TGGAGGTGGG GAAGCTAGGT TGATAACAGA AGAGAATGAA GAAGAACATA
 781  ATTTCTTTTT GGCTCCGGGA ACGTGTGTTG TTGATACAGG AATAACAAAC TCACAGACCT
 841  TAATTCCTGA CTGTCAGAAG AAATGGATTC AGTCAATAAT GGATATGCTC CAAAGGCAAG
```

```
 901  GTCTTAGACC TATTCCTGAA GCAGAAATTG GATTGGCGGT GATTTTCATG ACTACAAAGA
 961  ATTACTGTGA TCCTCAGGGC CATCCCAGTA CAGGATTAAA GACAACAACT CCAGGACCAA
1021  GCCTTTCACA AGGCGTGTCA GTTGATGAAA AACTAATGCC AAGCGCCCCA GTGAACACTA
1081  CAACATACGT AGCTGACACA GAATCAGAGC AAGCAGATAC ATGGGATTTG AGTGAAAGGC
1141  CAAAAGAAAT CAAAGTCTCC AAAATGGAAC AAAAATTCAG AATGCTTTCA CAAGATGCAC
1201  CCACTGTAAA GGAGTCCTGC AAAACAAGCT CTAATAATAA TAGTATGGTA TCAAATACTT
1261  TGGCTAAGAT GAGAATCCCA AACTATCAGC TTTCACCAAC TAAATTGCCA AGTATAAATA
1321  AAAGTAAAGA TAGGGCTTCT CAGCAGCAGC AGACCAACTC CATCAGAAAC TACTTTCAGC
1381  CGTCTACCAA AAAAAGGGAA AGGGATGAAG AAAATCAAGA AATGTCTTCA TGCAAATCAG
1441  CAAGAATAGA AACGTCTTGT TCTCTTTTAG AACAAACACA ACCTGCTACA CCCTCATTGT
1501  GGAAAAATAA GGAGCAGCAT CTATCTGAGA ATGAGCCTGT GGACACAAAC TCAGACAATA
1561  ACTTATTTAC AGATACAGAT TTAAAATCTA TTGTGAAAAA TTCTGCCAGT AAATCTCATG
1621  CTGCAGAAAA GCTAAGATCA AATAAAAAAA GGGAAATGGA TGATGTGGCC ATAGAAGATG
1681  AAGTATTGGA ACAGTTATTC AAGGACACAA AACCAGAGTT AGAAATTGAT GTGAAAGTTC
1741  AAAAACAGGA GGAAGATGTC AATGTTAGAA AAAGGCCAAG GATGGATATA GAAACAAATG
1801  ACACTTTCAG TGATGAAGCA GTACCAGAAA GTAGCAAAAT ATCTCAAGAA AATGAAATTG
1861  GGAAGAAACG TGAACTCAAG GAAGACTCAC TATGGTCAGC TAAAGAAATA TCTAACAATG
1921  ACAAACTTCA GGATGATAGT GAGATGCTTC CAAAAAAGCT GTTATTGACT GAATTTAGAT
1981  CACTGGTGAT TAAAAACTCT ACTTCCAGAA ATCCATCTGG CATAAATGAT GATTATGGTC
2041  AACTAAAAAA TTTCAAGAAA TTCAAAAAGG TCACATATCC TGGAGCAGGA AAACTTCCAC
2101  ACATCATTGG AGGATCAGAT CTAATAGCTC ATCATGCTCG AAAGAATACA GAACTAGAAG
2161  AGTGGCTAAG GCAGGAAATG GAGGTACAAA ATCAACATGC AAAAGAAGAG TCTCTTGCTG
2221  ATGATCTTTT TAGATACAAT CCTTATTTAA AAAGGAGAAG ATAACTGAGG ATTTTAAAAA
                                          End NBS1 >
2281  GAAGCCATGG GGATCCACCG GATCTAGATA ACTGATCATA ATCAGCCATA CCACA
```

Previous work on the protein-substrate interaction

The research topic presented in this thesis was my PhD topic since the beginning of 2005. In the time period from 2003 to 2005 I was working on a PhD thesis on the topic: "Investigation of protein-protein, protein-substrate and protein-DNA interactions by using time resolved UV-spectroscopy" supervised also by Prof. K.O.Greulich. The change of the research topic in 2005 happened due to the change of the research scope of the institute from Institute of Molecular Biotechnology (IMB) to Leibniz Institute for Age research, Fritz-Lipmann institute (FLI). In the following section the work done from 2003 to 2005 will be shortly summarized.

Investigation of protein-protein, protein-substrate and protein-DNA interactions by using time resolved UV-spectroscopy

The aim of the work was to develop the label free protein microarray analysis by measuring changes in intrinsic protein fluorescence

Detection of protein-protein interactions on microarrays by fluorescent labels is a very sensitive method. Nevertheless, label coupling to biological molecules can alter their native structure and thus their functionality. Moreover, some rare proteins may be lost during this time consuming and expensive labeling process. These disadvantages can be avoided by using label free detection techniques. In this short summary the principle of the label free optical method for analysis of protein – protein interactions by employing the native fluorescence of proteins will be introduced. Main results will be also presented.

Principle

Proteins usually contain various amounts of intrinsic fluorophores tyrosine and tryptophane. Those two aromatic amino acids have an absorbtion maximum around 280 nm and fluorescence from 300 to 350 nm depending on the environment. The fluorescence maximum as well as the life time of excited tryptophane highly depends on the environment. Alteration in the environment of these two aromatic amino acids may lead to variations of the excited state lifetime. Therefore a change of the fluorescence decay may be observed, when the target molecule binds to the immobilized protein. Furthermore, an increase in fluorescence intensity due to the fluorophores in the captured molecule can also provide information on protein-protein binding.

The intrinsic fluorophores were excited at around 280 nm by a frequency tripled Ti:Sa laser delivering pulses of approx. 200 fs length. The fluorescence decay kinetics of proteins immobilized on the slides after incubation with a binding partner or just a buffer were measured in a spectral range of 300 – 360 nm by Time Correlated Single Photon Counting technique or Streak camera (Hamamatsu). The hydrogel slides used for protein immobilization preserve proteins in their native state. Alternatively activated fused silica (quartz glass) slides were used. Both supports are distinguished by their low luminescence background upon excitation at 280 nm.

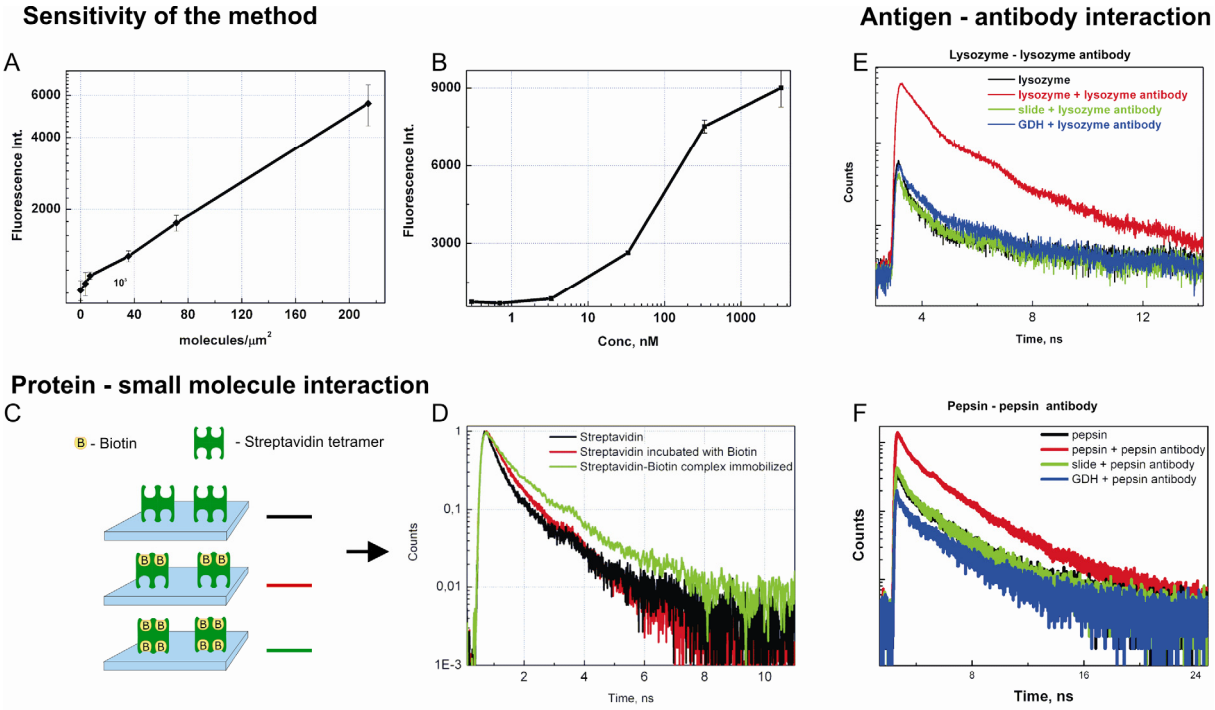

Figure 6.1 Detection of protein-substrate interaction on protein microarray. A – calibration curve of detection of lysozyme molecules. B – Antibody detection sensitivity, immobilized lysozyme was incubated with different concentrations of specific antibody. C and D – a prolongation of streptavidin tetramer fluorescence decay is observed upon biotin binding to immobilized protein. The effect is even stronger when the streptavidin tetramer is immobilized with all binding sites being occupied - E and F - An increase in fluorescence intensity (red curve) is observed when lysozyme or pepsin antibodies bind to immobilized lysozyme or pepsin respectively (black), while the level of unspecific binding is low (green and blue curves).

Results

The Figure 6.1 A and B demonstrate the sensitivity of the method. It was found that 7000 lysozyme molecules per μm^2 (or 0.16 ng/mm^2) immobilized on the microarray slide can be detected by the intrinsic protein fluorescence. Lysozyme slide incubation with the specific lysozyme antibody in different concentrations, shows that the lowest detectable concentration of the antibody in solution is 8 nM (Figure 6.1 B). An example of the fluorescence changes after this reaction is shown in Figure 6.1 E and F, where dramatic increase in fluorescence intensity is observed after the specific lysozyme (E) and pepsin (F) antibody binding to the immobilized corresponding antigens. The last example Figure 6.1 C and D demonstrates protein interaction with a small molecule. In this case streptavidin, immobilized on the slide, was incubated in the solution with biotin. Upon two biotin molecule binding to one streptavidin, the fluorescence life time of later is prolonged. Even stronger effect is found when the fluorescence decay of immobilized streptavidin in complex with four biotin molecules is recorded.

Conclusion

This work demonstrates that the time resolved UV spectroscopy is a suitable technique to detect binding of antibodies or small sized target molecules to proteins on the microarray. Two parameters can be used in this case: the fluorescence intensity increase is observed when large molecules containing lot of aromatic amino acids are bound; and changes in fluorescence life time can be detected upon binding of the small molecule.

CURRICULUM VITAE

Name:	**Paulius Grigaravičius**
Personal Details	
Date of birth:	30 03 1979
Place of birth:	Vilnius, Lithuania
Nationality:	Lithuanian
Personal Address:	Käthe-Kollwitz Str. 8 D-07743, Jena Germany
Phone:	+49 176 2432857
Working Address:	Leibniz Institute for Age Research - Fritz Lipmann Institute Beutenberg Str. 11 D-07745, Jena Germany
e-mail:	paulius@fli-leibniz.de
Phone:	+49 3641 656409
Fax:	+49 3641 656410

Education and research experience

2005 - present	PhD thesis "DNA repair after subcellular DNA damage with irradiation of different quality" Leibniz Institute for Age Research - Fritz Lipmann Institute, Jena (FLI), Germany Supervisor: Prof. K.O. Greulich
2005	Change of research object due to change of scope of the institute from IMB to FLI
2003 - 2005	PhD thesis "Investigation of protein-protein, protein-substrate and protein-DNA interactions by using time resolved UV-spectroscopy" Institute for Molecular Biotechnology (IMB), Jena, Germany Supervisor: Prof. K.O. Greulich
2001 - 2003	Master degree in Biophysical sciences (cum laude) Vilnius University, Faculty of Physics Supervisor: Prof. R. Rotomskis
1997 - 2001	Bachelor degree in Physical Sciences Vilnius University, Faculty of Physics Supervisor: Prof. R. Rotomskis
1994 - 1997	Vilnius lyceum of nature and precise sciences
1985 - 1994	Vilnius 21st Secondary School

Publications

1. P.Grigaravičius, T.Lenser, S.Monajembashi, K.O.Greulich "Late choice between NHEJ and HRR repair after DNA damage induction by a laser-microbeam" (Manuscript in preparation)

2. P.Grigaravičius, K.O.Greulich, S.Monajembashi "Laser microbeams and optical tweezers in ageing research" ChemPhysChem (in press)

3. P.Grigaravičius, A.Rapp, K.O.Greulich "A direct view by Immuno Fluorescent Comet-Assay (IFCA) on DNA damages induced by nicking and cutting enzymes, ionising 137Cs radiation, UV-A laser-microbeam irradiation and the radiomimetic drug bleomycin" Mutagenesis (in press)

4. P.Grigaravičius, S.Monajembashi, G.Pilarczyk, A.Rapp and K.O.Greulich "Laser microbeams and optical tweezers to study DNA repair and ageing" Proceedings of SPIE 2007 Vol. 6644

5. P.Grigaravičius, R.Dietrich, W.Fritzsche, K.O.Greulich, U.Horn, D.Knoll, S.Peters, H.-M.Striebel, P.Schellenberg „Protein chip analysis by probing time-resolved UV-fluorescence" Proceedings of SPIE 2007 Vol. 6633

6. P.Schellenberg, P.Grigaravičius, H.M.Striebel, K.O.Greulich: „Markerfreie Proteinchipanalytik: Analyse von Protein Chips mit zeitaufgelöster UV-Fluoreszenzspektroskopie" Bioforum, 10/2004, 34-35

7. H.M.Striebel, P.Schellenberg, P.Grigaravičius, K.O.Greulich: "Readout of protein microarrays using intrinsic time resolved UV fluorescence for label free detection" Proteomics 2004 4(6) 1703-11

8. B.Dietzek, W.Kiefer, A.Yartsev, V.Sundström, P.Schellenberg, P.Grigaravičius, G.Hermann, J.Popp, M.Schmitt: „The Exited-State Chemistry of Protochlorophyllide a: A Time-Resolved Fluorescence Study" ChemPhysChem 2006, 7 1727-1733

9. P.Grigaravičius, V.Gulbinas, U.-W.Grummt, R.Rotomskis: "Excited state relaxation of protonated 9-(4-diethylaminostyryl)-acridine" Lithuanian Journal of Physics 2002 Vol. 42, No. 2, 93-98

Publications1 - 4 are directly related to the presented work.

Publications 5 -8 are the result of Previous PhD work presented in Appendix

Scientific meetings

Invited talks

(Keynote) K.O.Greulich, P.Grigaravicius and S.Monajembashi "How we can reach a high healthy age? The secret of birds and what the laser can contribute to solving this question" Laser Application in Life Science (LALS), Taipei, Taiwan 04-06 12 2008

(Invited Lecture) P.Grigaravicius, T.Keining, S.Monajembashi, B.Schäfer, K.O.Greulich "Laser as an optical microtool for biology: DNA repair and ageing research" International school "Advanced methods in biophysics", Trakai, Lithuania 26-30 11 2007

(Invited) P.Grigaravicius, T.Keining, A.Rapp, S.Monajembashi and K.O.Greulich "Laser as a tool in DNA damage repair research: Does double strand break repair depend on nuclear environment?" Laser Application in Life Science (LALS), Moskau, Russia 11-14 05 2007

Contributed talks

P.Grigaravicius, T.Lenser, S.Monajembashi, K.O.Greulich „DNA damage and repair – dependence on irradiation type and quality" 11th Annual meeting of German Society for Radiation Biology Research (GBS), Tübingen, Germany, 6-8 10 2008

P.Grigaravicius, T.Lenser, S.Monajembashi, Z.- Q. Wang, K.O.Greulich "XRCC4 is an early acting NHEJ enzyme at laser induced double strand breaks" Research Workshop "Genome Stability in Health and Disease" Jerusalem, Israel, 21-25 09 2008

P.Grigaravicius, T.Lenser, S.Monajembashi, Z.- Q.Wang, K.O.Greulich "Live cell imaging reveals XRCC4 as an early acting molecule in double strand break response" 10th biennial meeting of the German Society for Research on DNA Repair (DGDR). Berlin, Germany 02-05 09 2008

P.Grigaravicius, A.Rapp and K.O.Greulich "Visualisation of DNA repair mechanisms by live cell imaging" Workshop on Cell Biology and Microscopy, Altleiningen Germany, 7.-11 12 2005

P.Grigaravicius, A.Rapp and K.O.Greulich "DNA damage induction by laser microbeam in a broad range of spectrum; New method for comet assay visualization: closer look at DNA stretching?" 9 Annual meeting of German Society for Radiation Biology Research (GBS), Braunschweig, 10-12 05 2006

P.Grigaravicius, A.Rapp and K.O.Greulich "Interaction of DNA double strand break pathways and effects of gene defects after UVA exposure" 8 Annual meeting of German Society for Radiation Biology Research (GBS), Buxtehude, Germany 6 – 8 04 2005

Posters

P.Grigaravicius, T.Keining, A.Rapp and K.O.Greulich „Spatiotemporal dynamics of DNA repair proteins Ku80, Xrcc4 and NBS1 after double strand break induction by laser microbeam“ 10th International Wolfsberg Meeting on Molecular Radiation Biology/Oncology, Ermatingen, Switzerland, 12-14 05 2007

P.Grigaravicius, T.Keining, A.Rapp and K.O.Greulich “Dynamics of DNA repair proteins Ogg1, Ku and XRCC4 at laser microbeam induced double strand breaks” Annual Meeting of the German Genetics Society, Jena, Germany 11-13 10 2007

P.Grigaravicius, A.Rapp and K.O.Greulich “Repair of DNA double strand breaks induced with laser microbeam of different quality; IFCA: ImmunoFluorescent Comet Assay” 9th biennial meeting of the German Society for Research on DNA Repair (DGDR), Hamburg, Germany 12 - 15 09 2006

P.Grigaravicius, A.Rapp, K.O.Greulich „Double strand break induction by blue light at 420 nm and detection of DNA fragmentation by the protein based neutral comet immunoassay“ VI International Comet Assay Workshop, Warszawa, Poland, 22-24 09 2005

P.Grigaravicius, A.Rapp, S.Monajembashi and K.O.Greulich “DNA damages induced by different laser microtools” Focus on Microscopy, Jena, Germany, 2005

P.Grigaravicius, P.Schellenberg, H.-M.Striebel, K.O.Greulich “Protein microarray analysis by using UV fluorescence spectroscopy: detection of antigen-antibody and protein-ligand binding” Chiptechnologien (Microarray Techiques), Frankfurt am Main, Germany 03-04 02 2005

Talk in the Advisory Board Meeting of the Leibniz Institute for Age Research - Fritz Lipmann Institute

P.Grigaravicius “The earliest events in DNA double strand break repair after damage induction with a laser-microbeam”

Reports on my work in the general press

Petra Spamer: Gesundes Altern (Healthy Aging) 07 05 2008, DIE WELT (a nationwide daily newspaper)

Eigenständigkeitserklärung

Hier mit erkläre ich, dass ich die vorliegende Arbeit selbständig und nur unter Zuhilfenahme der angegebenen Mittel und Literatur angefertigt habe.

Darüber hinaus erkläre ich, dass ich mich mit der vorgelegten Arbeit an keiner anderen Hoch - schule um den akademischen Grades *doctor rerum naturali um* (Dr. rer. nat.) beworben habe und dass ich weder früher noch gegenwärtig die Eröffnung eines Verfahren zum Erwerb des Titels des *doctor rerum naturalium* an einer anderen Hochschule beantragt habe.

Jena, den 15 Dezember 2008

Paulius Grigaravičius

Acknowledgments

In the following section all effectors such as determiners, helpers, supporters, advisors, stress makers and bystanders of my work will be discussed.

In the first line I would like to thank “Die Deutsche Bahn”! Since, without one ICE train being late in Jena Paradies I would never have been landed in the laboratory of Prof. K.O.Greulich, and therefore this work would not exist at all. And of course one has to note that reading articles in the train by constantly changing views of the wonderful German (mostly Thüringian and Bavarian) landscape significantly mediates better understanding and induces a lot of new ideas.

The most important person whom I would like to thank is Prof. K.O.Greulich who with great patience gave me an opportunity to do my PhD in his laboratory. Extremely I would like to thank him for his support not only in the research but also in politics and representation. I have to say that, in these years I have learned a lot from him. And was always supported not only by ideas, but also by his generating simply productive stress, which is an inescapable machinery of a successful work.

High impact on the work has also Alexander Rapp, from whom I had an opportunity to learn techniques of molecular biology, and also DNA repair. The existence of this work is hardly imaginable without his supervising in the first year of my PhD in the DNA repair field.

Further understanding of DNA double strand break repair couldn’t be developed without Prof. Z.Q.Wang as well as all members of his group. Constructive discussions in the seminars and journal clubs supervised by him particularly helped me to get an insight into cell biology and especially in DNA repair. Here I have to note that supporting played also a big role!

Most of AG Greulich group members are not in DNA repair research; however they are in charge in creating very friendly, funny and still productive working atmosphere in the group. The responsible people are Sabine, Helgard, Gabi, Marina, Silke, Leo, Konrad, Peter, Roland, Heike, Kornelia, Norman, Franzi, Kathrin, Melanie, Kerstin, Nikolina, and Maria. It was great pleasure and honour to work with these people. Especially I have to mention my diploma students Teresa and Julia who greatly contributed to this work and by whom I already could train my stress maker skills. There is still one and most important person left - Shamci Azar, sitting all these years left behind me and bringing incredibly quiet, smooth and do not forget - tasty surrounding in our office. From Shamci, again, I learned how to negotiate with firms, how to couple the laser beams into microscopes and how to be simply a good

man. And do not forget, that all these years she had to stand me almost every day.

By finishing the scientific part of acknowledgments I would like to thank Prof. Ričardas Rotomskis my supervisor during bachelor and master degree in Vilnius University. He was the person who sent me here to Jena, and the person from whom I've got the basics of good scientific practice. Additionally I would like to thank Prof. Peter Herrlich who basically initiated my research on DNA repair.

And last but not least I am gratefully thankful to Prof. K.O.Greulich, Amal, Anja, Kerstin, Maria and Leo for helping me with proofreading of this work, especially to Michela

Finally non-scientific helpers, motivators, supporters and bystanders have greatly influenced my life in Germany and therefore created a highly localized and warm "at HOME" feeling here in Jena.

Of course in the first line this is my family: parents Milda and Ričardas as well as sister Agne who always supported from a distance as well as sometimes from nearness. Unfortunately, all the time they were far away from here, but most important was the secure feeling to have them behind me - whatever happens! Also Saulius, Jonas and Julija my friends in Lithuania highly contributed by visiting me in Jena. It was always a great feeling to come back home to Vilnius to meet them and feel as if I haven't ever left this place.

Special thanks goes to the family Schrehardt and not only to Carola and Rüdiger, but also for all family members, who integrated me and who even made me to feel like having a second family here in Germany. Without them, the life in Jena wouldn't have had such a high quality. Of course a lot of friends highly contributed to this issue. I can hardly imagine my life without going to drink a beer or two and discuss human being problems with Anja, Venelina, Diana, Maria and/or Petra as well as talks and discussions with Michela or Amal.

Here I also have to point out the extremely friendliness of most of the people from the institute who always were ready to help and also to celebrate. Special thanks goes to people from AG Wang group: "drauge" Laura, "draugas" Antonio, Misha, Mareen, Tangliang, Sandra, Ralph, Tjard, Alicia, Benazir, Anke... and also from other groups: Tobias, Alex, Ralf, Marija, Ana, Kristin, Slavomir, Jan, Indri, Sandra, Eberhard, Fritz and…

Last but not least I would like to thank my flatmates and neighbours Christian, Kevin, Katja, Andrea, Christin, Bianca, Jana, Christian and Danny for their patience and worm friendliness.

All these people in one or another way have contributed to this work, therefore

THANK YOU VERY MUCH

Dėkoju jums nuo visos Širdies - Ačiū!